PHOTODEGRADATION OF SELECTED PHARMACEUTICALS USING MAGNETIC-CARBON DOT LOADED ON DIFFERENT TiO_2 NANOSTRUCTURES

EDNA DIMAKATSO MOSHOEU

Student number: 212105663

BTech: Chemistry

Dissertation submitted in fulfilment of the requirement for the degree of

MAGISTER TECHNOLOGIAE: CHEMISTRY

FACULTY OF APPLIED AND COMPUTER SCIENCES

DEPARTMENT OF CHEMISTRY

SUPERVISOR: Prof. S.J MODISE (BSc Hons, MSc, PhD Chemistry)

CO-SUPERVISORS: Dr O.E OSEGHE (BSc Hons, MSc, PhD Chemistry);

Prof. A.E OFOMAJA (BSc Hons, MSc, PhD Chemistry)

November 2020

DECLARATION

I, *Edna Dimakatso Moshoeu*, declare that this dissertation was composed by myself, that the work contained herein is my own except where explicitly stated otherwise in the text, and that this work has not been previously submitted for any other degree or professional qualification at another university.

…….....
(Candidate's signature)

……. day of……

DEDICATION

This work is dedicated to my mother, Germinah Ditlakala Moshoeu; my sister Patsy Mamorema Londani; my niece and nephew, Lutendo and Hulisani Londani.

ACKNOWLEDGEMENTS

I would like to express my profound appreciation and gratitude to the following for their contribution to this work:

I sincerely appreciate God Almighty for giving me life and strength to tackle this task. To Him alone be all the glory.

Special thanks to my supervisors; the late Prof. A.E. Ofomaja, Prof. S.J Modise and Dr E.O. Oseghe for their excellent support and tremendous guidance. Their encouragement, knowledge and sharing their ideas with me throughout the course of this research is greatly appreciated.

I would like to thank Vaal University of Technology through the Research Directorate for providing the research funding.

I would like to thank the Department of Chemistry who accepted my application in pursuit of this master's degree.

I also appreciate the assistance from my fellow research members Anza Makamu and Oyandi Sentse. They are wonderful and more of a family than just research fellows; their contributions have significantly led to the success of this project.

ABSTRACT

To replace the conventional wastewater treatment technology, photocatalysis has the best potential due to its utilization of visible light to photodegrade organic and inorganic contaminants. However, agglomeration of nanoparticles leads to serious decrease in photocatalytic performance when applied in slurry form, due to hindrance effect. TiO_2 semiconductor photocatalyst mediated advanced oxidation process is referred to as one of the most efficient technologies to degrade organic pollutants in water. However, TiO_2 semiconductor for water purification hinders large scale applicability due to poor activity under visible light and the recombination of photogenerated electron and hole pairs. The modification of TiO_2 semiconductor photocatalyst with carbon dots (CDs) is of high importance due to low toxicity, aqueous stability, enhanced surface area, economic feasibility, good biocompatibility and chemical inertness of CDs. Herein, strategies are highlighted to improve the activity of TiO_2 semiconductor photocatalyst by coupling it with CDs and Fe_2O_3. In this study, we study the morphological influence of TiO_2 nanostructures on photocatalytic degradation of tetracycline hydrochloride present in industrial wastewater. TiO_2 nanostructures, nanotubes, nanospheres and nanofibers were Synthesized using the hydrothermal technique. TiO_2 nanotubes, nanofibers and nanospheres were prepared by the hydrothermal treatment of TiO_2 nanoparticles with different NaOH concentrations (5, 10 and 12 N) at 120 and 140 ˚C; afterwards, HCl was added until it reached pH 2. Both the crystalline phase and coordination of the TiO_2 nanotubes, nanofibers and nanospheres were composed principally. Likewise, the surface area, pore volume and pore size of the TiO_2 nanotubes, nanofibers and nanospheres changed with the NaOH rinsing treatment. The photocatalytic activity for tetracycline degradation were strongly enhanced by the nanofibers and nanotubes in the basic and acid media, respectively, showing a relationship between their structure and the medium. TiO_2 nanostructures and the composite material were characterized by scanning electron microscope\SEM), X-Ray Diffraction (XRD), transmission electron microscope (TEM) and Fourier transform infrared (FTIR). BET surface area analysis was carried out using nitrogen adsorption desorption curves. The results show that TiO_2 morphology had great influence on photocatalytic degradation of tetracycline hydrochloride due to difference in specific surface area and pore volume of nanostructures. The

photocatalytic degradation experiments were carried out for three hours under visible-LED light. TiO_2 nanofibers show better degradation performance than nanotubes and nanospheres due to presence of large surface area for reaction, higher porosity with dispersion of active sites at different length scales of pores and presence of oxygen vacancies. Agricultural biomass pine bark serves as a carbon source and was doped into TiO_2-nanofibers (TNF) to fabricate the composite material (CD-TNF). CD-TNF composite nanofibers were prepared via a facile hydrothermal method. This study revealed that the photocatalytic efficiency of tetracycline (TC) under visible light irradiation of the composite nanofiber is higher than that of pure TiO_2-nanofiber. The anchored CDs can both enhance the light absorption and suppress photogenerated electron hole recombination which results in the enhancement of catalytic and antibacterial properties. The CDs can better capture and transfer photogenerated electrons through the Ti-O-C and Fe-O-C bonds. Moreover, CDs can improve the utilization of photogenerated electrons and the electrons in CDs are captured by O_2 to produce $O_2^{\bullet-}$ radicals and the role of $O_2^{\bullet-}$ radicals in the photocatalytic process is significantly improved. A new efficient photocatalyst consisting of TiO_2/CD/Fe_2O_3 composite material was Synthesized by the hydrothermal treatment and applied in the photodegradation of 5 mg/L tetracycline hydrochloride (TC) under visible-LED light. The CDs/TiO_2/Fe_2O_3 composite showed enhanced photocatalytic performance for tetracycline photodegradation when compared with TiO_2/CDs and pure TiO_2 under the visible light irradiation. The mechanism of the improved photocatalytic activity over CDs/TiO_2/Fe_2O_3 was also investigated. The influence of the interface formation between Fe_2O_3 and TiO_2/CDs affects severely the charges separation efficiency and enhances the electron transfer to keep on the existence of Fe^{3+}/Fe^{2+} moieties that take significant role in the reaction mechanism.

TABLE OF CONTENTS

Contents

LIST OF FIGURES

LIST OF TABLES

LIST OF ABBREVIATIONS AND SYMBOLS

Greek Symbol

Cos	Cosine
Θ	Theta
µm	Picometre
Λ	Wavelength

English Symbol/Abbreviation

A	Absorption coefficient photon energy
A_0	Adsorption in initial time
A_t	Adsorption of reactant time (t)
AOP	Advanced Oxidation Process
BET	Brunauer Emmett Teller
BJH	Barett Joiner Halenda
C	Concentration
CB	Conduction Band
Cm	Centimetre
cm^{-1}	per centimetre
C_0	Concentration reaction at initial time
C_t	Concentration of reactant time
CD	Carbon dots
CNTs	Carbon Nanotubes
CQD	Carbon quantum dots

CDTNF	Carbon dots TiO_2-Nanofiber
CVD	Chemical Vapour Deposition
D	Diameter
D%	Percentage Degradation
Ecb	Conduction band of electrons
Eg	Band Gap
eV	Electron Volt
Fe_2O_3	Iron (III) oxide or ferric oxide
FTIR	Fourier Transform Infrared Spectroscopy
HCl	Hydrochloric acid
H_2O_2	Hydrogen peroxide
IUPAC	International Union of Pure and Applied Chemistry
JCPDS	Joint Committee on Powder Diffraction Standards
K_{sp}	Solubility Product

SYMPOSIUM PRESENTATIONS AND PUBLICATIONS

Presentations

The results of this study were presented in the following conferences:

- "Photodegradation of tetracycline on different nanostructures of TiO_2". 3rd VUT Interdisciplinary Research and Postgraduate Conference 2018 held at Quest Conference Centre in Vanderbijlpark, South Africa from 17th – 18th October 2018. Oral presentation.

- "Photodegradation of tetracycline on different nanostructures of TiO_2". The 43rd National Convention of the South African Chemical Institute held at CSIR in Pretoria, South Africa from 2nd December 2018 – 7th December 2018. Poster presentation.

Publications

- Moshoeu, D.E., Sanni, S.O., Oseghe, E.O, Msagati, T.A.M., Mamba, B.B., and Ofomaja, A.E, 2020. Morphological influence of TiO_2 nanostructures on charge transfer and tetracycline degradation under LED light. *Chemistry Select*, 5, 1037-1040.

OUTLINE

This study is divided into 5 chapters.

Chapter 1:

The chapter covers the introduction, problem statement, aims and objectives of the research.

Chapter 2:

This chapter covers the literature review of the pollutants in the industrial wastewater and methods of their removal in wastewater. The advanced oxidation processes are introduced as a technique for the degradation of the pollutants. An in-depth review of the TiO_2/CDs/Fe_2O_3 composite nanofiber catalyst, its advantages and limitations are also discussed together with their synthesis methods.

Chapter 3:

The key aim of this chapter is to elucidate an experimental procedure of the research. A comprehensive outline of the chemical details, equipment used and procedures employed to attain the set research objectives is given.

Chapter 4:

This chapter describes three parts of the results and discussions. The chapter focuses on the Characterization of TiO_2 nanostructures, TiO_2-CDTNF and TiO_2/CDs/Fe_2O_3 composite nanofiber and the effect of experimental conditions for the degradation of tetracycline.

Chapter 5:

This chapter presents conclusions and recommendations of the study.

Chapter 1 INTRODUCTION

Chapter 1

1.1 Introduction

Water pollution is the contamination of water bodies such as rivers, lakes and oceans. However, over the years a billion tons of industrial, fertilizers and chemical waste were dumped untreated into these water bodies (Al-Mamun *et al.* 2019). In recent times, the occurrence and presence of toxic contaminants in wastewater are increasing and consequently contribute to the non-availability of clean and safe water (Khodadadi *et al.* 2018). There are different types of pollutants broadly classified into organic and inorganic pollutants. Organic pollutants consist of a wide range of compounds such as the polycyclic aromatic hydrocarbons (PAHs), pesticides and polychlorinated biphenyls (PCBs). Pharmaceuticals and personal care products (PPCPs) are attracting attention since they were recently detected in water bodies globally. Several antibiotics for pharmaceutical drugs have recently been identified and quantified in the environment and are specifically used to fight bacterial infections such as caffeine, tetracycline, carbamazepine, penicillin, ciprofloxacin and amoxicillin (Matongo *et al.* 2015).

TiO_2 photocatalyst will help in degrading these organic pollutants present in wastewater. They are one of the most frequently detectable antibiotics in surface water resources that receive discharges from agricultural effluents and municipal wastewater treatment plants (Xu *et al.* 2019). Their removal efficiencies are largely dependent on various parameters or factors or operating conditions of wastewater treatment and often insufficient even by full-scale wastewater treatment plants (Horikoshi and Serpone 2020). Tetracyclines have a high risk of the occurrence of antibiotic-resistant bacteria in activated sludge (Martins *et al.* 2017). Therefore, tetracycline-resistant genes have often been found at outfall of or downstream municipal wastewater treatment plants (Martins *et al.* 2017). Efficient methods for removing tetracyclines from wastewaters should be developed to reduce the environmental risk of these antibiotics. Several methods have been developed for the effective removal or degradation of tetracycline's in wastewaters (Khodadadi *et al.* 2018). Over the years, numerous conventional treatment techniques such as ozonation, reverse

osmosis, advanced oxidation technologies, Fenton oxidation, hydrogen peroxide and chemical oxidation technologies were used to degrade and remove organic pollutants present in wastewater; but research findings have it that some of the organic pollutants are not susceptible to conventional treatment (Gaur *et al.* 2018). Advanced oxidation processes (AOPs) utilize powerful hydroxyl or sulfate radicals as a major oxidizing agent for potable water treatment. AOPs were broadly applied for treatment of different types of wastewaters because the strong oxidants can readily degrade recalcitrant organic pollutants and remove certain inorganic pollutants in wastewater.

AOPs hold several advantages in the field of water treatment. They can effectively eliminate organic compounds in aqueous phase, rather than collecting or transferring pollutants into another phase. Due to its remarkable reactivity, hydroxyl radical ($OH^{\bullet}$) virtually reacts with almost every aqueous pollutant without discriminating. AOPs are applicable in many, if not all, scenarios where many organic contaminants must be removed at the same time. Some heavy metals can also be removed in forms of precipitated M(OH). In some AOPs' designs, disinfection can also be achieved, which makes these AOPs an integrated solution to some water quality problems. Since the complete reduction product of $OH^{\bullet}$ is H_2O (and CO_2), AOPs theoretically do not introduce any new hazardous substances into the water (Gaur *et al.* 2018).

Titanium dioxide (TiO_2) is a good polycrystalline semiconductor compound and is the most studied photocatalyst. TiO_2 semiconductor has gained enormous research interest as it is one of the most appropriate, green and cost-effective materials for the complete degradation of the hazardous particles into less toxic simpler molecules (Kumar *et al.* 2016). TiO_2 nanoparticles are considered a superb catalyst that is chemically stable, non-toxic, low cost and with relatively high photocatalytic activity (Totito 2013). It has been widely used in materials, chemical industry, electronics, photoelectricity, biology, life science and other fields (Tran and Jeong 2018). Despite the interesting analytical advantages of TiO_2, their limitation includes, wide band gap energy and high electron-hole recombination rate. It has a wide band gap energy and high electron-hole recombination rate which reduces its photocatalytic efficiency (Choi *et al.* 2018). However, TiO_2 semiconductor has been used for the degradation of organic contaminants in water, water splitting and solar energy conversion causing less harmful byproducts at comparatively cheaper costs (Tran and Jeong 2018). Previous studies indicate that the TiO_2 semiconductor is a magnificent photocatalyst that can

be operated under UV irradiation (Zhang *et al.* 2019). Efforts have been made to improve the photocatalytic efficiency by doping with noble metals and metal ions, coupling with narrow bandgap semiconductors and co-doping with "impurities". This helps to reduce the band gap energy of TiO_2, giving it access to a wide range of the solar spectrum and also slows down electron-hole recombination rate (Hantusch *et al.* 2018).

Photocatalytic efficiency can also be improved by adsorption affinity and external surface area of the material can be enlarged to elevate the possibility of pre-adsorption of organic compounds on the surface of the photocatalysts (Khan *et al.* 2017). However, the charge carrier separation process in the application of TiO_2 semiconductor can be utilized to overpower the electron-hole recombination and can also be strained by the wideband energy by changing the defect structure to trap electrons and holes on the surface (Khairy and Zakaria 2014).

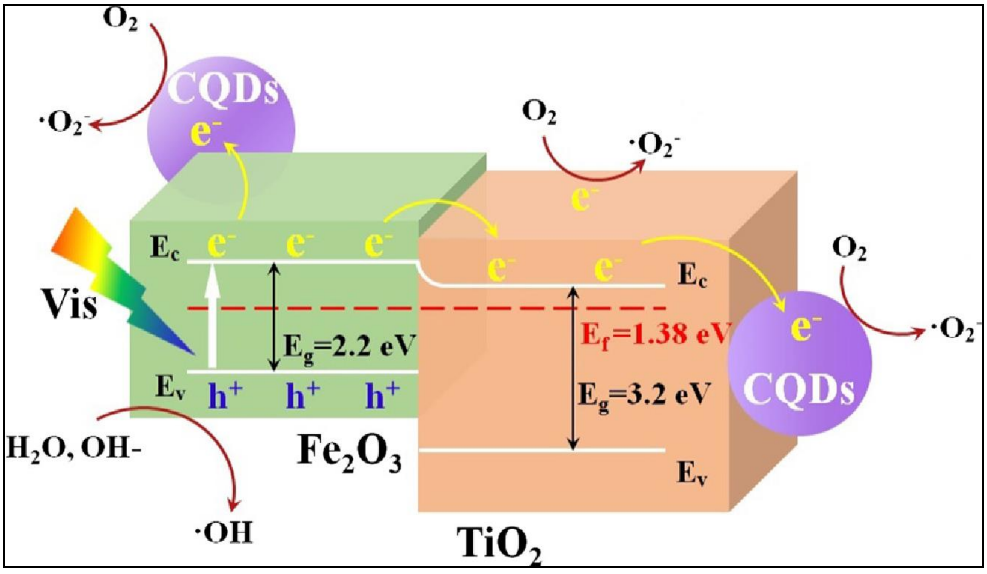

Figure 1.1: Schematic model for the photocatalytic process of $CDs/TiO_2/Fe_2O_3$ under visible light (Zhang *et al.* 2019).

In the mechanism photocatalytic process of $CDs/TiO_2/Fe_2O_3$ semiconductor (Fig. 1. 1), the distance between the valence band and the conduction band is called the band gap. TiO_2 has a problem with the wide band gap and to reduce it, impurities are introduced. It is expected that

by the time the impurities are introduced another level will be formed, and therefore the band gap is reduced (Zhu *et al.* 2018). When the catalyst is irradiated with the light source, electrons move from the valence band to the conduction band within that period; if there are no impurities to trap the electrons, the electrons will fall back to the hole and this is called electron-hole recombination (Zhang *et al.* 2019). Therefore, it has a fast electron-hole recombination rate to slow it down or to stop it; a trap must be introduced in the photocatalytic process. By the time the impurities are introduced, the visible light activates the catalysts. The electrons move from the valence band to the conduction band and instead of the electrons falling back to the hole they are trapped by the impurities or dopants, thereby preventing electron-hole recombination. This hole is so effective that it reacts with the surface water or hydroxyl group to produce non-selective hydroxyl radical ($OH^{\bullet}$) which can oxidize a vast range of organic contaminants present in wastewater. This hydroxyl radical reacts with the organic pollutants to oxidize or mineralize the organic pollutants.

In previous years, the synthesis of TiO_2 nanostructures such as nanotubes, nanorods, nanowires, nanofibers and nanospheres have been used in photocatalysis and are efficient to increase photocatalysis due to their high surface area, ion-exchange and photocatalytic abilities (Khan *et al.* 2017). Different TiO_2 morphologies and their nanostructures have been Synthesized using the hydrothermal and sol-gel methods. The sol-gel method is mostly used among all the methods for fabricating TiO_2 nanostructures as the size and growth of the nanostructures is well monitored and the method is advantageous for structures production in relatively shorter processing time. These TiO_2 nanostructures were applied to the degradation of organic pollutants but they have never been compared in the same photocatalytic system in order to identify the most efficient one (Haque *et al.* 2017). Another class of nanoparticles that have recently gain attention is carbon dots. Carbon dots (CDs) nanoparticles were initially discovered by Xu and co-workers. Throughout the electrophoretic ablution of carbon nanotubes and since then, there has been a hunt bustle in this aspect of research (Chansri and Sung 2016).

CDs are an emerging class of multicolour luminescent carbon nanoparticles and have received growing research major interest in varieties of technological applications in huge regions of biomedical, bioimaging, biosensing, photocatalysis and drug delivery (Asha Jhonsi and Thulasi 2016) since they were discovered. CDs are excellent nanomaterials due to their chemical stability, excellent biocompatibility, low toxicity and strong resistance to

photodegradation in comparison with other traditional semiconductor quantum dots and organic dyes (Sharma *et al.* 2019). Considering the unique and fluorescent properties of CDs, they are chosen as the most-liked substitution candidate for conventional semiconductor quantum dots that are found on poisonous metallic elements.

Long ago, an enormous effort has been spent on evolving synthesis methods for different types of CDs. Different physical or chemical methods such as laser irradiation, electrochemical oxidation, ultrasonic treatment, microwave irradiation, wet oxidation and hydrothermal treatment are ordinary approaches for the preparation of carbon quantum dots. However, there are some clear limitations to some of these synthetic methods such as the utilization of huge amounts of strong acids, costly equipment required and low quantum yield of the produced carbon quantum dots (Sharma *et al.* 2018). It has been reported that carbon helps in reducing the band gap energy and electron-hole recombination rate (Asha Jhonsi and Thulasi 2016). To explore the potentials of CDs obtained from pine bark which is considered as biomass or agro-waste, CDs will help to improve the efficiency of TiO_2 (Wang, Xiao, *et al.* 2011). Carbon dots-doped TiO_2 has been reported to exhibit excellent photocatalytic performance compared to bare TiO_2 (Martins *et al.* 2016). Therefore, photocatalytic materials of CDs/ TiO_2 systems are prepared to improve the photocatalytic activity of TiO_2 under visible light, such as Fe_2O_3/CDs, CDs/ Fe_2O_3@g-C_3N_4, CDs/ TiO_2, CDs/BiOBr, TiO_2/BiOI/CDs have been synthesized (Zhang *et al.* 2019).

There are various uses of magnetic nanoparticles in numerous fields, and they can be easily separated after the adsorption process by applying a magnetic field. Therefore, by applying external magnetic fields the use of magnetite nanoparticles as an adsorbent in water treatment provides a suitable and comfortable approach for separating and removing pollutants (Sadeghi-Niaraki, Ghasemi, Habibolahzadeh, *et al.* 2019). Magnetite is one of the nanoparticles used in wastewater treatment because of its specific large surface area, high reactivity in adsorption and it is recoverable from treated water via magnetic separation technology (Zhang *et al.* 2019). Although magnetite was initially existing naturally and without artificial aid magnet, there was no prospective application of magnetite in the sector of science and technology. Various research and development activities on the possibility of potential application of materials, environment and medical sciences have been carried out by scientists and technologists. These materials identified have many hidden characteristics having unlimited possibilities. So, they are focused to integrate iron formed magnetic

nanoparticles and their application in the area of materials, environment and medical sciences (Panneerselvam *et al.* 2011).

Furthermore, magnetic nanoparticles have outstanding paramagnetic properties, high chemical stabilities, ease of synthesis biocompatible, low toxicity and cytotoxicity (Zhang *et al.* 2019). Magnetic nanoparticles offer zero coercivity because of the superparamagnetic behaviour. However, due to the nano-size of the photocatalysts, it is difficult to separate the photocatalysts from the solution after the reaction. Recently, the main focus has been on synthesising photocatalysts with magnetic properties in order to be efficiently separated from solution when subjected to a magnetic field. Zhang *et al.* (2019) reported the synthesis and application of magnetically separable carbon dots-TiO_2 in the photocatalytic degradation of bisphenol (Cao *et al.* 2016). To the best of our knowledge, magnetically active carbon dots-TiO_2 has not been applied in the degradation of PPCPs.

1.2 Problem Statement

- South African aquatic systems are polluted with myriads of pollutants such as the pharmaceuticals and personal care products (Matongo *et al.* 2015).
- TiO_2 photocatalysis as an AOP is a promising technology for the treatment of wastewater containing pharmaceuticals. However, it has limitations of wide band gap energy and high electron-hole recombination rate.
- Different morphologies of TiO_2 have been Synthesized and applied for the degradation of organic pollutants, but they have never been compared in the same photocatalytic system in order to identify the most efficient.
- Another limitation of doped and un-doped TiO_2 is the problem of separation from the solution after the reaction.

1.3 Aim

The study is aimed at synthesizing cost-effective and efficient heterogeneous CD-TiO_2-Fe_2O_3 composite material for photodegradation of tetracycline present in water.

1.4 Objectives

- To Synthesize different shapes of TiO_2- nanospheres, nanotubes and nanofibers.
- Characterize using Scanning Electron Microscopy (SEM), X-Ray Diffraction (XRD) and Fourier Transform Infrared Spectroscopy (FTIR).
- To produce carbon dots from agro-waste (pine bark) using microwave synthesis.
- To fabricate composite materials of CD-TiO_2-Fe_2O_3 by co-precipitation.
- To apply composite materials CD-TiO_2-Fe_2O_3 in the photodegradation of tetracycline under visible-LED light.

References

Ahmad, R., Ahmad, Z., Khan, A.U., Mastoi, N.R., Aslam, M., and Kim, J., 2016. Photocatalytic systems as an advanced environmental remediation: Recent developments, limitations and new avenues for applications. *Journal of Environmental Chemical Engineering*, 4 (4), 4143–4164.

Akpan, U.G. and Hameed, B.H., 2010. The advancements in sol-gel method of doped-TiO2 photocatalysts. *Applied Catalysis A: General*, 375 (1), 1–11.

Al-Mamun, M.R., Kader, S., Islam, M.S., and Khan, M.Z.H., 2019. Photocatalytic activity improvement and application of UV-TiO2 photocatalysis in textile wastewater treatment: A review. *Journal of Environmental Chemical Engineering*, 7 (5).

Andrade-Guel, M., Díaz-Jiménez, L., Cortés-Hernández, D., Cabello-Alvarado, C., ávila-Orta, C., Bartolo-Pérez, P., and Gamero-Melo, P., 2018. Microwave assisted sol-gel synthesis of titaniumdioxide using hydrochloric and acetic acid ascatalysts. *Boletin de la Sociedad Espanola de Ceramica y Vidrio*, 1–7.

Archana, T., Vijayakumar, K., Arivanandhan, M., and Jayavel, R., 2019. TiO2 nanostructures with controlled morphology for improved electrical properties of photoanodes and quantum dot sensitized solar cell characteristics. *Surfaces and Interfaces*, 17 (May), 100350.

Asha Jhonsi, M. and Thulasi, S., 2016. A novel fluorescent carbon dots derived from tamarind. *Chemical Physics Letters*, 661, 179–184.

Awfa, D., Ateia, M., Fujii, M., Johnson, M.S., and Yoshimura, C., 2018. Photodegradation of pharmaceuticals and personal care products in water treatment using carbonaceous-TiO2 composites: A critical review of recent literature. *Water Research*, 142, 26–45.

Bakre, P. V., Volvoikar, P.S., Vernekar, A.A., and Tilve, S.G., 2016. Influence of acid chain length on the properties of TiO2 prepared by sol-gel method and LC-MS studies of methylene blue photodegradation. *Journal of Colloid and Interface Science*, 474, 58–67.

Bertoluzzi, L., Badia-Bou, L., Fabregat-Santiago, F., Gimenez, S., and Bisquert, J., 2013. Interpretation of cyclic voltammetry measurements of thin semiconductor films for solar fuel applications. *Journal of Physical Chemistry Letters*.

Bokare, A.D. and Choi, W., 2014. Review of iron-free Fenton-like systems for activating H2O2 in advanced oxidation processes. *Journal of Hazardous Materials*.

Camposeco, R., Castillo, S., Navarrete, J., and Gomez, R., 2016. Synthesis, characterization and photocatalytic activity of TiO2 nanostructures: Nanotubes, nanofibers, nanowires and nanoparticles. *Catalysis Today*, 266, 90–101.

Cao, M., Wang, P., Ao, Y., Wang, C., Hou, J., and Qian, J., 2016. Visible light activated photocatalytic degradation of tetracycline by a magnetically separable composite photocatalyst: Graphene oxide/magnetite/cerium-doped titania. *Journal of Colloid and Interface Science*, 467, 129–139.

Chansri, P. and Sung, Y.M., 2016. Reprint of "Investigations of electrochemical luminescence characteristics of ZnO/TiO2 nanotubes electrode and silica-based gel type solvents". *Surface and Coatings Technology*, 307, 1139–1143.

Choi, D., Ham, S., and Jang, D.J., 2018. Visible-light photocatalytic reduction of Cr(VI) via carbon quantum dots-decorated TiO2 nanocomposites. *Journal of Environmental Chemical Engineering*, 6 (1), 1–8.

Cuerda-Correa, E.M., Domínguez, J.R., Muñoz-Peña, M.J., and González, T., 2016. Degradation of Parabens in Different Aqueous Matrices by Several O3-Derived Advanced Oxidation Processes. *Industrial and Engineering Chemistry Research*.

Dedual, G., Macdonald, M.J., Alshareef, A., Wu, Z., Tsang, D.C.W., and Yip, A.C.K., 2014. Requirements for effective photocatalytic oxidative desulfurization of a thiophene-containing solution using TiO2. *Journal of Environmental Chemical Engineering*.

Dhaka, S., Kumar, R., Lee, S. hun, Kurade, M.B., and Jeon, B.H., 2018. Degradation of ethyl paraben in aqueous medium using advanced oxidation processes: Efficiency evaluation of UV-C supported oxidants. *Journal of Cleaner Production*.

F. Hasany, S., Ahmed, I., J, R., and Rehman, A., 2013. Systematic Review of the Preparation Techniques of Iron Oxide Magnetic Nanoparticles. *Nanoscience and Nanotechnology*.

Fazal, T., Razzaq, A., Javed, F., Hafeez, A., Rashid, N., Amjad, U.S., Ur Rehman, M.S., Faisal, A., and Rehman, F., 2020. Integrating adsorption and photocatalysis: A cost effective strategy for textile wastewater treatment using hybrid biochar-TiO2 composite. *Journal of Hazardous Materials*, 390 (May 2019), 121623.

Gaur, N., Narasimhulu, K., and PydiSetty, Y., 2018. Recent advances in the bio-remediation of persistent organic pollutants and its effect on environment. *Journal of Cleaner Production*, 198, 1602–1631.

Hama Aziz, K.H., Miessner, H., Mueller, S., Kalass, D., Moeller, D., Khorshid, I., and Rashid, M.A.M., 2017. Degradation of pharmaceutical diclofenac and ibuprofen in aqueous solution, a direct comparison of ozonation, photocatalysis, and non-thermal plasma. *Chemical Engineering Journal*.

Han, F., Kambala, V.S.R., Srinivasan, M., Rajarathnam, D., and Naidu, R., 2009. Tailored titanium dioxide photocatalysts for the degradation of organic dyes in wastewater treatment: A review. *Applied Catalysis A: General*.

Hanaor, D., Michelazzi, M., Chenu, J., Leonelli, C., and Sorrell, C.C., 2011. The effects of firing conditions on the properties of electrophoretically deposited titanium dioxide films on graphite substrates. *Journal of the European Ceramic Society*.

Hantusch, M., Bessergenev, V., Mateus, M.C., Knupfer, M., and Burkel, E., 2018. Electronic properties of photocatalytic improved Degussa P25 titanium dioxide powder. *Catalysis Today*, 307 (October 2017), 111–118.

Haque, F.Z., Nandanwar, R., and Singh, P., 2017. Evaluating photodegradation properties of

anatase and rutile TiO2 nanoparticles for organic compounds. *Optik*, 128, 191–200.

Heponiemi, A. and Lassi, U., 2012. Advanced Oxidation Processes in Food Industry Wastewater Treatment – A Review. *In*: *Food Industrial Processes - Methods and Equipment*.

Horikoshi, S. and Serpone, N., 2020. Can the photocatalyst TiO2 be incorporated into a wastewater treatment method? Background and prospects. *Catalysis Today*, 340 (August 2018), 334–346.

Hou, L., Wang, L., Royer, S., and Zhang, H., 2016. Ultrasound-assisted heterogeneous Fenton-like degradation of tetracycline over a magnetite catalyst. *Journal of Hazardous Materials*, 302, 458–467.

Hou, Y., Lu, Q., Wang, H., Li, H., Zhang, Y., and Zhang, S., 2016. One-pot electrochemical synthesis of carbon dots/TiO2 nanocomposites with excellent visible light photocatalytic activity. *Materials Letters*, 173, 13–17.

Huang, Y., Liang, Y., Rao, Y., Zhu, D., Cao, J.J., Shen, Z., Ho, W., and Lee, S.C., 2017. Environment-Friendly Carbon Quantum Dots/ZnFe2O4 Photocatalysts: Characterization, Biocompatibility, and Mechanisms for NO Removal. *Environmental Science and Technology*, 51 (5), 2924–2933.

Jia, J., Li, D., Wan, J., and Yu, X., 2016. Characterization and mechanism analysis of graphite/C-doped TiO2 composite for enhanced photocatalytic performance. *Journal of Industrial and Engineering Chemistry*, 33, 162–169.

Kalantari, K., Kalbasi, M., Sohrabi, M., and Royaee, S.J., 2016. Synthesis and characterization of N-doped TiO2 nanoparticles and their application in photocatalytic oxidation of dibenzothiophene under visible light. *Ceramics International*, 42 (13), 14834–14842.

Kalantari, K., Kalbasi, M., Sohrabi, M., and Royaee, S.J., 2017. crossmark, 43 (August 2016), 973–981.

Karci, A., Arslan-Alaton, I., Olmez-Hanci, T., and Bekbölet, M., 2012. Transformation of 2,4-dichlorophenol by H 2O 2/UV-C, Fenton and photo-Fenton processes: Oxidation products and toxicity evolution. *Journal of Photochemistry and Photobiology A:*

Chemistry.

Khairy, M. and Zakaria, W., 2014. Effect of metal-doping of TiO2 nanoparticles on their photocatalytic activities toward removal of organic dyes. *Egyptian Journal of Petroleum*, 23 (4), 419–426.

Khalid, N.R., Majid, A., Tahir, M.B., Niaz, N.A., and Khalid, S., 2017. Carbonaceous-TiO2 nanomaterials for photocatalytic degradation of pollutants: A review. *Ceramics International*, 43 (17), 14552–14571.

Khan, S.B., Hou, M., Shuang, S., and Zhang, Z., 2017. Morphological influence of TiO 2 nanostructures (nanozigzag, nanohelics and nanorod) on photocatalytic degradation of organic dyes. *Applied Surface Science*, 400, 184–193.

Khodadadi, M., Ehrampoush, M.H., Ghaneian, M.T., Allahresani, A., and Mahvi, A.H., 2018. Synthesis and characterizations of FeNi3@SiO2@TiO2 nanocomposite and its application in photo- catalytic degradation of tetracycline in simulated wastewater. *Journal of Molecular Liquids*, 255, 224–232.

Kim, H., Jin, C., Park, S., Lee, W.I., Chin, I.J., and Lee, C., 2013. Structure and optical properties of Bi2S3 and Bi2O3 nanostructures synthesized via thermal evaporation and thermal oxidation routes. *Chemical Engineering Journal*.

Kommineni, S., Zoeckler, J., Stocking, A., Liang, S., Flores, A., Kavanaugh, M., Rodriguez, R., Browne, T., Roberts, R., Brown, A., and Stocking, A., 2000. *Advanced Oxidation Processes: Literature Review, Removal of Methyl Tertiary Butyl Ether (MTBE) from Drinking Water: Air Stripping, Advanced Oxidation Process, Granular Activated Carbon, Synthetic Resin Sorbents*. National Water Research Institute.

Krishnan, S., Chandran, K., and Sinnathambi, C.M., 2016. Wastewater treatment technologies used for the removal of different surfactants: A comparative review. *International Journal of Applied Chemistry*.

Kumar, S., Sharma, S., Sood, S., Umar, A., and Kansal, S.K., 2016. Bismuth sulfide (Bi2S3) nanotubes decorated TiO2 nanoparticles heterojunction assembly for enhanced solar light driven photocatalytic activity. *Ceramics International*, 42 (15), 17551–17557.

Li, Z., Guo, C., Lyu, J., Hu, Z., and Ge, M., 2019. Tetracycline degradation by persulfate

activated with magnetic Cu/CuFe2O4 composite: Efficiency, stability, mechanism and degradation pathway. *Journal of Hazardous Materials*, 373 (March), 85–96.

Lin, C.C., Ho, J.M., and Wu, M.S., 2015. Continuous preparation of Fe3O4 nanoparticles using a rotating packed bed: Dependence of size and magnetic property on temperature. *Powder Technology*.

Liu, C., Li, Y., Wei, L., Wu, C., Chen, Y., Mei, L., and Jiao, J., 2014. CdS quantum dot-sensitized solar cells based on nano-branched TiO2 arrays. *Nanoscale Research Letters*.

Lu, J., Wang, Z., Zhang, Y., and Zhou, X., 2013. Hydrothermal synthesis of Bi2S3 nanorods from a single-source precursor and their promotional effect on the photocatalysis of TiO2. *Journal of Nanomaterials*.

Mahshid, S., Askari, M., Sasani Ghamsari, M., Afshar, N., and Lahuti, S., 2009. Mixed-phase TiO2 nanoparticles preparation using sol-gel method. *Journal of Alloys and Compounds*.

Martins, A.C., Cazetta, A.L., Pezoti, O., Souza, J.R.B., Zhang, T., Pilau, E.J., Asefa, T., and Almeida, V.C., 2017. Sol-gel synthesis of new TiO2/activated carbon photocatalyst and its application for degradation of tetracycline. *Ceramics International*, 43 (5), 4411–4418.

Martins, N.C.T., Ângelo, J., Girão, A.V., Trindade, T., Andrade, L., and Mendes, A., 2016. N-doped carbon quantum dots/TiO2 composite with improved photocatalytic activity. *Applied Catalysis B: Environmental*, 193, 67–74.

Matongo, S., Birungi, G., Moodley, B., and Ndungu, P., 2015. Pharmaceutical residues in water and sediment of Msunduzi River, KwaZulu-Natal, South Africa. *Chemosphere*, 134, 133–140.

Matsuzawa, S., Tanaka, J., Sato, S., and Ibusuki, T., 2002. Photocatalytic oxidation of dibenzothiophenes in acetonitrile using TiO2: Effect of hydrogen peroxide and ultrasound irradiation. *Journal of Photochemistry and Photobiology A: Chemistry*.

Mohamed, M.M., Bayoumy, W.A., Goher, M.E., Abdo, M.H., and Mansour El-Ashkar, T.Y., 2017. Optimization of α-Fe 2 O 3 @Fe 3 O 4 incorporated N-TiO 2 as super effective photocatalysts under visible light irradiation. *Applied Surface Science*, 412, 668–682.

Muruganandham, M., Suri, R.P.S., Jafari, S., Sillanpää, M., Lee, G.J., Wu, J.J., and Swaminathan, M., 2014. Recent developments in homogeneous advanced oxidation processes for water and wastewater treatment. *International Journal of Photoenergy*.

Oseghe, E.O. and Ofomaja, A.E., 2018a. Study on light emission diode/carbon modified TiO2 system for tetracycline hydrochloride degradation. *Journal of Photochemistry and Photobiology A: Chemistry*, 360 (April), 242–248.

Oseghe, E.O. and Ofomaja, A.E., 2018b. Facile microwave synthesis of pine cone derived C-doped TiO2 for the photodegradation of tetracycline hydrochloride under visible-LED light. *Journal of Environmental Management*, 223 (July), 860–867.

Panneerselvam, P., Morad, N., and Tan, K.A., 2011. Magnetic nanoparticle (F3O4) impregnated onto tea waste for the removal of nickel(II) from aqueous solution. *Journal of Hazardous Materials*, 186 (1), 160–168.

Park, Y., Kim, W., Park, H., Tachikawa, T., Majima, T., and Choi, W., 2009. Carbon-doped TiO2 photocatalyst synthesized without using an external carbon precursor and the visible light activity. *Applied Catalysis B: Environmental*.

Ren, Y.N., Xu, W., Si, Z.X., Zhou, L.X., and Zheng, Y.Q., 2018. Photocatalytic degradation of tetracycline antibiotics under visible light using uranyl isophthalate coordination polymers. *Polyhedron*, 152, 195–201.

Rimoldi, L., Meroni, D., Cappelletti, G., and Ardizzone, S., 2017. Green and low cost tetracycline degradation processes by nanometric and immobilized TiO2 systems. *Catalysis Today*, 281, 38–44.

Sadeghi-Niaraki, S., Ghasemi, B., adeh, A.H., Ghasemi, E., and Ghahari, M., 2019. Preparation of (Fe,Cr)2O3@TiO2 cool pigments for energy saving applications. *Journal of Alloys and Compounds*, 779, 367–379.

Sadeghi-Niaraki, S., Ghasemi, B., Habibolahzadeh, A., Ghasemi, E., and Ghahari, M., 2019. Nanostructured Fe2O3@TiO2 pigments with improved NIR reflectance and photocatalytic ability. *Materials Chemistry and Physics*, 235 (May), 121769.

Safari, G.H., Hoseini, M., Seyedsalehi, M., Kamani, H., Jaafari, J., and Mahvi, A.H., 2014. Photocatalytic degradation of tetracycline using nanosized titanium dioxide in aqueous

solution. *International Journal of Environmental Science and Technology*, 12 (2), 603–616.

Saitoh, T., Shibata, K., and Hiraide, M., 2014. Rapid removal and photodegradation of tetracycline in water by surfactant-assisted coagulation-sedimentation method. *Journal of Environmental Chemical Engineering*, 2 (3), 1852–1858.

Shao, S., Hu, Y., Cheng, C., Cheng, J., and Chen, Y., 2018. Simultaneous degradation of tetracycline and denitrification by a novel bacterium, Klebsiella sp. SQY5. *Chemosphere*, 209, 35–43.

Sharma, S., Dutta, V., Singh, P., Raizada, P., Rahmani-Sani, A., Hosseini-Bandegharaei, A., and Thakur, V.K., 2019. Carbon quantum dot supported semiconductor photocatalysts for efficient degradation of organic pollutants in water: A review. *Journal of Cleaner Production*, 228, 755–769.

Sharma, S., Umar, A., Sood, S., Mehta, S.K., and Kansal, S.K., 2018. Photoluminescent C-dots: An overview on the recent development in the synthesis, physiochemical properties and potential applications. *Journal of Alloys and Compounds*, 748, 818–853.

Shen, G.R., Cheng, Y.T., and Tsai, L.N., 2005. Synthesis and characterization of Ni-P-CNT's nanocomposite film for MEMS applications. *IEEE Transactions on Nanotechnology*.

Shen, T., Wang, Q., Guo, Z., Kuang, J., and Cao, W., 2018. Hydrothermal synthesis of carbon quantum dots using different precursors and their combination with TiO2 for enhanced photocatalytic activity. *Ceramics International*, 44 (10), 11828–11834.

Sobczyński, A., Duczmal, L., and Zmudziński, W., 2004. Phenol destruction by photocatalysis on TiO2: An attempt to solve the reaction mechanism. *Journal of Molecular Catalysis A: Chemical*.

Song, Z., Ma, Y.L., and Li, C.E., 2019. The residual tetracycline in pharmaceutical wastewater was effectively removed by using MnO2/graphene nanocomposite. *Science of the Total Environment*, 651, 580–590.

Sun, D., Cao, Y., Xu, Y., Zhang, G., and Sun, Y., 2016. Tunable synthesis of core-shell α-Fe2O3/TiO2 composite nanoparticles and their visible-light photocatalytic activity. *Chemical Research in Chinese Universities*.

Tomić, N., Grujić-Brojčin, M., Finčur, N., Abramović, B., Simović, B., Krstić, J., Matović, B., and Šćepanović, M., 2015. Photocatalytic degradation of alprazolam in water suspension of brookite type TiO2 nanopowders prepared using hydrothermal route. *Materials Chemistry and Physics*.

Totito, T.C., 2013. Photocatalytic activity of supported TiO 2 nanocrystals, (November), 1–153.

Tran, M.H. and Jeong, H.K., 2018. Modification of titanium dioxide by solution plasma. *Journal of Physics and Chemistry of Solids*, 121 (April), 292–297.

Tseng, Y.H., Kuo, C.S., Huang, C.H., Li, Y.Y., Chou, P.W., Cheng, C.L., and Wong, M.S., 2006. Visible-light-responsive nano-TiO2 with mixed crystal lattice and its photocatalytic activity. *Nanotechnology*.

Wang, D., Xiao, L., Luo, Q., Li, X., An, J., and Duan, Y., 2011. Highly efficient visible light TiO2 photocatalyst prepared by sol-gel method at temperatures lower than 300°C. *Journal of Hazardous Materials*, 192 (1), 150–159.

Wang, J.Y., Yu, J.X., Liu, Z.H., He, Z.K., and Cai, R.X., 2005. A simple new way to prepare anatase TiO2 hydrosol with high photocatalytic activity. *Semiconductor Science and Technology*.

Wang, Q., Zheng, H., Long, Y., Zhang, L., Gao, M., and Bai, W., 2011. Microwave-hydrothermal synthesis of fluorescent carbon dots from graphite oxide. *Carbon*.

Wu, M.C., Huang, W.K., Lin, T.H., and Lu, Y.J., 2019. Photocatalytic hydrogen production and photodegradation of organic dyes of hydrogenated TiO 2 nanofibers decorated metal nanoparticles. *Applied Surface Science*, 469 (August 2018), 34–43.

Wu, Q. and Zhang, Z., 2019. The fabrication of magnetic recyclable nitrogen modified titanium dioxide/strontium ferrite/diatomite heterojunction nanocomposite for enhanced visible-light-driven photodegradation of tetracycline. *International Journal of Hydrogen Energy*, 44 (16), 8261–8272.

Xu, D., Xiao, Y., Pan, H., and Mei, Y., 2019. Toxic effects of tetracycline and its degradation products on freshwater green algae. *Ecotoxicology and Environmental Safety*, 174 (December 2018), 43–47.

Yang, L., Sun, W., Luo, S., and Luo, Y., 2014. White fungus-like mesoporous Bi2S3 ball/TiO2 heterojunction with high photocatalytic efficiency in purifying 2,4-dichlorophenoxyacetic acid/Cr(VI) contaminated water. *Applied Catalysis B: Environmental*.

Yu, Y., Yu, J.C., Yu, J.G., Kwok, Y.C., Che, Y.K., Zhao, J.C., Ding, L., Ge, W.K., and Wong, P.K., 2005. Enhancement of photocatalytic activity of mesoporous TiO2 by using carbon nanotubes. *Applied Catalysis A: General*, 289 (2), 186–196.

Zhang, B., Maimaiti, H., Zhang, D.D., Xu, B., and Wei, M., 2017. Preparation of coal-based C-Dots/TiO2 and its visible-light photocatalytic characteristics for degradation of pulping black liquor. *Journal of Photochemistry and Photobiology A: Chemistry*, 345, 54–62.

Zhang, J., Kuang, M., Wang, J., Liu, R., Xie, S., and Ji, Z., 2019. Fabrication of carbon quantum dots/TiO2/Fe2O3 composites and enhancement of photocatalytic activity under visible light. *Chemical Physics Letters*, 730 (May), 391–398.

Zheng, X., Fu, W., Kang, F., Peng, H., and Wen, J., 2018. Enhanced photo-Fenton degradation of tetracycline using TiO2-coated α-Fe2O3 core–shell heterojunction. *Journal of Industrial and Engineering Chemistry*, 68, 14–23.

Zhu, J., Chen, F., Zhang, J., Chen, H., and Anpo, M., 2006. Fe3+-TiO2 photocatalysts prepared by combining sol-gel method with hydrothermal treatment and their characterization. *Journal of Photochemistry and Photobiology A: Chemistry*, 180 (1–2), 196–204.

Zhu, Z., Cai, H., and Sun, D.W., 2018. Titanium dioxide (TiO2) photocatalysis technology for nonthermal inactivation of microorganisms in foods. *Trends in Food Science and Technology*, 75 (February), 23–35.

Chapter 2 LITERATURE REVIEW

2.1 Background

The increasing rate of environmental pollution without a methodical solution has become one of the centres of scientific attention for human health with intense industrial development (Zhang *et al.* 2019). One of the top ten problems that humanity is facing in the world is water pollution. Water pollution has become increasingly worse, with the development of industrialized production and increase in population (Sharma *et al.* 2019). The adverse effects of toxic pollutants in water bodies have drawn global consideration. The dumping of chemicals has led to contamination of lakes, rivers, oceans and groundwater aquifers. Lately, a serious threat to the environment is the textile dyeing industry which is releasing non-biodegradable organic pollutants into the ecosystem. The key issue for recycling of wastewater is the effective removal of hazardous contaminants (Gaur *et al.* 2018). Interestingly, Advanced Oxidation Processes (AOPs) is the latest technology employed in the removal of these resistant and recalcitrant pollutants from water and wastewater (Cao *et al.* 2016). In South Africa so many antibiotics for pharmaceuticals which are drugs have been found in the environment such as caffeine, tetracycline and carbamazepine. The next section discuss some salient point about tetracycline in wastewater.

2.1.1 Tetracycline

Every year, the number of consumers and variety of drugs increase and as a result antibiotics and drug compounds are continuously and rapidly being produced and consumed in large quantities (Shao *et al.* 2018). The average annual consumption of pharmaceuticals is 15 g per person in the industrialized countries, although this is increasing and anticipated to reach 50-150 g (Awfa *et al.* 2018). Antibiotics are one of the major pharmaceutical products widely used for veterinary and medical purposes (Khodadadi *et al.* 2018). The annual consumption of antibiotics in the world is estimated to be 100 000- 200 000 tonnes (Matongo *et al.* 2015). After consumption, such antibiotics are not completely metabolized in bodies and 30-90% of them remain active after expulsion from the body of the user (Cao *et al.* 2016). Hence, it can

be concluded that at best 30 000 tonnes and at worst 180 000 tonnes of active antibiotics are entering the environment per year (Khodadadi *et al.* 2018). Based on environmental conditions these have a relatively long-life of about 180 days in the environment (Khodadadi *et al.* 2018). As a result, the increased use of these compounds affects both human health and the environment (Saitoh *et al.* 2014).

The second largest group of antibiotics in the world are tetracyclines (TCs), in terms of production and consumption, and they account for almost 29% of all antibiotics consumed (Safari *et al.* 2014). TCs are obtained via natural fermentation of fungi or through semi-synthetic processes and are classified as arising micro-pollutants since their collection in the environment can influence long-term effects such as endocrine disruption, antibiotic resistance and toxicity on living organisms (Rimoldi *et al.* 2017). TCs are being used repetitively for humans, livestock and agricultural purposes and are effective against many microorganisms. TC is the most used antibiotic for humans and animals but is not fully absorbed only (50-80%) is absorbed (Khodadadi *et al.* 2018). The non-absorbed tetracycline, on active non-metabolized compounds, is expelled into household or livestock sewage and eventually finds its way to the environment to pollute water resources. TC concentrations of 5.4–9.3 ng/L have been measured in surface water resources and underground water resources. TC was measured in the range 0.8-6.8 µg/L, in samples from Nanming River in China. TCs' presence in water and soils samples can cause some sensitivities and toxicity, due to the sustained activity of TC (Song *et al.* 2019).

Furthermore, the presence of antibiotics in the environment can affect different species of bacteria and cause increase in their resistance. Long-term exposure to antibiotics even in small amounts can lead to microbial resistance (Khodadadi *et al.* 2018). TC affects the kidneys and nervous system in the human body and in many cases also affects spermatogenesis (Khodadadi *et al.* 2018). Furthermore, it also has mutagenic and teratogenic effects. The molecular formula for tetracycline is $C_{22}N_{24}N_2O_8$ and the structure is given in Fig. 2.1 (Cao *et al.* 2016). Traces of tetracycline and its metabolites have been found in many different environments, due to their extensive use over the years; more and more residues of pharmaceuticals antibiotics have been detected in the environmental sample like wastewaters, drinking water and soils leading to the human health and ecological damages (Zheng *et al.* 2018). Furthermore, due to their physicochemical properties, these antibiotics are mostly excreted after use in the pristine un-metabolized form since they are difficult to be

metabolized completely and their residues are expelled through urine and faeces to the environment (Cao *et al.* 2016). Tetracyclines and other antibiotics have been proven to be a modern group of potential pollutants, which may be chronically toxic to humans and animals, disrupt indigenous microbial populations and domesticate multi-resistant bacterial strains (Cao *et al.* 2016). To prevent adverse effects of TC, it should be removed from aquatic environments using specific methods.

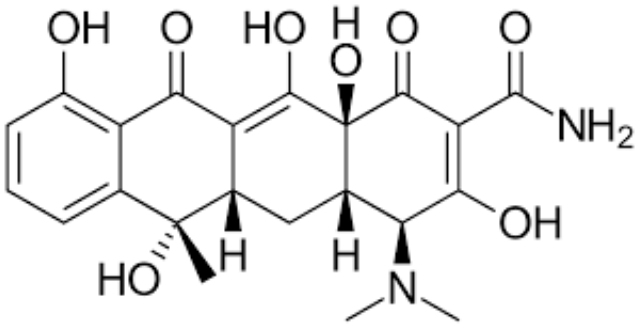

Figure 2. 1: The molecular structure of tetracycline.

2.1.2 Wastewater Treatment

For antibiotics such as tetracycline, the conventional biological treatments employed in wastewater are not efficient to decompose, due to their bactericide's properties; making it very important to explore new cost-effective technologies for their effective treatments (Martins *et al.* 2017). Several new alternative treatments for tetracycline are being considered, in this regard, including direct anodic oxidation, electro-degradation, ozonation adsorption and photocatalysis.

2.1.3 Advanced Oxidation Processes (AOPs)

Recently, advanced oxidation processes (AOPs) with their capability in the degradation of a wide range of organic chemicals have drawn attention in treating wastewater and it has been proven as suitable alternatives for rapid degradation of recalcitrant and non-biodegradable compounds in water (Sharma *et al.* 2019). The wastewater treatment methodology depends on the type and concentration of contaminants present, level of pollutants allowed in the discharge, volume of the wastewater to be treated and treatment procedure cost. There are several organic pollutants which are not easily degradable such as effluent from chemical, agrochemical, pharmaceutical, cosmetic and pulp, and paper industry. Therefore, conventional wastewater treatment plants are not sufficient to remove these class of pollutants to desirable level.

Various physical, chemical and biological treatment methods have been applied for wastewater treatment. However, these methods have several disadvantages and cannot be implemented for large scale treatment as disposing large amounts of chemical sludge make this treatment process inefficient. For instance, sludge formation occurs while coagulation and flocculation via chemicals generates large amounts of sludge and chemicals which contain hazardous materials in precipitation methods. Adsorption processes have been widely used for the treatment of various pollutants present in wastewater but the major drawback in adsorption process is the contaminant is only adsorbent regularly, resulting in additional cost. Technologies such as reverse osmosis, nanofiltration and ultrafiltration have been used for full scale treatment and reuse of water and chemicals. These methods have several operational difficulties in addition to high cost. Therefore, for complete removal of contaminants from the environment, physical methods may not be suitable (Krishnan *et al.* 2016). Similarly, aerobic and anaerobic biological wastewater treatment methods have been employed but these methods also do not completely remove the high concentration of organic contaminants present in the wastewater (Khan *et al.* 2017). In addition, chemical methods such as the oxidation process are effective and relevant to large scale wastewater treatment. Generally, chemical treatment methods use air, oxygen, ozone and oxidants (NaOCl and H_2O_2). Basic chemical oxidation process occurs with air and oxygen but for highly polluted wastewater it is no longer sufficient. Therefore, there is a need for a simple, cost-effective and eco-friendly method which can effectively treat wastewater (Wu *et al.* 2019). AOPs work

on the principle of hydroxyl radicals ($HO^{\bullet}$) production. Hydroxyl radicals can be produced from ozone, hydrogen peroxide (H_2O_2), oxidants or photo-catalysis in combination with ultraviolet (UV) radiation.

AOPs like ozonation (O_3), ozone combined with H_2O_2 and UV irradiation or both, O_3 combined with catalysts, UV/H_2O_2, Fenton and photo Fenton processes; and in all processes ($HO^{\bullet}$) is primarily responsible for the organic pollutant degradation in some cases. $HO^{\bullet}$ being a random strong chemical oxidant, on production, attacks nearly all organic contaminants and breaks them completely. As a result, the concentration of organic pollutants decreases from a few hundred ppm to less than 5 ppb. Organic radical ($^{\bullet}R$) is formed when $HO^{\bullet}$ takes away the hydrogen atom from an organic compound (R-H) as in equation (1). Later $^{\bullet}R$ forms several products and by-products through several successive chemical reactions.

$$R - H + HO^{\cdot} \rightarrow H_2O + R \quad \text{..... (1)}$$

2.1.3.1 Ozonation

When ozone is added to water then $HO^{\bullet}$ and superoxide radical ($O_2^{\bullet -}$) are formed through a complex series of reactions. At higher pH, the disintegration of ozone is better in water. The performance of the process can be determined by close of ozone, alkalinity of water and contact time. Oxidants of organic species occur when combination of reaction with molecular ozone and reactions with $HO^{\bullet}$ takes place (equation (2)) (Krishnan *et al.* 2016).

$$3O_2 + OH^- \rightarrow 2HO^{\cdot} + 4O_2 \quad \text{..... (2)}$$

Degradation of the organic compounds can be facilitated by the addition of H_2O_2 in the decomposition of ozone which leads to the formation of $HO^{\bullet}$. In water, H_2O_2 partially dissociates to produce hydroperoxide ion which rapidly reacts with ozone to produce $HO^{\bullet}$ (equation (3)).

$$2O_3 + H_2O_2 \rightarrow 2HO^{\cdot} + O^{\cdot} + 3O_2 \quad \text{..... (3)}$$

The ozonation process can be speed up using homogeneous or heterogeneous catalysts. The concentration of ozone in inlet gas and the ozonation time are the predominant factors for the enhancement of the degradation rate. The oxidation of various contaminants can be studied using Fe_2O_3, MnO_2, TiO_2-Me, Fe^{2+}, Fe^{3+} and Mn^{2+}. The ozone/catalyst system appears to be more effective as compared to the oxidation with ozone alone at higher pH for the reduction of COD and TOC. Bokare and Choi (2014) studied the application of the synergistic effects of various AOPs in wastewater treatment and they observed that decomposition of the Acid Orange 7, Hydrocortisone and Verampil hydrochloride were strongly improved by synergistic effect of photocatalytic reactions occurring on TiO_2 photocatalyst (Bokare and Choi 2014). When ozone decomposes readily and generates hydrogen peroxide (equation (4) and equation (5)) as an intermediate by absorbing UV radiation (λ = 254 nm) ozonation process can be speed up, which finally decomposes to $HO^{\bullet}$ as it comprises H_2O_2/O_3, H_2O_2/UV and O_3/UV as compared to O_3 or UV alone (Krishnan *et al.* 2016).

$$O_3 + H_2O + hv \rightarrow O_2 + H_2O_2 \;\; at\; hv < 300\; nm \quad \text{..... (4)}$$

$$2O_3 + H_2O_2 \rightarrow 2HO^{\cdot} + 3O_2 \quad \text{..... (5)}$$

Ozone technology has been used in petroleum refineries, textile industries, pharmaceutical industries, food industry, pulp and paper industry, cosmetic industry, distilleries, olive mill and electronic chip manufacturing to treat pollutants present in wastewater (Bakre *et al.* 2016).

2.1.3.2 Hydrogen peroxide

The photolytic dissociation of hydrogen peroxide in water forms the hydroxyl radicals by UV irradiation at a wavelength of 254 nm (equation 6). Studied conducted revealed that the rate of photolysis of aqueous hydrogen peroxide is directly proportional to alkaline pH (Safari *et al.* 2014). The efficiency of the UV/Ozone system can be reduced as interfering compounds and turbidity absorbs the UV light.

$$H_2O + hv \rightarrow 2HO^{\cdot} \quad at\ hv < 300\ nm \quad \text{..... (6)}$$

UV/H_2O_2 systems have several advantages like high reaction rate, flexibility in the design of reactor, use of UV lamps (provides disinfection of the water), low cost and easy availability of hydrogen peroxide which leads to lesser footprint in the treatment plant. Apart from these, AOP has some drawbacks such as bromate formation that hinders this process (reduced by lowering pH and increasing peroxide to ozone ratio), hydrogen peroxide has poor UV absorption characteristics, etc. UV/H_2O_2 methods have been used for the treatment of phenolic complexes present in olive mill wastewater. In addition, in textile industry, UV/H_2O_2 method has been used for the removal of dyes and it was found that increase in UV dosage and H_2O_2 concentration increases the rate of decolorization (Muruganandham *et al.* 2014).

2.1.3.3 Fenton's reagent, Fenton-like and Photo-Fenton processes

Radicals are produced where Fe^{2+} ions act as a catalyst and where iron (II) reacts with hydrogen peroxide for this reaction. Fenton's process is a simple method that takes place at ambient temperature and pressure and does not require any special apparatus or chemicals to produce $HO^{\bullet}$. This method is an attractive way for oxidation as hydrogen peroxide and iron salts are readily available, easy to handle and environmentally safe. The destruction of organic compounds takes places by reacting with the $HO^{\bullet}$ (equation 7):

$$Fe^{2+} + H_2O_2 \rightarrow Fe^{3+} + OH^- + HO\cdot \text{..... (7)}$$

The rate of degradation of organic pollutants with Fenton-Fenton like reagents strongly accelerates irradiation with UV-Vis light at wavelengths greater than 300 nm. Fe^{2+} is generated by the photolysis of Fe^{3+} complexes. The occurrence of Fenton reactions in the presence of hydrogen peroxide is shown in (equation 8) (Karci *et al.* 2012).

$$Fe^{2+} + h\gamma \rightarrow Fe^{3+} + OH^- + HO\cdot \text{ ..... (8)}$$

This process is initiated by the production of hydroxyl radical for the degradation of organic compounds, primarily by oxidation reactions, similar to other AOPs. However, to prevent precipitation of the iron, the Fenton process is accurate and requires pH control. A reactor helps to facilitate the proper mixing of the Fe (II) and H_2O_2. Optimal hydroxyl radical formation and degradation of the contaminants is achieved by the Fenton processes method. The cost of using this system would possibly be raised by the extraction of iron from the effluent water during the process.

Chromium and copper are elements with several redox states that can be used to decompose H_2O_2 into $HO^{\bullet}$ through conventional ways for fenton-like processes. However, each non-ferrous catalyst in the Fenton like system could counterbalance the practical gains of better catalyst stability and working at neutral pH. Hence, the activation process for H_2O_2 is influenced by the composition of the catalyst and is specific to its nature (Bokare and Choi 2014). Toxic compounds such as phenols and herbicides in wastewater can be degraded by this method. However, to keep the low pH value the maintenance and operation cost increases because of change requirement from this system. The advanced oxidation pre-treatment using Fenton reagent has been found to be very effective, for enhancing the biodegradability of wastewater containing surfactants.

The Fenton, Photo-Fenton and Fenton-like methods are popular methods for AOP due to their flexibility, simplicity and integration into existing water remediation process such as

coagulation (Bokare and Choi 2014). Due to a rapid reaction between iron and H_2O_2, $HO^{\bullet}$ are generated in the shortest time compared to other AOPs, as well. This method shows high elimination for the degradation of linear alkyl benzene sulfonate (ABS) surfactants (Hou, Wang, *et al.* 2016). One major drawback of using the Fenton process is the production of sludge that contains iron hydroxide as a by-product. Large quantities of flocs of various sizes have been observed during several studies conducted (Bokare and Choi 2014). The disposal of the sludge formed must be included when estimating the cost of this process. Nonetheless, this method has been found as an effective method for the removal of the flocs, as well as COD. Until now, Fenton and Photo-Fenton processes have been used to treat effluents from dye and chemical manufacturing, pulp bleaching and agricultural processing. In addition to this, Fenton pretreatment can be used to improve biological wastewater treatment. In terms of operating expenses for the treatment of toxic and industrial wastewater, Fenton's reaction has exhibited to be more efficient as it has been considered as easy to handle (Heponiemi and Lassi 2012).

2.1.3.4 Titanium dioxide (TiO_2)

Heterogeneous photocatalysis using titanium dioxide (TiO_2) is an efficient and advanced method for oxidation in the industrial effluent treatment process. When the TiO_2 is illuminated by UV, a conduction band of electrons (ecb) and valence band holes (h^+) (equation 9) are generated. When these band electrons interact with surface adsorbed oxygen, superoxide radical's anions are produced (equation 10). Hydroxyl radicals are produced when band holes interact with water (equation 11).

$$TiO_2 + hv \rightarrow ecb + h^+ \quad \text{..... (9)}$$

$$ecb + O_2 \rightarrow O_2^{-\cdot} \quad \text{..... (10)}$$

$$h^+ + H_2O \rightarrow H^+ + HO^{\cdot} \quad \text{..... (11)}$$

Many organic complexes can be degraded by oxidation (Ren *et al.* 2018); it has been shown in the presence of UV/TiO_2. In AOP, the degradation of organic compounds takes place by reacting with the hydroxyl radicals with the rest of the process. Also, because TiO_2 nanoparticles are non-toxic, chemically and biologically inert and inexpensive (Fazal *et al.* 2020) they are deemed suitable for wastewater treatment. In addition, TiO_2 has a comparatively higher oxidative power as compared to other oxidizing species. Suspended TiO_2 particles were used in most of the studies that relate to the photocatalytic oxidation of contaminants. Recycling and recovery of these nanoparticles becomes cumbersome and expensive; this is a disadvantage of using suspended systems. This results in the requirement for employing new methods for using immobilized TiO_2 to create systems with an immobilized active phase. Different techniques to generate immobilized TiO_2 have been studied for the photodegradation of surfactants present in produced water using white plaster cement.

Photocatalytic oxidation is considered a developing technology since there aren't many industrial applications of the process. Though, many studies indicate successful use of the photocatalytic process in the treatment of effluents from winery and distillery, olive mill, dairy industry, molasses, candy and sugar industry, fresh-cut vegetable industry, etc (Zhu *et al.* 2018). For decreasing counts of bacteria, moulds and yeasts photocatalysis was found to be effective. Kommineni *et al.* (2000) studied the Hydroxyl Systems Incorporated and stipulated the costs for TiO_2/UV AOP system. The estimated cost is averagely $ 1.01 for a flow 1380 m^3/h at 2000 µg/L per 3.79 m^3 of treated water. Compared to the other processes, this system appears to be the least cost effective (Kommineni *et al.* 2000). Table 1.1 shows the typical findings observed in the degradation of various organic pollutants by using AOPs.

Table 1.1: Typical findings observed in the degradation of organic pollutants by using AOPS

Pollutants	Initial Concentration	Experimental setup		Conclusion
		AOPs applied	Optimum conditions	
Carbamazepine and Trimethoprim	-	-	-	UV H_2O_2 = TMP and CBZ degradation up to 91.2 and 99.7% respectively, DCF and SMX were completely degraded. (Kommineni *et al.* 2000)
Diclofenac (DCF) and ibuprofen	50 mg/L	Ozonation, photocatalysis and non-thermal plasma	Ozone generator = 130± 5 mg/L ozone gas at a power of 30W and an oxygen gas flow rate of 10 L/h, pH 5.6 (DCF), 5.7 (IBP)	Direct ozonation in darkness (effective in DCF degradation) possesses the highest energy yield of 28 g/kWh but it was not effective for IBP (2.5 g/kWh) (Hama Aziz *et al.* 2017)
Methyl paraben (MP)	32.8 µM	UV/persulfate	Low-pressure mercury UV lamps = 254 nm, pH 6.5, room temperature, persulfate = 1 mM	98.9% of MP was removed within 90 min using the UV/persulfate, TOC removal -53% (Dhaka *et al.* 2018)
Methylparaben, Ethylparaben, Propylparaben, Butylparaben	5 ppm	O_3/Fenton, O_3/H_2O_2, O_3/UV, O_3/UV/ H_2O_2, O_3/photo-Fenton, O_3/UV/TiO_2, and O_3/UV/TiO_2/ H_2O_2	pH 8 and T- 20 ˚C, for O_3/Fenton and O_3/photo-Fenton systems, pH 3.5.	Ozonation process = 94.85-99.22% removal of four parabens, O_3/UV/TiO_2/H_2O_2 – most effective method (Cuerda-Correa *et al.* 2016)

2.1.4 TiO_2 as a photocatalyst

Compared with other photocatalysts, anatase TiO_2 is well-known as the most popular material for environment and energy applications due to its superior photocatalytic ability (Hou, Lu, *et al.* 2016). For the degradation of organic contaminants in water and air TiO_2 nanoparticle is an important photocatalyst material because of its high efficiency, inexpensiveness, easy production, photochemical and biological stability and it is friendly to the environment and human beings (Wang, Xiao, *et al.* 2011). Generally, TiO_2 has three polymorphs: anatase and rutile belong to tetragonal and brookite in orthorhombic crystal phase. The formation of a specific phase of TiO_2 has been known from hierarchies in the enthalpy as follows: brookite (0.71 $kJmol^{-1}$), anatase (2.61 kJ mol^{-1}) and rutile (147 kJ mol^{-1}). Therefore, TiO_2 crystal structure has a strong correlation with synthesis temperature, and the crystal structure of anatase in fact can be transformed irreversibly to the stable phase of rutile at an elevated temperature, tending to more compressed unit cells (Tran and Jeong 2018).

Hanaor *et al.* (2011) had reported that fine powders of TiO_2 show the phase transformation at the high temperature from ~600 ˚C to 700 ˚C (Hanaor *et al.* 2011). Anatase TiO_2 has a direct band gap of 3.2 eV while rutile TiO_2 has a smaller indirect optical band gap of 3.0 eV, its photoactivity is restricted in the UV region. As UV rays make just 3-5% of the entire spectrum of the sunlight, considerable attention has recently been given to enhance the absorption of visible light by TiO_2 catalyst with a viewpoint of industrial applications (Kalantari *et al.* 2017). Anatase phase is deemed more active for the photocatalysis based on its surface chemistry. However, it also introduces low quantum efficiency due to fast recombination of photo-generated electrons and holes. Previous reports have revealed that mixed-phase composites of anatase and rutile possess a synergy effect which can enhance the photocatalytic performance of TiO_2. The mixture of brookite, anatase and rutile based on polyethylene glycol and tartaric acid or metal-doped rutile with improved quantum efficiency have been reported for the new method for controlling phase transition which performed photocatalyst activities superior to their pure precursors (Tran and Jeong 2018).

TiO_2 nanoparticles have been most widely used as a photocatalyst because of its strong oxidizing properties for the decomposition of pollutants and organic compounds under UV illumination (Mohamed *et al.* 2017). The photocatalytic properties of TiO_2 are derived from the formation of holes and electrons, which are formed by irradiation of TiO_2 by UV light in

the narrow band gap forming reactive species of $OH^{\bullet}$ and $O_2^{\bullet-}$ (Ahmad *et al.* 2016). Matsuzawa *et al.* (2002) reported the photocatalytic oxidation of DBT and 4,6-dimethyldibenzothiophene using TiO_2 photocatalyst and H_2O_2 as oxidant under UV irradiation. Dedual *et al.* (2014) reported that DBT can be removed from the model fuel using TiO_2 photocatalyst, H_2O_2 and methanol as solvent under UV irradiation (Kalantari *et al.* 2016).

2.1.5 Sol-gel and hydrothermal method

For the preparation of TiO_2-based photocatalysts various methods are available such as electrochemical, continuous reaction, multi-gelation, supercritical carbon dioxide, thin films and spin-coating and SILAR, two-step wet chemical, precipitation, thermal (ethanol thermal, hydrothermal and solvothermal), chemical solvent and chemical vapour decomposition (CSD & CVD), ultrasonic irradiation at extremely low temperature, Aerogel and Xerogel. Nevertheless, the benefits derived from preparing TiO_2 by sol-gel method (Scheme 1), which include synthesis of nanosized crystallized powder of high purity at relatively low temperature, possibility of stoichiometry controlling process, preparation of composite materials and production of homogeneous materials have driven many researchers to use the method in preparing TiO_2 based photocatalysts.

Sol-gel technology has been in existence from as long ago as the mid-1800s and was used almost a century later by Schott Glass Company (Jena, Germany) (Akpan and Hameed 2010). Sol-gel technology finds applications in the development of new materials for catalysis, photo-chronic applications, and solid-state electrochemical devices; and in a diverse range of scientific and engineering fields such as ceramic industry, nuclear industry and electronic industry (Akpan and Hameed 2010). The sol-gel is one of the most exploited methods, it is used mainly to produce thin film and powder catalysts (Akpan and Hameed 2010). Studies revealed that different variants and modifications of the process have been concentrated under stoichiometry-control. Han *et al.* (2009) recently undertook a review on tailored titanium dioxide photocatalysts for the degradation of organic dyes in wastewater treatment (Akpan and Hameed 2010). Reducing reaction times and nanometric particles sizes have been obtained by numerous authors that have studied different synthesis methods for finding the anatase and rutile phases (Archana *et al.* 2019).

The sol-gel method allows the formation of nanostructured materials with controlled porosity and shape as either powders or films. This process provides excellent chemical homogeneity and the possibility of deriving unique metastable structures at low reaction temperatures (Andrade-Guel *et al.* 2018). Mahshid *et al.* (2009) used the sol-gel method to produce titanium oxide with two different polymorphs; it has been reported that water/titanium molar ratio (r) has been employed to control the hydrolysis and condensation of titanium isopropoxide in solution (Andrade-Guel *et al.* 2018).

(Wang *et al.* 2005) reported a simple and novel method for preparing anatase TiO_2 hydrosol with high visible light photocatalytic activity. Firstly, they prepared amorphous TiO_2 by adding tetrabutyl titanate dropwise into water to obtain anatase TiO_2 by processing amorphous TiO_2 with diluted HNO_3 solution at 70 ˚C. Tseng *et al.* (2006) prepared TiO_2 with a mixed crystal lattice of anatase, brookite and rutile phases by sol-gel process with tetra butyl orthotitanate and HNO_3 as precursor and catalyst, at the calcination temperature of 150-600 ˚C, respectively. They studied the visible light photocatalytic activity of the as-prepared TiO_2 with NO_x as model compound and found that TiO_2 prepared at 200 ˚C had high visible light photocatalytic activity. Park *et al.* (2009) recently reported the visible light photocatalytic activity of TiO_2 prepared by a typical sol-gel method at lower temperatures. They found that the as-prepared TiO_2 samples had visible light photocatalytic activity, the calcination temperature obviously affected the photocatalytic activity and the best photocatalytic activity was around 250 ˚C (Wang, Xiao, *et al.* 2011).

The sol-gel method and impregnation technique have been employed to dope TiO_2 widely. Solid-solution containing titanium and doping ions could be formed by the sol-gel method (Fig. 2.2) and the doping ion could be incorporated into TiO_2 lattice, while doping iron into titania by impregnation technique. Fe_2TiO_5 or α-Fe_2O_3 can be easily produced on the surface of TiO_2 during calcination at high temperature (Zhu *et al.* 2006).

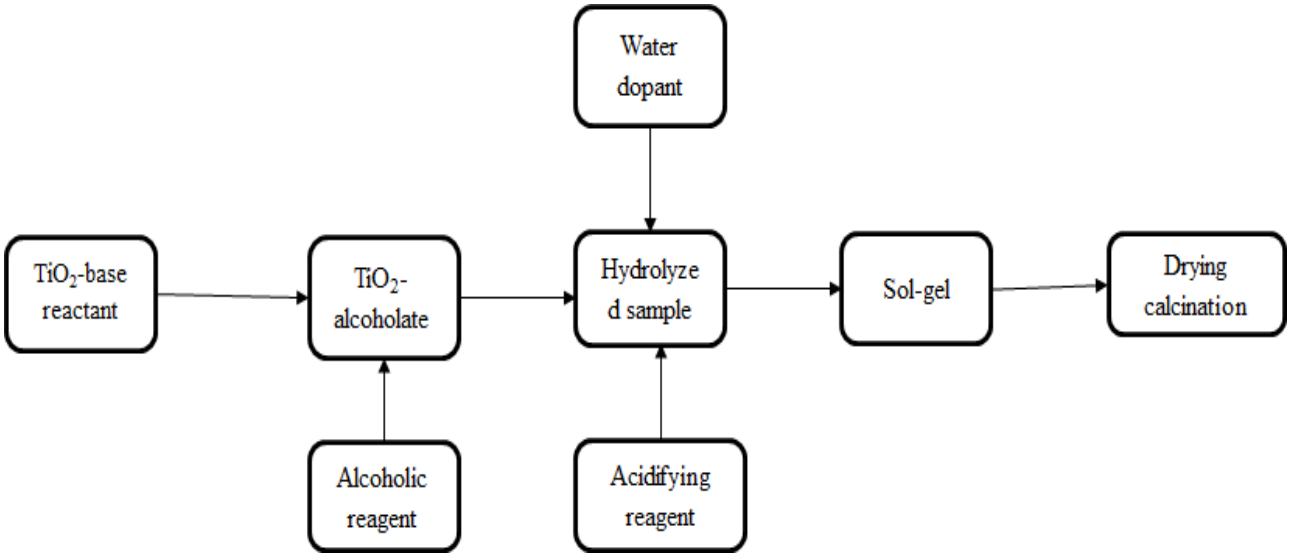

Figure 2. 2: Process flow chart for the preparation of TiO_2-based photocatalysts by sol-gel method (Akpan and Hameed 2010).

2.1.6 Semiconductor photocatalysis

One of the considered efficient methods to tackle environmental pollution and energy crisis is semiconductor-based photocatalysis. Amongst all the semiconductors, titanium dioxide (TiO_2) plays a considerable role in the field of environmental protection applications, owing to its high oxidation ability, non-toxicity, low cost, environmental-friendly nature, chemical and thermal stability and relatively efficient photocatalytic activity (Martins *et al.* 2017). These properties trade TiO_2 as an adequate photocatalyst for decomposition of diverse pollutants in an aqueous solution. On the other hand, TiO_2 has a large band gap (3.2eV), high charge carrier, recombination, low surface area and the photonic efficiency of TiO_2 is poor under visible light, because it can only be activated in the ultraviolet (UV) region (Shen *et al.* 2018). Therefore, UV light constitutes only a small fraction, it can only use about 3-5% of the total energy of the solar spectrum (Khairy and Zakaria 2014). These undesired properties restrict its uses in various applications.

To overcome these limitations, the combination of TiO_2 with various materials such as carbon nanostructures has been adopted. Novel nanostructures such as nanofibers, nanotubes and nanoparticles derived from TiO_2 have been employed in photocatalysis. Due to their high specific surface area, ion-exchange and photocatalytic abilities these structures have been Synthesized. TiO_2 nanostructures possess unique properties and advantages for photocatalytic reactions. For example, TiO_2 nanostructures has a higher surface area as compared with TiO_2 bulk, which could significantly lead to an increase in surface reaction sites and reduce the electron-hole recombination rate. Moreover, due to their shorter distance for diffusion of these carriers, the one nanostructure geometry allows a high charge carrier transfer rate. Therefore, these effects are commendable for photocatalytic reactions.

The TiO_2 nanostructures could be Synthesized by five main methods, including chemical vapour deposition (CVD), template based, anodic oxidation, solvothermal and hydrothermal synthesis. The hydrothermal treatment is a low-cost and simple method for the control of the shape and size with different morphology, among these methods. Over the last few decades to Synthesize TiO_2 nanostructures, the method developed by Kasuga *et al*. (1998) has been mostly used. The shape of TiO_2 nanostructures plays a significant role in determining their photocatalytic activity since TiO_2 nanostructures with different morphologies have shown clear differences in their ability to photodegrade organic contaminants. The study of the morphology effect of various TiO_2 nanostructures (e.g. nanotubes, nanofibers and nanowires) on photodegradation of dyes have been reported by Camposeco *et al.* (2016). The results on this work showed that tubular morphology has the maximum photocatalytic efficiency, attributed to its tubular geometry and high hydroxylation degree which result in a greater number of active sites through the generation of oxygen vacancies (Ov). Recently, studies show that the morphology also greatly influences the photocatalytic activity of TiO_2.

Kasuga *et al*. (1998) reported the synthesis of TiO_2 nanotubes by the hydrothermal treatment. Other kinds of morphologies can be obtained: nanotubes, nanosheets, nanorods/nanowires and nanoribbons/nanobelts have also been observed through the hydrothermal treatment. The alkaline hydrothermal treatment is the most well used because of numerous unique properties and advantages such as high reactivity, low-cost, relatively non-polluting set-up and simple method for the control of the shape and size with different morphology. When synthesizing TiO_2 nanostructures by the hydrothermal method, the TiO_2 nanostructures are strongly influenced by the starting material (TiO_2), the hydrothermal conditions and the washing

process. The next structures have been proposed in several studies: H_2TiO_7, $H_2Ti_4O_9.H_2O$, $H_2Ti_2O_5.H_2O$ and lepidocrocite $HxTi_2$-x/4x/$4O_4$ (x-0.7, vacay). Recently, the nanostructures and formation mechanisms are still a topic of discussion. The photocatalytic performances of hydrothermally Synthesized nanostructures are lower with regards to commercial TiO_2 particles (Camposeco *et al.* 2016).

2.1.7 Carbon dots as a photocatalyst

Carbon quantum dots (CQDs) with advantages of low toxicity, low production cost and high chemical stability, have recently attracted increasing attention in the photocatalytic field, especially when coupled with TiO_2 (Huang *et al.* 2017). CQDs refer to zero-dimensional carbon material with size below 10 nm, which are composed of sp^2/sp^3 hybridized carbon atoms and various surface functional groups. The excellent conductivity of CQDs promote the transfer of photo-generated electrons more significantly when coupled with TiO_2, which is beneficial for the separation of electron-hole pairs and the enhancement of TiO_2 photocatalytic activity (Shen *et al.* 2018). To date, authors reported various methods to prepare CQDs such as chemical, ablation, electrochemical carbonization, laser ablation, microwave irradiation and hydrothermal treatment. CQDs Synthesized by the hydrothermal carbonization method comparatively exhibit more attractive properties including low cost, high efficiency, non-toxicity, environmentally friendly features and so on. A solution of organic precursor is necessary in a typical hydrothermal process, which is generally transferred to an autoclave and further reacted at high temperature.

The organic precursors for the synthesis of CQDs have been extensively studied up to now and various precursors such as glucose, sucrose, citric acid, chitosan and even orange juice have been reported (Shen *et al.* 2018). However, most researchers only aimed at searching for new-type of organic precursors to prepare CQDs and seldom paid close attention to direct differences between various precursors. The different structures of precursors such as carbon atom numbers, carbon chain length and functional groups, play crucial roles in the hydrothermal carbonization process, resulting in the CQDs with different structures and chemical properties. Therefore, it is of great significance to investigate the effects of precursors on the properties of CQDs, especially on the photocatalytic properties after

coupling with TiO_2 (Shen *et al.* 2018). Conventional carbonaceous materials such as carbon black, graphite and graphitized materials have been widely used in heterogeneous catalysis (Khalid *et al.* 2017).

The combination of TiO_2 nanomaterials with carbon materials recently attracted considerable interest and exhibited distinct potential including activated carbon, carbon nanotubes, graphene, graphite, carbon dots and carbon doping. They have recently been proven to be excellent photosensitizers which can further enhance photocatalytic activity of TiO_2-based composites. This can also be attributed to the following aspects:

- Carbon materials possess metallic conductivity as one of the many possible electronic materials.
- Carbon materials hold on intense electron-accepting capacity and can store the photo-induced electrons to prevent the recombination of the photogenerated electron-hole (e^--h^+) pairs.
- Carbon materials present an intense and wide range of visible light absorption in the range of 400-800 nm, hence aggregating a number of thermal energies which can promote the movement of the photo-excited electrons from the bulk of the TiO_2 into the oxidation reaction sites and further generate a series of active species.
- Carbon element is always demonstrated transferring into the lattice of TiO_2 through replacing some lattice Ti atoms and forms C-O or C=O bond in the process of carbon doping, which produces a hybrid orbital just below the conduction band of TiO_2 and improves the utilization efficiency of visible light (Jia *et al.* 2016). For the synthesis of carbon dots/titanium dioxide (CDs/TiO_2) nanocomposites, several methods have been reported so far such as the sol-gel process, thermal oxidation and solvothermal synthesis (Hou, Lu, *et al.* 2016). Most of the synthesis techniques are related to multiple steps:
- The synthesis of CDs
- The synthesis of TiO_2
- The preparation of CD/TiO_2 nanocomposites

For example, Wang, Zheng, *et al.* (2011) reported a hydrothermal synthesis for the fabrication of CDs/TiO_2 nanocomposites. P25 solution was firstly maintained at 150 ˚C for 24 h to prepare TiO_2 nanowires and CDs/TiO_2 nanocomposites were Synthesized through a mixture of TiO_2 nanowires and Vitamin C with another hydrothermal reactor at 90 ˚C for 4 h

(Wang, Zheng, *et al.* 2011). Liu *et al.* (2014) prepared CDs through a modified pyrolysis approach and the TiO_2 nanorod and nanospheres were Synthesized by a two-phase hydrothermal method. Thereafter, CDs/TiO_2 composite with enhanced visible light-driven photocatalytic activity were obtained by a hydrothermal coupling process (Liu *et al.* 2014).

Among these carbon materials, carbon nanotubes (CNTs) have been attracting considerable attention due to their special structure, their extraordinary mechanical and unique electronic properties and their potential applications since their discovery (Sharma *et al.* 2018). Their superior mechanical strength makes them good candidates for advanced composites (Shen *et al.* 2005). Depending on the helicity and the diameter of the tube, they can either be semiconducting, semi-metallic or metallic. Such variety opens a promising field in nanoscale electro-device applications. They can be ideal hydrogen storage materials due to their large specific surface area, hollow and layered structures. Recently, researchers found that CNTs are efficient adsorbents for dioxin, fluoride, lead and cadmium (Zhang *et al.* 2017). Thus, CNTs can be used as a promising material in environmental cleaning (Yu *et al.* 2005). CNTs can conduct electrons and have a high adsorption capacity. It was also found that carbon is utilized by adding Fenton based oxidation compounds via utilizing Fe^{2+} and H_2O_2 components to improve the separation of photogenerated charge carriers and to facilitate the adsorption of the pollutant molecules at the carbon catalyst interface as reported in the work of Hou *et al.* (2016) for the $Bi_{12}TiO_{20}$ photocatalyst (Mohamed *et al.* 2017).

2.1.8 Hematite (α-Fe_2O_3) as a photocatalyst

One of typical n-type semiconductors for photodegrading atmospheric and aquatic organic contaminants is called hematite (α-Fe_2O_3), which presents excellent photocatalytic activity compared with traditional photocatalysts such as ZnO and TiO_2 (Zheng *et al.* 2018). The Hematite (α-Fe_2O_3) has a low band gap (2.2 eV) and could absorb visible light well among ZnO and TiO_2 semiconductors. It also has the advantages of high chemical stability and low cost. The advanced nature of (α-Fe_2O_3) as it is non-toxic and magnetic, can facilitate the promising applications in photocatalytic water splitting and water treatment (Zheng *et al.* 2018). Nonetheless, low diffusion length and high electron-hole recombination result in visible light trapping and photo-corrosion.

Coupling α-Fe_2O_3, ZnO and TiO_2 helps to improve their photocatalytic response. (Sadeghi-Niaraki, Ghasemi, Habibolahzadeh, *et al.* 2019). Many researchers adhere to the synthesis of TiO_2-based photocatalysts with visible light response; this may include the doping of metal ions, non-metal ions and preparation of composite semiconductors. Numerous semiconductors metal oxide such as TiO_2, ZnO, Bi_2O_3, In_2O_3, SnO_2, Fe_2O_3, Ag_3PO_4, $FeWO_4$, $Bi_{12}TiO_{20}$, $InMoO_3$-TiO_2; and sulfides such as ZnS and CdS have been used for the degradation of organic contaminants and generating less harmful by-products at relatively cheaper costs (Kumar *et al.* 2016). The photogenerated electrons could be transferred from one semiconductor to another semiconductor by coupling semiconductors to further promote the charge separation. The coupling of TiO_2 with α-Fe_2O_3 can strengthen the photocatalytic activity under visible light irradiation and TiO_2/Fe_2O_3 as a photocatalyst has been widely used for degradation of organic pollutants and solar water splitting (Zhang *et al.* 2019). Therefore, TiO_2 and Fe_2O_3 are used in photocatalytic activity and cool pigment applications.

The high recombination rate of photogenerated electrons and holes hampers its photocatalytic performance in a mono-component α-Fe_2O_3 because of the short lifetime (<10 ps) of photogenerated charge carriers and small diffusion length of the hole (Zhang *et al.* 2019). The photocatalytic performance of TiO_2/Fe_2O_3 composite under visible light irradiation still needs to be enhanced. Lin *et al.* (2015) prepared TiO_2/Fe_2O_3 composite by calcining commercial P25 nanoparticles mixture and Fe_3O_4 powder. The Synthesized TiO_2/Fe_2O_3 had more visible light than bare P25 and Fe_2O_3.

Sun *et al.* (2016) used the hydrothermal method to Synthesize uniform α-Fe_2O_3/TiO_2 core-shell nanoparticles where the photocatalytic performance increased with the TiO_2 contents. Meanwhile, α-Fe_2O_3/TiO_2 composites were prepared by α-FeOOH nanoparticles using hydrothermal method and the uniform TiO_2 shell was prepared using TBOT via sol-gel reaction at 45 ˚C for 24 h. They reported that the thickness, density and crystal structure of TiO_2 coating shells affected the photocatalytic performance (Sadeghi-Niaraki, Ghasemi, adeh, *et al.* 2019). Kim *et al.* (2013) developed Bi_2S_3 loaded TiO_2 composite system which led to reduce recombination rate of electrons and holes and it was reported that this composite exhibited higher photocatalytic hydrogen production as compared to bare Bi_2S_3 and TiO_2. Lu *et al.* (2013) Synthesized TiO_2/Bi_2S_3 heterojunction for the degradation of methyl orange under UV light. It was concluded that the assistant effect of Bi_2S_3 on TiO_2 highly improved the photocatalytic activity. Yang *et al.* (2014) reported the synthesis of Bi_2S_3

sensitized TiO_2 nanotubes arrays and studied the growth and morphologies of the hierarchical nanostructures (Kumar *et al.* 2016). Owing to the great opportunities provided by coupling of metal oxides such as TiO_2 with other desirable compounds we concluded to present unique assembly of Bi_2S_3 nanotubes-TiO_2 heterostructures as efficient photocatalytic material (Kumar *et al.* 2016).

References

Ahmad, R., Ahmad, Z., Khan, A.U., Mastoi, N.R., Aslam, M., and Kim, J., 2016. Photocatalytic systems as an advanced environmental remediation: Recent developments, limitations and new avenues for applications. *Journal of Environmental Chemical Engineering*, 4 (4), 4143–4164.

Akpan, U.G. and Hameed, B.H., 2010. The advancements in sol-gel method of doped-TiO2 photocatalysts. *Applied Catalysis A: General*, 375 (1), 1–11.

Al-Mamun, M.R., Kader, S., Islam, M.S., and Khan, M.Z.H., 2019. Photocatalytic activity improvement and application of UV-TiO2 photocatalysis in textile wastewater treatment: A review. *Journal of Environmental Chemical Engineering*, 7 (5).

Andrade-Guel, M., Díaz-Jiménez, L., Cortés-Hernández, D., Cabello-Alvarado, C., ávila-Orta, C., Bartolo-Pérez, P., and Gamero-Melo, P., 2018. Microwave assisted sol-gel synthesis of titaniumdioxide using hydrochloric and acetic acid ascatalysts. *Boletin de la Sociedad Espanola de Ceramica y Vidrio*, 1–7.

Archana, T., Vijayakumar, K., Arivanandhan, M., and Jayavel, R., 2019. TiO2 nanostructures with controlled morphology for improved electrical properties of photoanodes and quantum dot sensitized solar cell characteristics. *Surfaces and Interfaces*, 17 (May), 100350.

Asha Jhonsi, M. and Thulasi, S., 2016. A novel fluorescent carbon dots derived from tamarind. *Chemical Physics Letters*, 661, 179–184.

Awfa, D., Ateia, M., Fujii, M., Johnson, M.S., and Yoshimura, C., 2018. Photodegradation of pharmaceuticals and personal care products in water treatment using carbonaceous-TiO2 composites: A critical review of recent literature. *Water Research*, 142, 26–45.

Bakre, P. V., Volvoikar, P.S., Vernekar, A.A., and Tilve, S.G., 2016. Influence of acid chain length on the properties of TiO2 prepared by sol-gel method and LC-MS studies of methylene blue photodegradation. *Journal of Colloid and Interface Science*, 474, 58–67.

Bertoluzzi, L., Badia-Bou, L., Fabregat-Santiago, F., Gimenez, S., and Bisquert, J., 2013. Interpretation of cyclic voltammetry measurements of thin semiconductor films for solar fuel applications. *Journal of Physical Chemistry Letters*.

Bokare, A.D. and Choi, W., 2014. Review of iron-free Fenton-like systems for activating H2O2 in advanced oxidation processes. *Journal of Hazardous Materials*.

Camposeco, R., Castillo, S., Navarrete, J., and Gomez, R., 2016. Synthesis, characterization and photocatalytic activity of TiO2 nanostructures: Nanotubes, nanofibers, nanowires and nanoparticles. *Catalysis Today*, 266, 90–101.

Cao, M., Wang, P., Ao, Y., Wang, C., Hou, J., and Qian, J., 2016. Visible light activated photocatalytic degradation of tetracycline by a magnetically separable composite photocatalyst: Graphene oxide/magnetite/cerium-doped titania. *Journal of Colloid and Interface Science*, 467, 129–139.

Chansri, P. and Sung, Y.M., 2016. Reprint of "Investigations of electrochemical luminescence characteristics of ZnO/TiO2 nanotubes electrode and silica-based gel type solvents". *Surface and Coatings Technology*, 307, 1139–1143.

Choi, D., Ham, S., and Jang, D.J., 2018. Visible-light photocatalytic reduction of Cr(VI) via carbon quantum dots-decorated TiO2 nanocomposites. *Journal of Environmental Chemical Engineering*, 6 (1), 1–8.

Cuerda-Correa, E.M., Domínguez, J.R., Muñoz-Peña, M.J., and González, T., 2016. Degradation of Parabens in Different Aqueous Matrices by Several O3-Derived Advanced Oxidation Processes. *Industrial and Engineering Chemistry Research*.

Dedual, G., Macdonald, M.J., Alshareef, A., Wu, Z., Tsang, D.C.W., and Yip, A.C.K., 2014. Requirements for effective photocatalytic oxidative desulfurization of a thiophene-containing solution using TiO2. *Journal of Environmental Chemical Engineering*.

Dhaka, S., Kumar, R., Lee, S. hun, Kurade, M.B., and Jeon, B.H., 2018. Degradation of ethyl paraben in aqueous medium using advanced oxidation processes: Efficiency evaluation of UV-C supported oxidants. *Journal of Cleaner Production*.

F. Hasany, S., Ahmed, I., J, R., and Rehman, A., 2013. Systematic Review of the Preparation Techniques of Iron Oxide Magnetic Nanoparticles. *Nanoscience and Nanotechnology*.

Fazal, T., Razzaq, A., Javed, F., Hafeez, A., Rashid, N., Amjad, U.S., Ur Rehman, M.S., Faisal, A., and Rehman, F., 2020. Integrating adsorption and photocatalysis: A cost effective strategy for textile wastewater treatment using hybrid biochar-TiO2 composite. *Journal of Hazardous Materials*, 390 (May 2019), 121623.

Gaur, N., Narasimhulu, K., and PydiSetty, Y., 2018. Recent advances in the bio-remediation of persistent organic pollutants and its effect on environment. *Journal of Cleaner Production*, 198, 1602–1631.

Hama Aziz, K.H., Miessner, H., Mueller, S., Kalass, D., Moeller, D., Khorshid, I., and Rashid, M.A.M., 2017. Degradation of pharmaceutical diclofenac and ibuprofen in aqueous solution, a direct comparison of ozonation, photocatalysis, and non-thermal plasma. *Chemical Engineering Journal*.

Han, F., Kambala, V.S.R., Srinivasan, M., Rajarathnam, D., and Naidu, R., 2009. Tailored titanium dioxide photocatalysts for the degradation of organic dyes in wastewater treatment: A review. *Applied Catalysis A: General*.

Hanaor, D., Michelazzi, M., Chenu, J., Leonelli, C., and Sorrell, C.C., 2011. The effects of firing conditions on the properties of electrophoretically deposited titanium dioxide films on graphite substrates. *Journal of the European Ceramic Society*.

Hantusch, M., Bessergenev, V., Mateus, M.C., Knupfer, M., and Burkel, E., 2018. Electronic properties of photocatalytic improved Degussa P25 titanium dioxide powder. *Catalysis Today*, 307 (October 2017), 111–118.

Haque, F.Z., Nandanwar, R., and Singh, P., 2017. Evaluating photodegradation properties of anatase and rutile TiO2 nanoparticles for organic compounds. *Optik*, 128, 191–200.

Heponiemi, A. and Lassi, U., 2012. Advanced Oxidation Processes in Food Industry Wastewater Treatment – A Review. *In*: *Food Industrial Processes - Methods and Equipment*.

Horikoshi, S. and Serpone, N., 2020. Can the photocatalyst TiO2 be incorporated into a wastewater treatment method? Background and prospects. *Catalysis Today*, 340 (August 2018), 334–346.

Hou, L., Wang, L., Royer, S., and Zhang, H., 2016. Ultrasound-assisted heterogeneous

Fenton-like degradation of tetracycline over a magnetite catalyst. *Journal of Hazardous Materials*, 302, 458–467.

Hou, Y., Lu, Q., Wang, H., Li, H., Zhang, Y., and Zhang, S., 2016. One-pot electrochemical synthesis of carbon dots/TiO2 nanocomposites with excellent visible light photocatalytic activity. *Materials Letters*, 173, 13–17.

Huang, Y., Liang, Y., Rao, Y., Zhu, D., Cao, J.J., Shen, Z., Ho, W., and Lee, S.C., 2017. Environment-Friendly Carbon Quantum Dots/ZnFe2O4 Photocatalysts: Characterization, Biocompatibility, and Mechanisms for NO Removal. *Environmental Science and Technology*, 51 (5), 2924–2933.

Jia, J., Li, D., Wan, J., and Yu, X., 2016. Characterization and mechanism analysis of graphite/C-doped TiO2 composite for enhanced photocatalytic performance. *Journal of Industrial and Engineering Chemistry*, 33, 162–169.

Kalantari, K., Kalbasi, M., Sohrabi, M., and Royaee, S.J., 2016. Synthesis and characterization of N-doped TiO2 nanoparticles and their application in photocatalytic oxidation of dibenzothiophene under visible light. *Ceramics International*, 42 (13), 14834–14842.

Kalantari, K., Kalbasi, M., Sohrabi, M., and Royaee, S.J., 2017. crossmark, 43 (August 2016), 973–981.

Karci, A., Arslan-Alaton, I., Olmez-Hanci, T., and Bekbölet, M., 2012. Transformation of 2,4-dichlorophenol by H 2O 2/UV-C, Fenton and photo-Fenton processes: Oxidation products and toxicity evolution. *Journal of Photochemistry and Photobiology A: Chemistry*.

Khairy, M. and Zakaria, W., 2014. Effect of metal-doping of TiO2 nanoparticles on their photocatalytic activities toward removal of organic dyes. *Egyptian Journal of Petroleum*, 23 (4), 419–426.

Khalid, N.R., Majid, A., Tahir, M.B., Niaz, N.A., and Khalid, S., 2017. Carbonaceous-TiO2 nanomaterials for photocatalytic degradation of pollutants: A review. *Ceramics International*, 43 (17), 14552–14571.

Khan, S.B., Hou, M., Shuang, S., and Zhang, Z., 2017. Morphological influence of TiO 2

nanostructures (nanozigzag, nanohelics and nanorod) on photocatalytic degradation of organic dyes. *Applied Surface Science*, 400, 184–193.

Khodadadi, M., Ehrampoush, M.H., Ghaneian, M.T., Allahresani, A., and Mahvi, A.H., 2018. Synthesis and characterizations of FeNi3@SiO2@TiO2 nanocomposite and its application in photo- catalytic degradation of tetracycline in simulated wastewater. *Journal of Molecular Liquids*, 255, 224–232.

Kim, H., Jin, C., Park, S., Lee, W.I., Chin, I.J., and Lee, C., 2013. Structure and optical properties of Bi2S3 and Bi2O3 nanostructures synthesized via thermal evaporation and thermal oxidation routes. *Chemical Engineering Journal*.

Kommineni, S., Zoeckler, J., Stocking, A., Liang, S., Flores, A., Kavanaugh, M., Rodriguez, R., Browne, T., Roberts, R., Brown, A., and Stocking, A., 2000. *Advanced Oxidation Processes: Literature Review, Removal of Methyl Tertiary Butyl Ether (MTBE) from Drinking Water: Air Stripping, Advanced Oxidation Process, Granular Activated Carbon, Synthetic Resin Sorbents*. National Water Research Institute.

Krishnan, S., Chandran, K., and Sinnathambi, C.M., 2016. Wastewater treatment technologies used for the removal of different surfactants: A comparative review. *International Journal of Applied Chemistry*.

Kumar, S., Sharma, S., Sood, S., Umar, A., and Kansal, S.K., 2016. Bismuth sulfide (Bi2S3) nanotubes decorated TiO2 nanoparticles heterojunction assembly for enhanced solar light driven photocatalytic activity. *Ceramics International*, 42 (15), 17551–17557.

Li, Z., Guo, C., Lyu, J., Hu, Z., and Ge, M., 2019. Tetracycline degradation by persulfate activated with magnetic Cu/CuFe2O4 composite: Efficiency, stability, mechanism and degradation pathway. *Journal of Hazardous Materials*, 373 (March), 85–96.

Lin, C.C., Ho, J.M., and Wu, M.S., 2015. Continuous preparation of Fe3O4 nanoparticles using a rotating packed bed: Dependence of size and magnetic property on temperature. *Powder Technology*.

Liu, C., Li, Y., Wei, L., Wu, C., Chen, Y., Mei, L., and Jiao, J., 2014. CdS quantum dot-sensitized solar cells based on nano-branched TiO2 arrays. *Nanoscale Research Letters*.

Lu, J., Wang, Z., Zhang, Y., and Zhou, X., 2013. Hydrothermal synthesis of Bi2S3 nanorods

from a single-source precursor and their promotional effect on the photocatalysis of TiO2. *Journal of Nanomaterials*.

Mahshid, S., Askari, M., Sasani Ghamsari, M., Afshar, N., and Lahuti, S., 2009. Mixed-phase TiO2 nanoparticles preparation using sol-gel method. *Journal of Alloys and Compounds*.

Martins, A.C., Cazetta, A.L., Pezoti, O., Souza, J.R.B., Zhang, T., Pilau, E.J., Asefa, T., and Almeida, V.C., 2017. Sol-gel synthesis of new TiO2/activated carbon photocatalyst and its application for degradation of tetracycline. *Ceramics International*, 43 (5), 4411–4418.

Martins, N.C.T., Ângelo, J., Girão, A.V., Trindade, T., Andrade, L., and Mendes, A., 2016. N-doped carbon quantum dots/TiO2 composite with improved photocatalytic activity. *Applied Catalysis B: Environmental*, 193, 67–74.

Matongo, S., Birungi, G., Moodley, B., and Ndungu, P., 2015. Pharmaceutical residues in water and sediment of Msunduzi River, KwaZulu-Natal, South Africa. *Chemosphere*, 134, 133–140.

Matsuzawa, S., Tanaka, J., Sato, S., and Ibusuki, T., 2002. Photocatalytic oxidation of dibenzothiophenes in acetonitrile using TiO2: Effect of hydrogen peroxide and ultrasound irradiation. *Journal of Photochemistry and Photobiology A: Chemistry*.

Mohamed, M.M., Bayoumy, W.A., Goher, M.E., Abdo, M.H., and Mansour El-Ashkar, T.Y., 2017. Optimization of α-Fe 2 O 3 @Fe 3 O 4 incorporated N-TiO 2 as super effective photocatalysts under visible light irradiation. *Applied Surface Science*, 412, 668–682.

Muruganandham, M., Suri, R.P.S., Jafari, S., Sillanpää, M., Lee, G.J., Wu, J.J., and Swaminathan, M., 2014. Recent developments in homogeneous advanced oxidation processes for water and wastewater treatment. *International Journal of Photoenergy*.

Oseghe, E.O. and Ofomaja, A.E., 2018a. Study on light emission diode/carbon modified TiO2 system for tetracycline hydrochloride degradation. *Journal of Photochemistry and Photobiology A: Chemistry*, 360 (April), 242–248.

Oseghe, E.O. and Ofomaja, A.E., 2018b. Facile microwave synthesis of pine cone derived C-doped TiO2 for the photodegradation of tetracycline hydrochloride under visible-LED light. *Journal of Environmental Management*, 223 (July), 860–867.

Panneerselvam, P., Morad, N., and Tan, K.A., 2011. Magnetic nanoparticle (F3O4) impregnated onto tea waste for the removal of nickel(II) from aqueous solution. *Journal of Hazardous Materials*, 186 (1), 160–168.

Park, Y., Kim, W., Park, H., Tachikawa, T., Majima, T., and Choi, W., 2009. Carbon-doped TiO2 photocatalyst synthesized without using an external carbon precursor and the visible light activity. *Applied Catalysis B: Environmental*.

Ren, Y.N., Xu, W., Si, Z.X., Zhou, L.X., and Zheng, Y.Q., 2018. Photocatalytic degradation of tetracycline antibiotics under visible light using uranyl isophthalate coordination polymers. *Polyhedron*, 152, 195–201.

Rimoldi, L., Meroni, D., Cappelletti, G., and Ardizzone, S., 2017. Green and low cost tetracycline degradation processes by nanometric and immobilized TiO2 systems. *Catalysis Today*, 281, 38–44.

Sadeghi-Niaraki, S., Ghasemi, B., adeh, A.H., Ghasemi, E., and Ghahari, M., 2019. Preparation of (Fe,Cr)2O3@TiO2 cool pigments for energy saving applications. *Journal of Alloys and Compounds*, 779, 367–379.

Sadeghi-Niaraki, S., Ghasemi, B., Habibolahzadeh, A., Ghasemi, E., and Ghahari, M., 2019. Nanostructured Fe2O3@TiO2 pigments with improved NIR reflectance and photocatalytic ability. *Materials Chemistry and Physics*, 235 (May), 121769.

Safari, G.H., Hoseini, M., Seyedsalehi, M., Kamani, H., Jaafari, J., and Mahvi, A.H., 2014. Photocatalytic degradation of tetracycline using nanosized titanium dioxide in aqueous solution. *International Journal of Environmental Science and Technology*, 12 (2), 603–616.

Saitoh, T., Shibata, K., and Hiraide, M., 2014. Rapid removal and photodegradation of tetracycline in water by surfactant-assisted coagulation-sedimentation method. *Journal of Environmental Chemical Engineering*, 2 (3), 1852–1858.

Shao, S., Hu, Y., Cheng, C., Cheng, J., and Chen, Y., 2018. Simultaneous degradation of tetracycline and denitrification by a novel bacterium, Klebsiella sp. SQY5. *Chemosphere*, 209, 35–43.

Sharma, S., Dutta, V., Singh, P., Raizada, P., Rahmani-Sani, A., Hosseini-Bandegharaei, A.,

and Thakur, V.K., 2019. Carbon quantum dot supported semiconductor photocatalysts for efficient degradation of organic pollutants in water: A review. *Journal of Cleaner Production*, 228, 755–769.

Sharma, S., Umar, A., Sood, S., Mehta, S.K., and Kansal, S.K., 2018. Photoluminescent C-dots: An overview on the recent development in the synthesis, physiochemical properties and potential applications. *Journal of Alloys and Compounds*, 748, 818–853.

Shen, G.R., Cheng, Y.T., and Tsai, L.N., 2005. Synthesis and characterization of Ni-P-CNT's nanocomposite film for MEMS applications. *IEEE Transactions on Nanotechnology*.

Shen, T., Wang, Q., Guo, Z., Kuang, J., and Cao, W., 2018. Hydrothermal synthesis of carbon quantum dots using different precursors and their combination with TiO2 for enhanced photocatalytic activity. *Ceramics International*, 44 (10), 11828–11834.

Sobczyński, A., Duczmal, L., and Zmudziński, W., 2004. Phenol destruction by photocatalysis on TiO2: An attempt to solve the reaction mechanism. *Journal of Molecular Catalysis A: Chemical*.

Song, Z., Ma, Y.L., and Li, C.E., 2019. The residual tetracycline in pharmaceutical wastewater was effectively removed by using MnO2/graphene nanocomposite. *Science of the Total Environment*, 651, 580–590.

Sun, D., Cao, Y., Xu, Y., Zhang, G., and Sun, Y., 2016. Tunable synthesis of core-shell α-Fe2O3/TiO2 composite nanoparticles and their visible-light photocatalytic activity. *Chemical Research in Chinese Universities*.

Tomić, N., Grujić-Brojčin, M., Finčur, N., Abramović, B., Simović, B., Krstić, J., Matović, B., and Šćepanović, M., 2015. Photocatalytic degradation of alprazolam in water suspension of brookite type TiO2 nanopowders prepared using hydrothermal route. *Materials Chemistry and Physics*.

Totito, T.C., 2013. Photocatalytic activity of supported TiO 2 nanocrystals, (November), 1–153.

Tran, M.H. and Jeong, H.K., 2018. Modification of titanium dioxide by solution plasma. *Journal of Physics and Chemistry of Solids*, 121 (April), 292–297.

Tseng, Y.H., Kuo, C.S., Huang, C.H., Li, Y.Y., Chou, P.W., Cheng, C.L., and Wong, M.S., 2006. Visible-light-responsive nano-TiO2 with mixed crystal lattice and its photocatalytic activity. *Nanotechnology*.

Wang, D., Xiao, L., Luo, Q., Li, X., An, J., and Duan, Y., 2011. Highly efficient visible light TiO2 photocatalyst prepared by sol-gel method at temperatures lower than 300°C. *Journal of Hazardous Materials*, 192 (1), 150–159.

Wang, J.Y., Yu, J.X., Liu, Z.H., He, Z.K., and Cai, R.X., 2005. A simple new way to prepare anatase TiO2 hydrosol with high photocatalytic activity. *Semiconductor Science and Technology*.

Wang, Q., Zheng, H., Long, Y., Zhang, L., Gao, M., and Bai, W., 2011. Microwave-hydrothermal synthesis of fluorescent carbon dots from graphite oxide. *Carbon*.

Wu, M.C., Huang, W.K., Lin, T.H., and Lu, Y.J., 2019. Photocatalytic hydrogen production and photodegradation of organic dyes of hydrogenated TiO 2 nanofibers decorated metal nanoparticles. *Applied Surface Science*, 469 (August 2018), 34–43.

Wu, Q. and Zhang, Z., 2019. The fabrication of magnetic recyclable nitrogen modified titanium dioxide/strontium ferrite/diatomite heterojunction nanocomposite for enhanced visible-light-driven photodegradation of tetracycline. *International Journal of Hydrogen Energy*, 44 (16), 8261–8272.

Xu, D., Xiao, Y., Pan, H., and Mei, Y., 2019. Toxic effects of tetracycline and its degradation products on freshwater green algae. *Ecotoxicology and Environmental Safety*, 174 (December 2018), 43–47.

Yang, L., Sun, W., Luo, S., and Luo, Y., 2014. White fungus-like mesoporous Bi2S3 ball/TiO2 heterojunction with high photocatalytic efficiency in purifying 2,4-dichlorophenoxyacetic acid/Cr(VI) contaminated water. *Applied Catalysis B: Environmental*.

Yu, Y., Yu, J.C., Yu, J.G., Kwok, Y.C., Che, Y.K., Zhao, J.C., Ding, L., Ge, W.K., and Wong, P.K., 2005. Enhancement of photocatalytic activity of mesoporous TiO2 by using carbon nanotubes. *Applied Catalysis A: General*, 289 (2), 186–196.

Zhang, B., Maimaiti, H., Zhang, D.D., Xu, B., and Wei, M., 2017. Preparation of coal-based

C-Dots/TiO2 and its visible-light photocatalytic characteristics for degradation of pulping black liquor. *Journal of Photochemistry and Photobiology A: Chemistry*, 345, 54–62.

Zhang, J., Kuang, M., Wang, J., Liu, R., Xie, S., and Ji, Z., 2019. Fabrication of carbon quantum dots/TiO2/Fe2O3 composites and enhancement of photocatalytic activity under visible light. *Chemical Physics Letters*, 730 (May), 391–398.

Zheng, X., Fu, W., Kang, F., Peng, H., and Wen, J., 2018. Enhanced photo-Fenton degradation of tetracycline using TiO2-coated α-Fe2O3 core–shell heterojunction. *Journal of Industrial and Engineering Chemistry*, 68, 14–23.

Zhu, J., Chen, F., Zhang, J., Chen, H., and Anpo, M., 2006. Fe3+-TiO2 photocatalysts prepared by combining sol-gel method with hydrothermal treatment and their characterization. *Journal of Photochemistry and Photobiology A: Chemistry*, 180 (1–2), 196–204.

Zhu, Z., Cai, H., and Sun, D.W., 2018. Titanium dioxide (TiO2) photocatalysis technology for nonthermal inactivation of microorganisms in foods. *Trends in Food Science and Technology*, 75 (February), 23–35.

Chapter 3 METHODOLOGY

3.1 Method

3.1.1 Materials

Ammonia solution, 25% NH_4OH (Labchem), hydrochloric acid, 32% HCl (Merck), 97% titanium (IV) isopropoxide (Sigma-Aldrich, India), tert-Butanol (Sigma-Aldrich, Germany), ethanol, C_2H_5OH (Glassworld), sodium hydroxide pellets, NaOH (Ace), ferrous sulphate heptahydrate, $FeSO_4.7H_20$ (Ace), potassium iodide, KI (Ace), ferric chloride, $FeCl_3.6H_20$ (Labchem), sulphuric Acid, 98% H_2SO_4 (Labchem), tetracycline hydrochloride (Europe) and isopropanol C_3H_80 (Ace).

3.1.2 Apparatus

The following apparatus were used in the experiment: Microwave Russel Hobbs, 45L, 1000W cooking power, Model number RHEM45BM (Game store). ThermoFisher Scientific vacuum, Model number 3628A, 1400W, 42.2L, Ambient +10 ˚C/50 ˚C to 280 ˚C. LAGBO 1 Rectangular Muffle Furnace 9x4x4 inner chamber, Model number MARS160, Part number LAGBO160 (M.G Scientific Manufacturer). Jouan C3i Bench Top centrifuge max speed 14 000 rpm, microprocessor control, induction drive motor, quick change rotor system includes 4x280 mL swing out rotor, 4x280 mL round buckets and adapters. Bransonic Ultrasonic Baths Branson, 1207K44, MFr number: CPX-952-317R, MH series, Model 3800, 120V, 1.5 gal. BAOSHISHAN 100 mL Teflon-lined Hydrothermal Synthesis Autoclave Reactor 220 ˚C, 3Mpa 304 steel High Pressure Digestion Tank PTFE vessel acid and Alkali Resistance 100mL (imported from the USA). ThermoFisher Scientific STARA3215 pH meter, 810TUWMMD ROSS ultra-gel-filled epoxy body pH/ATC electrode with 3m cable, pH 4, 7, 10 buffer and rinse pouches.

3.1.3 Chemicals

The following chemicals were used in this experiment: Tetracycline hydrochloride (Sigma-Aldrich, Europe), Isopropanol (Ace), Ethanol (Glassworld), 1.4-Benzoquinone 99% pur

(Acros Organics), Tert-Butanol (Sigma-Aldrich, Germany), Titanium (IV) isopropoxide 98% (Sigma-Aldrich, India), Potassium iodide (ACE), Ammonia solution 25% (ACE), Ferric chloride, $FeCl_3.6H_2O$ (Labchem), Ferrous sulphate Heptahydrate $FeSO_4.7H_2O$ (Merck), Sulphuric acid, H_2SO_4 98% (Labchem), Sodium hydroxide, NaOH (Ace), Hydrochloric acid, HCl 32% (Merck) and H_2O (Deionized and ultrapure water).

3.2 Synthesis of TiO_2 nanostructures

3.2.1 Synthesis of TiO_2 catalyst

10 g of TiO_2 precursor- titanium isopropoxide was added in a 120 mL solvent of 40 mL ethanol and 80 mL deionized water. The solution was sonicated for 10 min. Thereafter, the solution was mixed by stirring for 1 hour at room temperature. The solution was then allowed to cool, filtered and washed 2 times with 50 mL ethanol. The as-prepared material was allowed to dry under vacuum at 60 ˚C. Finally, the material was calcined in a furnace at 400 ˚C for 1 h with a heating rate of 2 ˚C/min. The obtained nano powders were the TiO_2 catalyst.

3.2.2 Synthesis of nanospheres

TiO_2 nanospheres were prepared by the hydrothermal method. 10 g of TiO_2 titanium isopropoxide was added in a solution of 40 mL ethanol and 80 mL deionized water. Thereafter, the solution was set under constant stirring for 1 hour at room temperature. The solution was filtered and washed with 2 times 50 mL of deionized water and 50 mL ethanol. The as-prepared material was allowed to dry under vacuum at 60 ˚C. Finally, the material was calcined in a furnace at 400 ˚C for 2 hours with a heating rate of 2 ˚C/min. The nano powders were named nanospheres (NS).

3.2.3 Synthesis of nanotubes

TiO_2 nanotubes were prepared by the hydrothermal treatment. 3 g of anatase Synthesized by the hydrothermal method and 60 mL of 10 N sodium hydroxide aqueous solution were mixed

in a sealed cylindrical Teflon-lined autoclave Parr reactor at 140 ˚C for 24 hours. The obtained solution was filtered with HCl until reaching pH 2 and thereafter it was washed with abundant deionized water to reach pH 7. Then the washed material was dried under vacuum at 80 ˚C for 12 hours. The sample was calcined in a furnace at 400 ˚C for 2 hours with a heating rate of 2 ˚C/min. The hydrothermally pretreated samples were named TiO_2 nanotubes.

3.2.4 Synthesis of nanofibers

TiO_2 nanofibers were prepared by the hydrothermal treatment. 3 g of anatase Synthesized by the hydrothermal method and 60 mL of 5 N sodium hydroxide aqueous solution were mixed in a sealed cylindrical Teflon-lined autoclave Parr reactor at 120 ˚C for 48 hours. The obtained solution was filtered with HCl until it reached pH 2, thereafter it was washed with abundant deionized water to reach pH 7. Finally, the material was dried under vacuum at 80º C for 12 hours. The sample was calcined in a furnace at 400 ˚C for 2 hours with a heating rate of 2 ˚C/min. The hydrothermally pretreated samples were TiO_2 nanofibers.

3.3 Synthesis of carbon quantum dots

10 g of the pine bark was weighed and dispersed in a cylindrical Teflon-lined autoclave Parr reactor. 50 mL of ultrapure water was added in the autoclave. The sample was left in the oven for 24 hours at 180 ˚C. Then the sample was removed from the oven and cooled for 2 hours. A dark brown crude solution was recovered from the autoclave. 50 mL of ultrapure water was added in the solution; the solution was centrifuged at 2000 rpm for 10 min. A clear yellow/brown solution was obtained and filtered through an ultrafiltration membrane. The solution was freeze dried for 48 h, then the carbon dots were obtained. 4 g of the carbon dots was dispersed in a 500 mL volumetric flask to have the carbon dots in a liquid form. The liquid was kept in the refrigerator so that the concentration of active constituents does not change over their prescribed usage life.

Table 3. 1: Synthesis of the composite material CD-TiO_2

Carbon dots	Deionized water	Ethanol
40 mL	0 mL	20 mL
30 mL	10 mL	20 mL
20 mL	20 mL	20 mL
10 mL	30 mL	20 mL
0 mL	40 mL	20 mL

Approximately 2 g of the TiO_2 catalyst was dispersed in 60 mL solvent of different volumes of carbon dots + deionized water + ethanol (

Table 3. 1). The resulting solution was kept stirring for 30 min and transferred into the Teflon- lined stainless-steel autoclave. The solution was heated in an oven for 4 hours at 140 ˚C. The solution was allowed to cool room temperature and centrifuged to remove the supernatant and the residue was washed with 20 mL ethanol; the solution was thoroughly centrifuged. The sample was allowed to dry under vacuum at 60 ˚C. The obtained composite material was named CD-TiO_2.

3.4 Preparation of magnetic CD-TiO_2-Fe_2O_3

0.021 g of $FeSO_4.7H_2O$ and 0.031 g of $FeCl_3.6H_2O$ (1% of Fe_2O_3) were weighed and dissolved under inert atmosphere in 80 mL of ultrapure water with vigorous stirring, nitrogen gas was applied in the solution to prevent the solution from oxidizing. The solution was heated to 80 ˚C and then 10 mL of ammonium hydroxide solution (25%) was added. 1.98 g

of CD-TNF composite was added to the solution and kept stirring for 30 minutes. Afterwards the solution was filtered and washed several times with deionized water and ethanol to remove impurities. The as-prepared composite material was allowed to dry under vacuum at 60 ˚C for 12 hours. The obtained composite material was named CD-TiO_2-Fe_2O_3.

0.063 g of $FeSO_4.7H_2O$ and 0.093 g of $FeCl_3.6H_2O$ (3% of Fe_2O_3) were weighed and dissolved under inert atmosphere in 80 mL of ultrapure water with vigorous stirring, nitrogen gas was applied in the solution to prevent the solution from oxidizing. While the solution was heated to 80 ˚C, 10 mL of ammonium hydroxide solution (25%) was added. 1.94 g of CD-TNF composite was added to the solution and kept stirring for 30 minutes. Afterwards the solution was filtered and washed several times with deionized water and ethanol to remove impurities. The as-prepared composite material was allowed to dry under vacuum at 60 ˚C for 12 hours. The obtained composite material was named CD-TiO_2-Fe_2O_3.

0.105 g of $FeSO_4.7H_2O$ and 0.155 g of $FeCl_3.6H_2O$ (5% of Fe_2O_3) were weighed and dissolved under inert atmosphere in 80 mL of ultrapure water with vigorous stirring; nitrogen gas was applied in the solution to avoid the solution from oxidizing. While the solution was heated to 80 ˚C, 10 mL of ammonium hydroxide solution (25%) was added. 1.90 g of CD-TNF composite was added to the solution and kept stirring for 30 minutes. Afterwards the solution was filtered and washed several times with deionized water and ethanol to remove impurities. The as-prepared composite material was allowed to dry under vacuum at 60 ˚C for 12 hours. The obtained composite material was named CD-TiO_2-Fe_2O_3.

3.5 Characterization of TiO_2 nanostructures, CD/TNF and CD/TNF/Fe_2O_3 composite material

The composite material CD-TiO_2-Fe_2O_3/TiO_2-nanostructures/CD-TNF catalyst was characterized using the following analytical equipment and methods:

3.5.1 Scanning Electron Microscope (SEM)

SEM shows the scanning electron microscopy images of samples Synthesized at 250 ˚C and 300 ˚C. The image of the surface morphology of the CD-TiO_2-Fe_2O_3 and the shape of TiO_2 nanostructures were taken with JSM-7900F Schottky Field Emission Scanning Electron Microscope and the samples were coated with a thin layer of about 10 nm of a non-conductive material electrically grounded layer of metal beam to minimize negative charge accumulation from the electron.

3.5.2 Transmission Electron Microscopy (TEM) Measurement

A transmission electron microscopy (TEM) was employed to visualize the size measurement and the shape of the Synthesized TiO_2 nanostructures. A 200Kv Ultra High-Resolution Transmission Electron Microscope (JEOL-2010) was used. TEM grids were prepared by placing a drop of the particle solution on a carbon-coated copper grid followed by drying at room temperature.

3.5.3 Liquid Chromatography-Mass Spectroscopy (LC-MS)

LC-MS was employed to determine the degradation intermediates of TC in the CD-TiO_2-Fe_2O_3 system. The degradation intermediates of TC were detected by HPLC-MS/MS system (Waters Xevo TQ-S) with a Waters BEH C18 column (2.1 mm x 50 mm, 10 cm).

3.5.4 Fourier Transform Infrared (FTIR)

The FTIR spectra of the TiO_2 nanostructures and CD-TiO_2-Fe_2O_3 material were recorded on a Perkin-Elmer (USA) FTIR Spectra 400 spectrometer in the range 650-4000 cm^{-1} to interpret the functional groups present in the catalyst.

3.5.5 Thermogravimetric Analysis (TGA)

The thermogravimetric analysis determines the weight loss as a function of temperature. TGA was used to measure the thermal stability and changes in the weight loss of the sample as a function of temperature in an inert environment. The composite material (CD-TiO_2-Fe_2O_3) was subjected to heat ranging from 30–700 ˚C in an inert environment at a heating rate of 10 ˚C.min^{-1} using Perkin Elmer (USA) Simultaneous Thermal Analyzer 600 instrument.

3.5.6 X-ray Diffraction (XRD)

Crystalline properties of the Synthesized nanoparticles were investigated by an X'Pert PRO X-ray diffractometer (PANalytical, PW3040/60 XRD) equipped with monochromatic CuKα anode; radiation wavelength of (λ = 0.154 nm) was used to obtain the XRD patterns. The samples were placed in an aluminum stainless steel holder and the span of the scanning process was kept at 45 kV and 40 mA between 10° to 70° 2θ, the exposure time for each sample was 20 minutes and positioned with a scan step size of 0.02°.

3.5.7 Ultraviolet-Diffuse Reflectance Spectroscopy (UVDRS)

The Ultraviolet-Diffuse Spectroscopy was used to determine the band gap energy and absorbance of the composite material CD-TiO_2-Fe_2O_3. The measurement was performed by placing the sample in front of the incident light window and concentrating the light reflected from the sample on the detector using a sphere with a barium sulfate-coated inside. The obtained value becomes the reflectance (relative reflectance) with respect to the reflectance of the reference standard white board, which is taken to be 100% when light is directed at the sample at an angle of 0 ˚C. Specular reflected light exits the integrating sphere and is not detected. As a result, only diffuse reflected light is measured.

3.5.8 Photoluminescence Intensity

Photoluminescence spectroscopy is a contactless, non-destructive method of probing the electronic structure of materials. The spectral distribution of a Jasco spectrofluorometer FP-8600 instrument from a semiconductor was analyzed non-destructively to determine the

electronic band gap on CD-TiO_2-Fe_2O_3 composite material. PL usually is excited with a laser having photon energy higher than the composite material band gap. The laser light penetrates to a depth $d = \alpha^{-1}$, where α is the absorption coefficient at the wavelength of the laser emission and the electron-hole pairs were created uniformly in this volume.

3.5.9 Nitrogen desorption-adsorption

N_2 desorption-adsorption isotherms were measured at 77 K using a conventional volumetric apparatus for the surface texturing properties namely BET surface area, total pore volume (V_p) and mean pore radius (r). Before starting the measurement, the samples were out-gassed at 473K for 3 h under a decreased pressure of 10^{-5} Torr. To assume complete pore saturation, the total pore volume was taken from the desorption branch of the isotherm at P/P_o= 0.95.

3.6 Measurement of photocatalytic activity

The photocatalytic performance of the Synthesized TiO_2 nanoparticles was characterized by the photodegradation technique using tetracycline as a model pharmaceutical under LED lamp. The LED lamp was used as the light source. Photocatalysis experiments were carried out in an 800 mL glass beaker containing 200 mL of tetracycline solution and then 0.05 g of the catalyst was added in the solution. The solution was sonicated for 5 min, then kept in the dark for 1 h while stirring. After stirring for an hour, the solution was transferred into a self-designed photodegradation reactor. This was to ensure that all light came from one direct source. The LED lamp was fitted on top of the reactor. All the experiments were carried out in a dark room to eliminate other light sources. The experiment lasted for 120 min and sampling was done at 20 min intervals. The degradation trend was monitored using the UV-Vis spectrometer (UV-1900i; SHIMADZU). The percentage degradation of the TC was determined by the equation given below:

$$\% \text{ Degradation} = [\, 1 - \frac{C}{C_o} \,] * 100 \ldots\ldots\ldots (12)$$

where C is the concentration of tetracycline at the given time and C_o is the initial concentration.

Figure 3. 1: Image of a self-designed photo-reactor for TC photodegradation.

3.7 Reusability and change in the composition of the catalyst

To check the reusability of the catalyst after an experiment, TiO_2 catalyst was separated by centrifugation, washed several times with distilled water and ethanol, dried under vacuum and used in the reaction with a fresh mixture of tetracycline in the same photodegradation conditions.

3.8 Electrochemical studies

Modification of glass carbon (GC) electrode using CD-TiO_2-Fe_2O_3 composite nanofiber

The surface of the glassy carbon (GC) was polished using 0.05 and 1 µm alumina. The electrode was washed in an ultrasonic bath for 15 min using ethanol solution, then distilled water was used to rinse the electrode that was dried with infrared lamp. For electrochemical studies, 20 µL of the CD-TiO_2-Fe_2O_3 composite nanofiber suspension was deposited on the GC electrode and left to dry under infrared lamp for 30 min. This new modified GC electrode was denoted as GC/CD-TiO_2-Fe_2O_3 composite nanofiber electrode. The modified electrodes were dipped into an electrochemical cell containing an acetate buffer solution at pH 4.5.

3.8.1 Electrochemical Characterization of the modified working electrodes

Bare and GC/CD-TiO_2-Fe_2O_3 sensor were electrochemically characterized using CV and DPV in solution containing potassium ferrocyanide. This was done by cycling a potential from -100 mV to 600 mV at a scan rate of 50 mV/s and DPV was done by cycling a potential from -1.2 to 0.2 V, to compare the peak current signal of the bare GC electrode and GC/CD-TiO_2-Fe_2O_3 sensor.

3.8.2 Electrochemical detection of 2-chlorophenol and arsenic ions

All three-electrode setup configurations were used in an electrochemical cell, consisting of GC/CD-TiO_2-Fe_2O_3 as the working electrodes, Ag/AgCl containing KCl as reference electrode and platinum wire as the counter electrode. A solution of potassium Ferrocyanide (5 mM) was prepared from an acetate solution (0.1 M) and poured into the electrochemical cell equipped with three electrodes. The system was subjected to cyclic voltammetry (CV) from -

200 mV to 600 mV at a scanning speed of 100 mV/s. The voltammetry was recorded on a bare glassy carbon electrode surface and then on an electrode modified by a mixture of CD-TiO_2-Fe_2O_3. To accumulate analytes on the electrode surface, the modified electrodes were immersed in a stirred (300 rpm) acetate buffer solution.

Chapter 4 RESULTS AND DISCUSSIONS

4.1 Characterization of TiO_2 Nanostructures

The following section of results discusses the successful synthesis TiO_2 nanostructures.

4.1.1 Characterization results of TiO_2 nanostructures

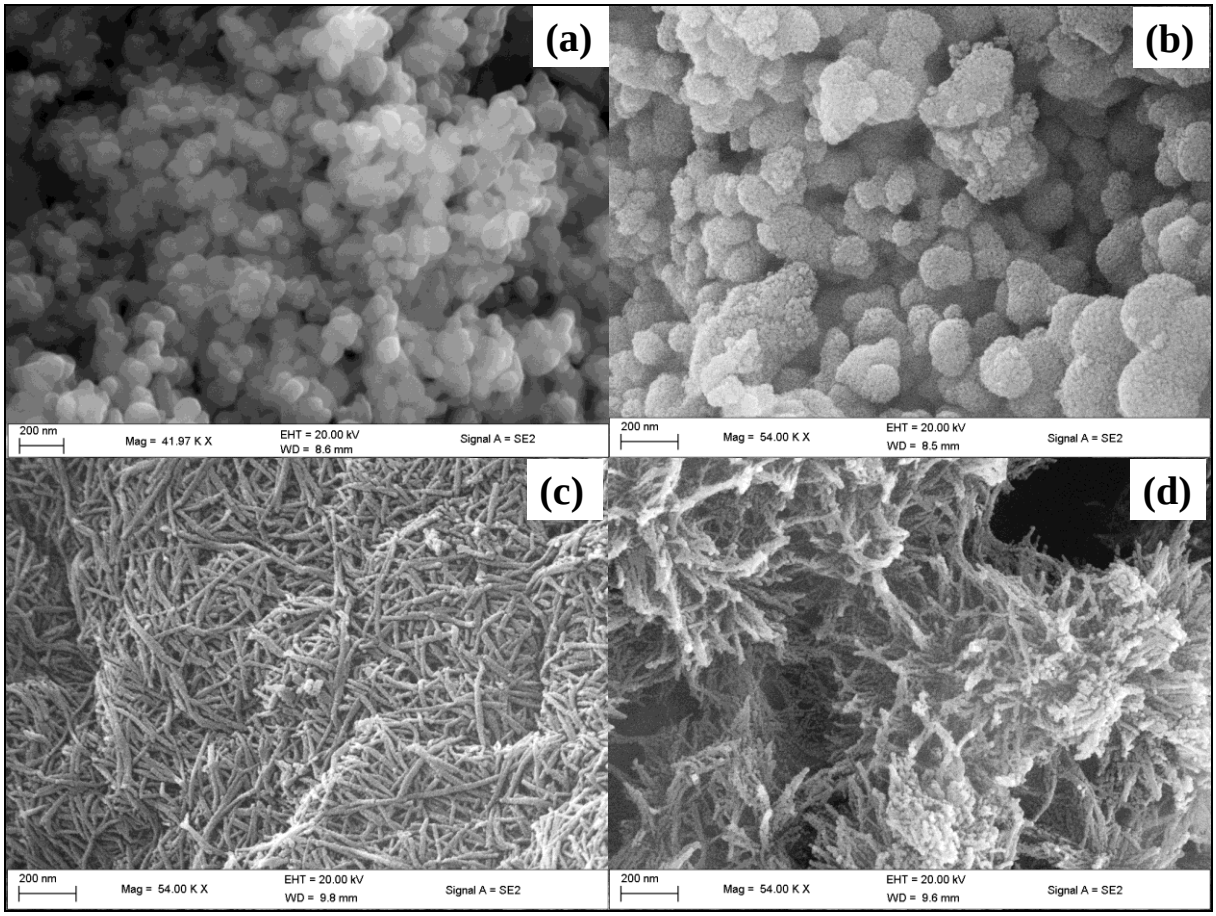

Figure 4. 1: SEM micrographs of a) TiO_2-amophores (T-AM), b) TiO_2-nanospheres (T-NS), c) TiO_2-nanotubes (T-NT) and TiO_2-nanofibers (T-NF).

SEM were used in order to confirm different morphologies under controlled conditions. From the SEM images, it was observed that desired shapes were obtained where a slight particle aggregation occurred in Fig. 4.1(a). The starting material of TiO_2-Amophores (T-AM) shows

non-uniform spherical TiO_2 nanoparticles. In Fig. 4.1(b) T-NS is spherical in terms of shape, the particles are uniform, the particles became agglomerated and this will invariably lead to a decrease in the surface area. Fig. 4.1(c) T-NT shows that the shapes are nanotubes, they are uniform. Fig. 4.1(d) also shows the shape of nanofibers (T-NF), they are uniform and the surface area is rough. The agglomerates of TiO_2 nanostructures were also observed around large particles. These shapes are desirable for the photodegradation studies and possess good photocatalytic properties (Camposeco *et al.* 2016).

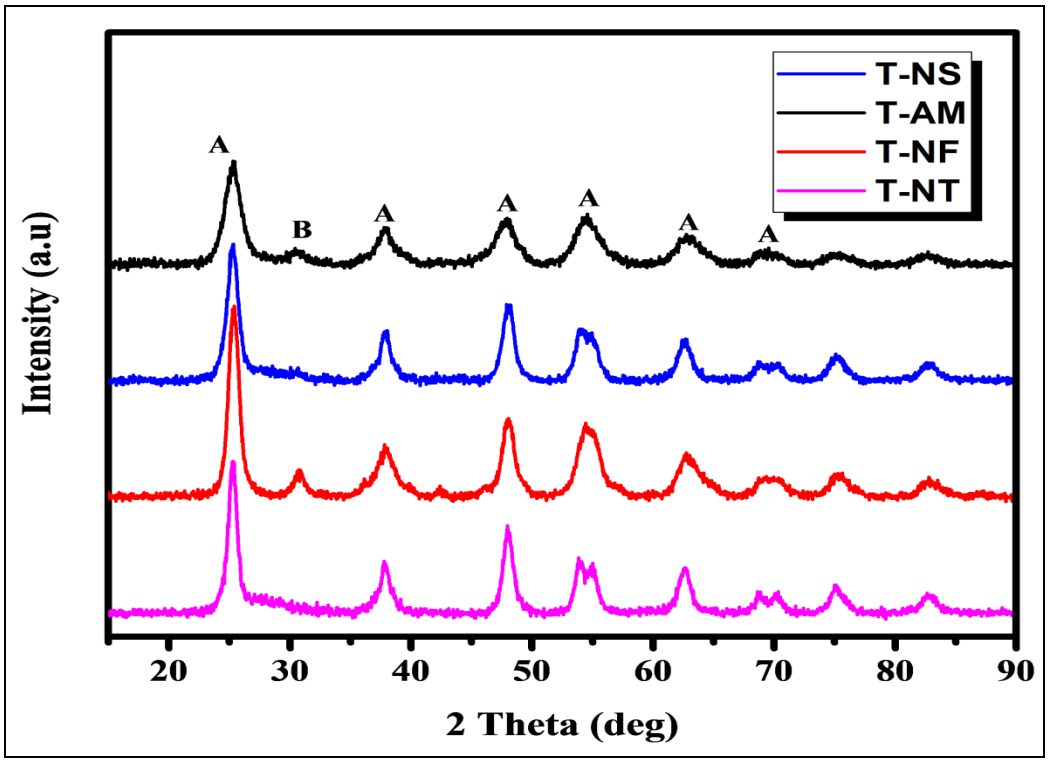

Figure 4. 2: XRD diffraction patterns of the TiO_2 nanostructures (T-AM, TNS, TNF and TNT) where A and B correspond to the anatase and brookite phase, respectively.

Fig. 4.2 shows the XRD patterns of the TiO_2 nanostructures (T-NT, T-NF, T-NS and T-AM) annealed at 350 ˚C. The characteristic reflections of anatase phase at 2θ of 25.38˚ [101], 37.72˚ [004], 48.5˚ [020], 54.77˚ [105] and 62.51˚ [204] are observed for all TiO_2 materials. The experimental XRD pattern agrees with the JCPDS: 21-1272 anatase phase TiO_2 and the XRD pattern of TiO_2. The reflection at 2θ of 33.45˚ [121] was assigned to the TiO_2 brookite phase according to JCPDS: 76-1934 is seen only for TiO_2-nanofibers (T-NF) and TiO_2-amorphous (T-AM). Based on the results, the XRD patterns of all TiO_2 nanostructures show a

good degree of crystallinity and TiO_2 exists in both anatase and brookite phase. TiO_2-nanofiber is the most crystalline photocatalyst because it has the sharpest diffraction peak compared to the other TiO_2 nanostructures. This may be due to the synthesis of T-NF. The T-NF aqueous solution was kept in the oven for 48 h at 120 ˚C as compared to the other TiO_2 nanostructures which were kept in the oven for 24 h which exerts an important effect on the morphological and desired physicochemical properties. The crystallite size of both the anatase and brookite TiO_2 phase was determined by applying the Scherrer's equation (equation 13):

$$D = \frac{K\lambda}{\beta cos\theta} \quad \text{..... (13)}$$

where D is the crystallite size (nm), $\boldsymbol{\lambda}$ (0.15418 nm) is the wavelength of the X-ray radiation, K is the Scherrer constant, usually taken as 0.89, $\boldsymbol{\beta}$ is the full-width-at-half-maximum of the anatase peak [1 0 1] plane (in radians) and 2θ corresponding to the anatase peak 25.38˚ (Martins *et al.* 2016). In addition, the presence of brookite phase in the T-AM may be due to the use of Ti(IV) alkoxide as starting material, which agrees with other studies, reported in the literature (Camposeco *et al.* 2016).

It is interesting to observe the disappearance of the brookite phase upon calcining (T-NS). According to Tomić *et al.* (2015), the duration of hydrothermal treatment plays a role in the transition from anatase to brookite phase. The shorter the treatment time, the smaller the percentage of brookite in the sample. The opposite is the case when the treatment time is longer. Hence, there is the presence of brookite in the T-NF as opposed to T-NF due to the treatment time. The result of the pore size has resulted from the disparity in the duration of the hydrothermal treatment.

Table 4. 1: Crystal properties of TiO_2 nanostructures

TiO_2 nanostructures	2θ (°)	Crystal size (nm)
T-NT	37.7	8.3
T-NF	48.5	9
T-NS	9.78	8.3
T-AM	-	7.2

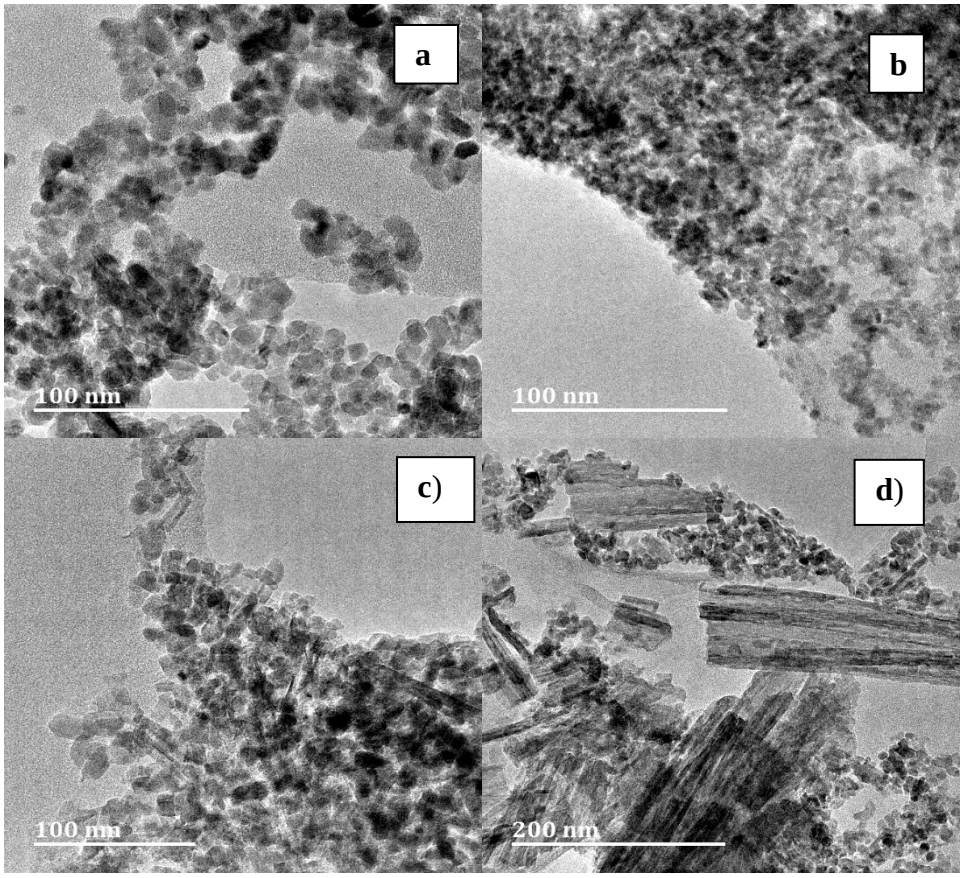

Figure 4. 3: TEM images for TiO_2 nanostructures a) T-AM b) T-NT c) T-NS and d) T-NF.

The morphology of the T-AM, T-NS, T-NF and T-NT samples is examined by TEM. TEM images are displayed in Fig. 4.3(a-d). TEM revealed that the hydrothermal treatment is efficient in the formation of TiO_2 nanostructures and they are successfully Synthesized. The T-AM Synthesized by the sol-gel method in Fig. 4.3(a) comprises particles of a diameter

between 4-6 nm and showed sphere-like TiO_2 nanoparticles. Changes in the precursor of TiO2 at the same temperature produced change in the obtained morphology, hence the Synthesized samples revealed different morphologies. Fig. 4.3(b) shows a cluster set of nanotubes (T-NT) that was achieved with the anatase TiO2 precursor. The T-NT (Fig. 4.3(c) shows a uniform nanotubular morphology with multilayered walls and diameter between 3-4 nm, with lengths of approximately 8 nm and open ends. The T-NF in Fig. 4. 3(d) consisted of a fiber-like morphology with diameters between approximately 8-10 nm and length between 15-20 nm. In summary, T-NF nanostructures are dense, longer and thicker than T-NT, while all TiO2 nanostructures are randomly orientated crystallites and are spherical.

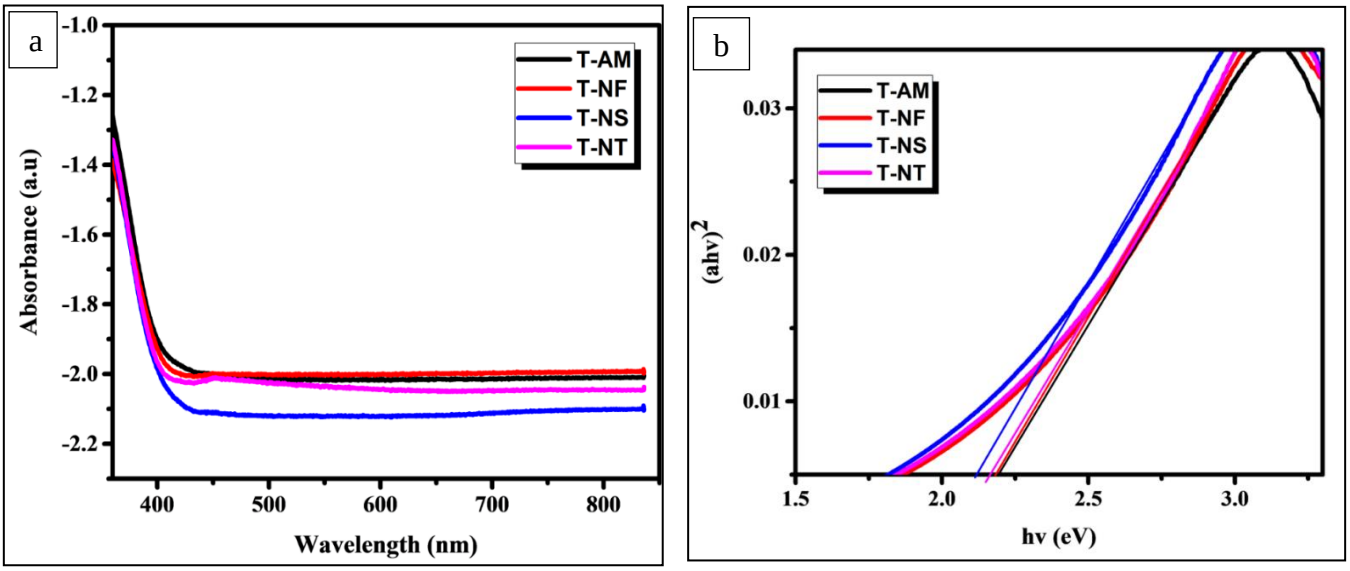

Figure 4. 4: (a) UV-Vis diffuse reflectance spectra of TiO_2 nanostructures (b) Tauc plot-Vis diffuse reflectance spectra of TiO_2 nanostructures.

UV-Vis diffuse reflectance spectra (DRS) of all TiO_2 nanostructures were recorded as shown in Fig. 4.4(a). The spectrum of all TiO_2 nanostructures shows a sharp peak at about 350 nm. According to DRS results, the light scattering from the materials occurs mostly in the UV region, which implies the materials are photoactive in this region. Additionally, the light scattering by T-AM and T-NF are higher than that of T-NT and T-NS which is consistent with the former's white colour. In comparison, the absorption edge of T-NF shows a notable red shift towards the visible region. This change can be due to the fact that the hydrothermal

and annealing treatment modified the UV-Vis absorption characteristics of the fiber structure. Tauc plots are shown in Fig. 4.4(b). Tauc plot is used to estimate the band gap energy of the materials proposed in equation (14).

$$(ahv)_2 = A\left(hv - E_g\right) \quad \textbf{(14)}$$

$E_g = \frac{1240}{\lambda}$ was used and $\boldsymbol{\lambda}$ implies the absorption edge; where a, hv, are the absorption coefficient photon energy constant and E_g is referred to band gap energy can be estimated from the intercept point between the x-axis line and the line tangent of the curve in the inflection point (Oseghe and Ofomaja 2018a). The E_g is an important parameter to evaluate the activity of the photocatalysts, where usually the materials with best performances are often shown by the materials that have the lowest E_g values (Martins *et al.* 2016). Materials T-NF and T-AM had the highest band gap energy while T-NS and T-NT had the least.

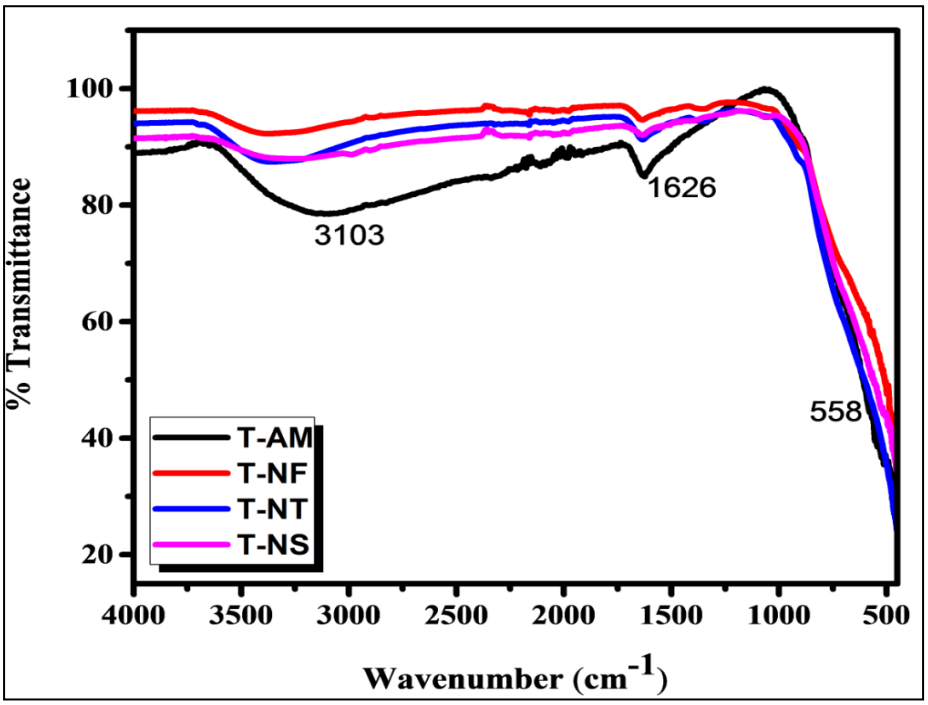

Figure 4. 5: FTIR spectra of TiO_2 nanostructures: T-AM; T-NF; T-NT and T-NS.

The FTIR analysis was carried out to identify the functional groups on the surface of the materials in Fig. 4.5. The results show two distinguished peaks distinctive to different functional groups spectra in the 500-4000 cm^{-1}. The region of the TiO_2 nanostructures investigated in this work featured at the peak 558 cm^{-1} corresponds to the O-Ti-O bonds. The peak observed at 1626 cm^{-1} corresponds to the O-H stretching and the broad peak at 3101 cm^{-1} corresponds to the O-H bending. This confirms that there is a molecule of water, which has been absorbed on the surface of the catalysts (Khairy and Zakaria 2014). This can be explained by creation of new active sites in the catalysts which results in higher activity of TiO2.

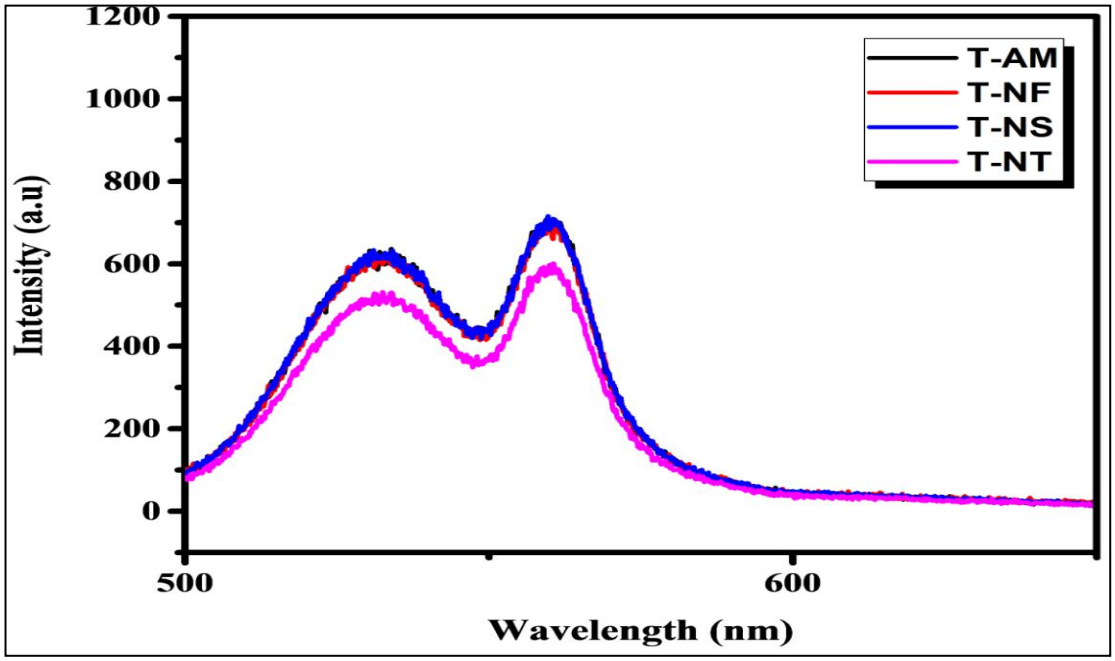

Figure 4. 6: Room temperature PL spectrum of TiO_2 nanostructures excitation wavelength of 360 nm.

PL spectroscopy is used to determine the photoluminescence properties and active sites on the surface of the catalysts. The PL spectrum of TiO_2 at room temperature is depicted in Fig. 4.6. Heterojunction is at an excitation wavelength of 360 nm. In the spectrum, two strong comparative emission peaks were observed at 530 and 570 nm in the visible region. The prominent emission peak at 419 nm corresponds to the direct recombination of photogenerated electrons and holes from conduction band at 530 and 570 nm originated from

the indirect recombination due to the oxygen vacancies thereby causing defects at the surface (Kumar et al. 2016).

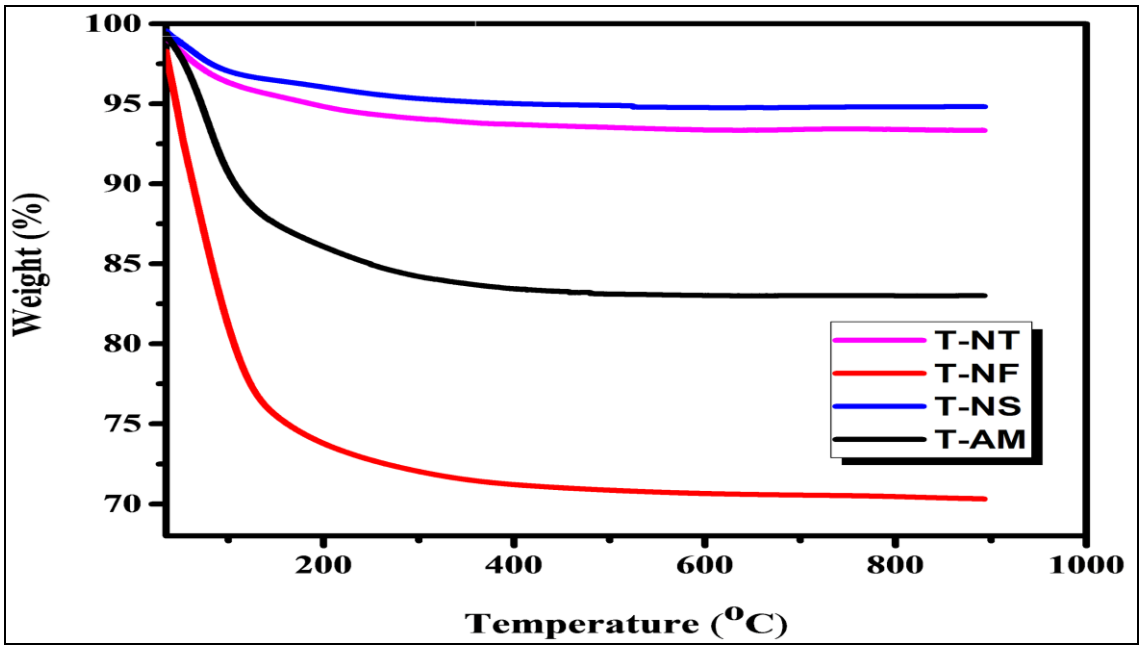

Figure 4. 7: Thermogravimetric analysis spectra recorded for TiO_2 nanostructures.

Fig. 4.7 shows the thermogravimetric analysis (TGA) thermograms of TiO_2 nanostructures at temperature 100-900 ˚C. The thermogram of T-NS displays a weight loss of 2.5 wt% at room temperature up to 150 ˚C, which corresponds to water evaporation and hydroxyl group on the materials and it is thermally most stable. A second weight loss of 4 wt% (T-NT) was observed from 100 ˚C up to 150 ˚C, which is associated with the removal of adsorbed water and may include the evaporation of a small amount of ethanol. The third weight loss (T-AM) of 15 wt% from 150 up to 200 ˚C is because of the TiIV alkoxide starting material which evaporates upon calcination resulting in a drop in the % weight loss. The fourth weight loss of 27.5 wt% in the range of 150 to 250 ˚C can be attributed to the desorption of the crystal water and the degradation of the skeletal $-CH_2-CH_2-CH_2-CH_3$ organic. The high percentage in case of T-NF can be explained by the higher purity and absence of ethanol as well as a loss

of TiO_2 in the centrifugation process and the duration of the alkaline hydrothermal which may have resulted in more surface adsorbed and hydroxyl group.

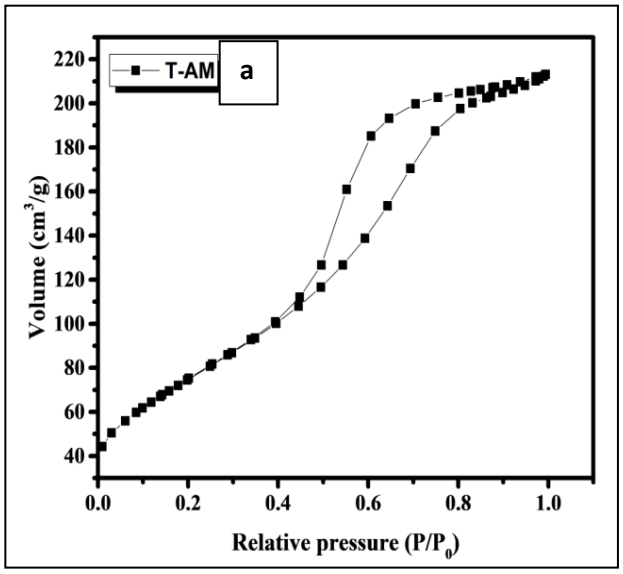
T-AM
a
Volume (cm3/g)
Relative pressure (P/P0)

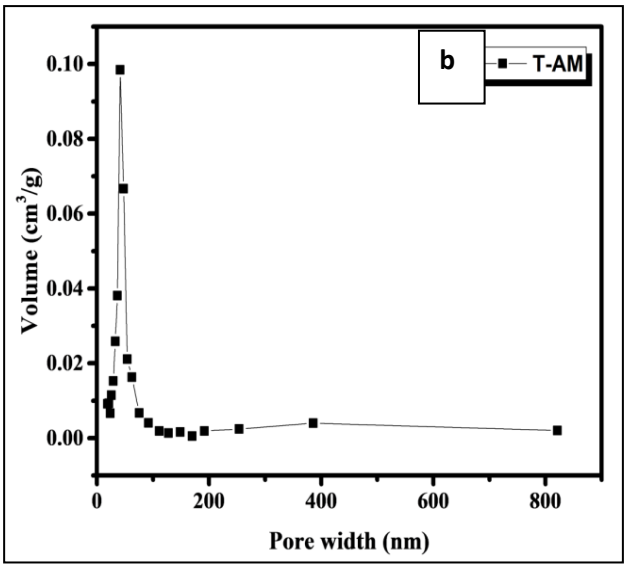
T-AM
b
Volume (cm3/g)
Pore width (nm)

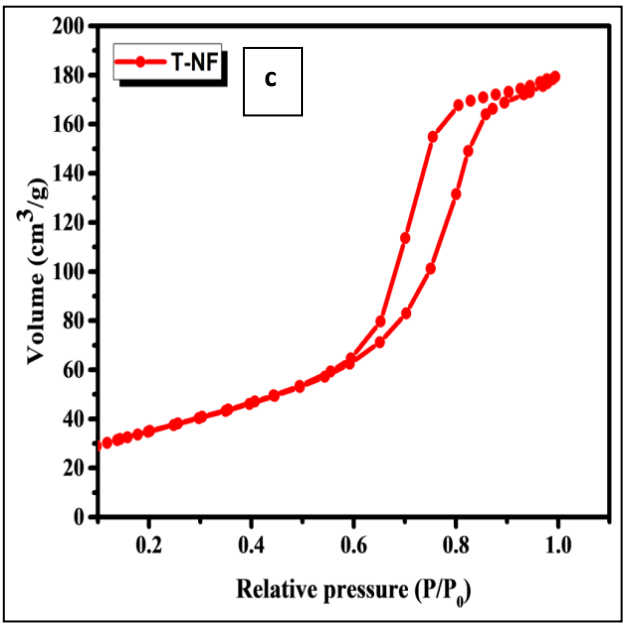
T-NF
c
Volume (cm3/g)
Relative pressure (P/P0)

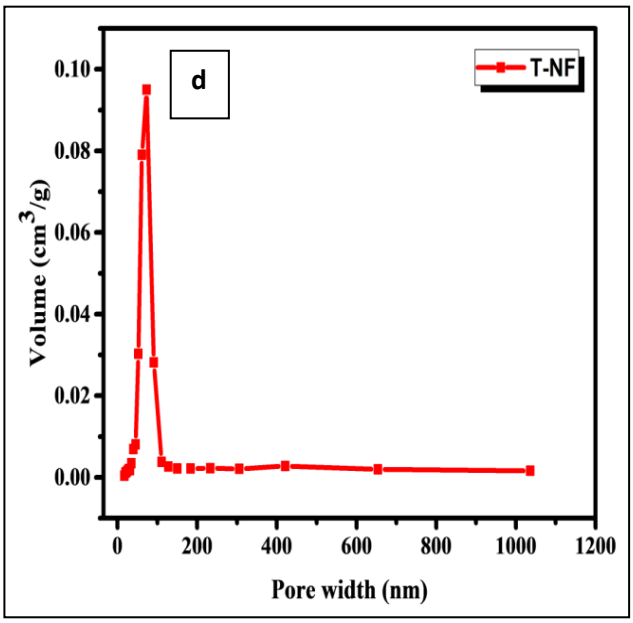
T-NF
d
Volume (cm3/g)
Pore width (nm)

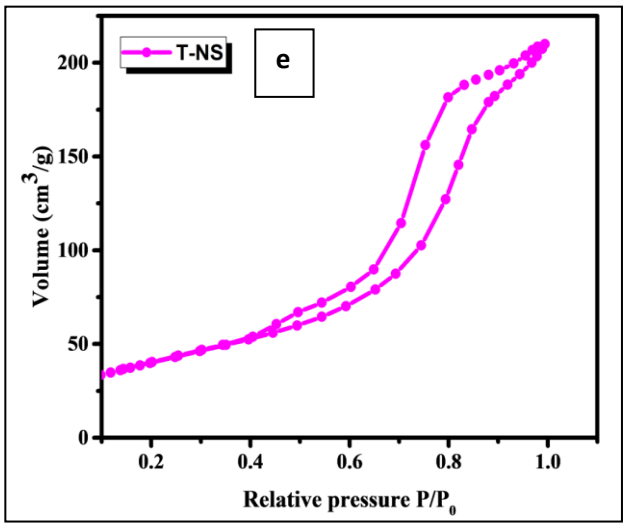
T-NS
e
Volume (cm3/g)
Relative pressure P/P0

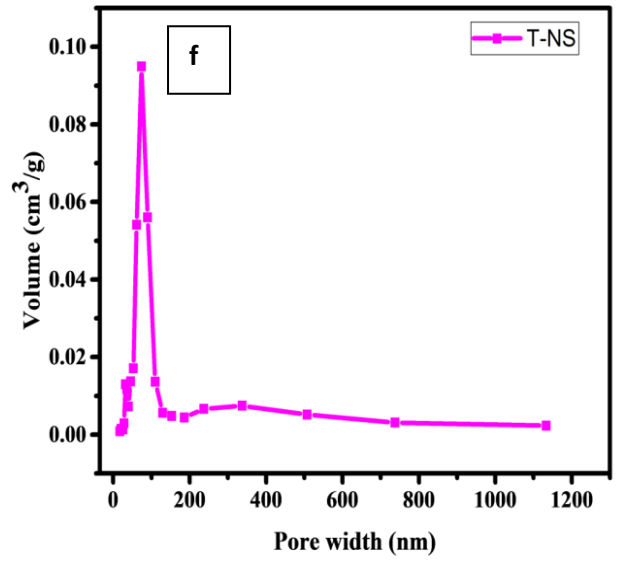
T-NS
f
Volume (cm3/g)
Pore width (nm)

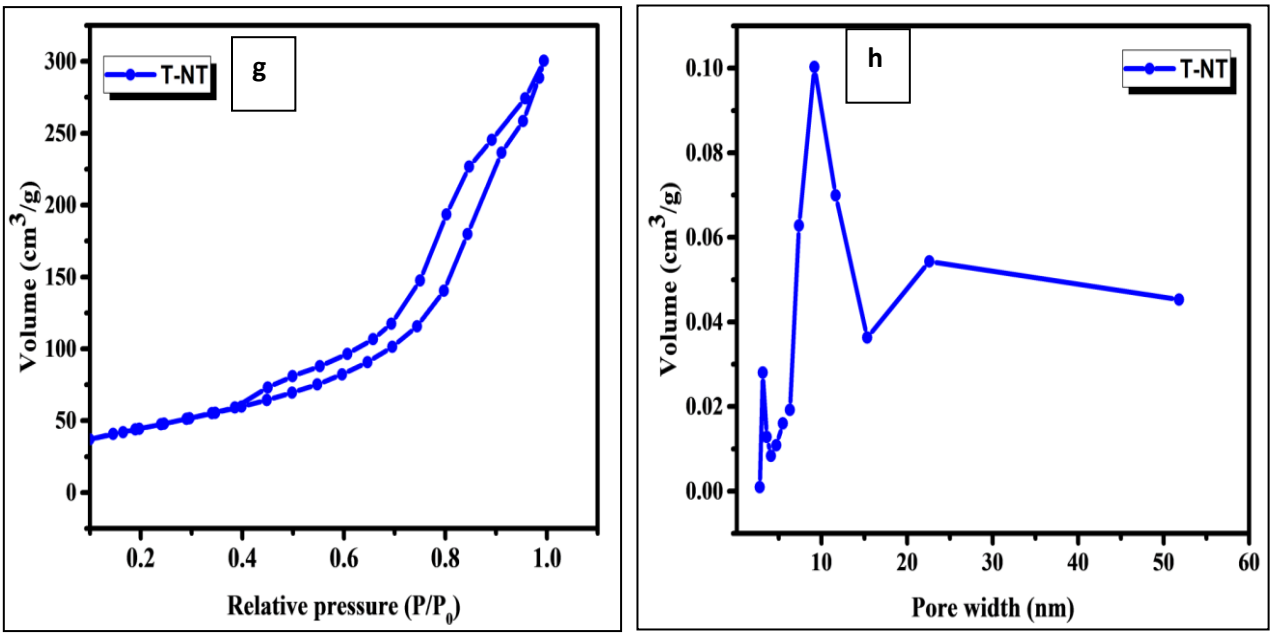

Figure 4. 8: (a-d) Nitrogen adsorption-desorption isotherms and corresponding DFT pore size distribution of TiO_2 nanostructures.

Fig. 4.8 shows the Brunauer-Emmett-Teller (BET) surface area and Barett-Joiner-Halenda pore structure of TiO_2 nanostructures. Samples are investigated by nitrogen adsorption-desorption isotherms. The BET surface area was found to be 162.53, 144.99, 274.37 and 126.59 cm^2/g for T-NT, T-NS, T-NF and T-AM, respectively. The isotherm for the Synthesized TiO_2 nanostructures shows characteristics of hysteresis loops. Therefore, they can be characterized as type IV isotherm (Khan et al. 2017), according to the International Union of Pure and Applied Chemistry (IUPAC) classification. The characteristic hysteresis loops at the relative pressure between 0.2 and 1 revealed the presence of mesopores nature of the Synthesized materials (Madurai Ramakrishnan et al. 2019). The pore size distribution analysis of TiO_2 nanostructures displays that it contains multiple pores, which could be attributed to the inner pore of the particles and the inner-pore between the particles and further it is found to be in the mesoporous range. Its average pore volume was found to be 0.33, 0.32, 0.46 and 0.28 cm^3/g for T-NT, T-NS, T-NF and T-AM respectively. In the T-NT sample, the smaller pores (<10 nm) could correspond to the pores inside of the nanotube, considering that the sizes of the pores are approximately equal to the inner diameter of this

nanostructure, as was seen in TEM images. Alternatively, the T-NF and T-NS samples exhibit a tri-modal pore size distribution. Very small pores (3-10 nm) and larger pores (100 nm) are apparent, which can be attributed to the voids in the aggregation of nanofibers (Rosales et al. 2019). Changes in average pore diameter can be caused by variations in aggregations that can be formed between the nanostructures.

Table 4. 2: Summary of BET specific surface and total pore volume at single point P/P0= 0.99 of TiO_2 nanostructures hydrothermally treated.

Sample	Surface BET (m^2/g)	Pore Volume (cm^3/g)
T-NT	162.53	0.46
T-NS	144.99	0.32
T-NF	274.37	0.33
T-AM	126.59	0.28

4.1.2 Photocatalytic activity results of TiO_2 nanostructures

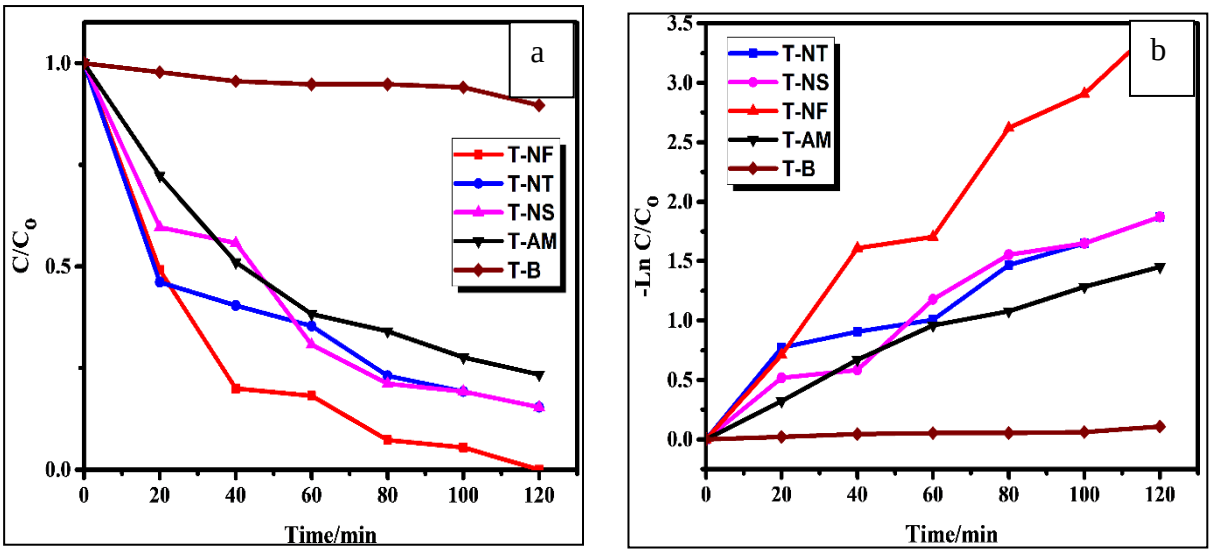

Figure 4. 9: a) Photocatalytic degradation of TiO_2 nanostructures in 5 mL TC without pH adjustment b) Kinetics pseudo 1st order of TiO_2 nanostructures.

The photocatalytic degradation of TC under LED light was carried out with the TiO_2 nanostructure catalysts. TC concentration did not decrease after equilibration in the dark for 1 hour, due to the lack of physical TC adsorption on the surface of TiO_2 nanostructures. The photocatalytic results under LED light are shown in Fig. 4.9 (a). The catalytic degradation rate under UV-Vis LED light reduced in the order of T-NF > T-NT >T-NS > T-AM > T-B (without catalyst). The T-NF photocatalyst displayed the maximum degradation up to (100%) under LED light in 120 min as compared to T-NT (85%), T-NS (85%), T-AM (77%) and T-B (12%) under similar experimental conditions. The photocatalytic experiments showed that the prepared unique T-NF is a promising catalyst in the field of environmental remediation.

The excellent catalytic activity of the T-NF can be attributed to its unique morphology, excellent crystallinity, small size, high surface area and enhanced visible light absorption. Generally, the photocatalytic efficiency of the catalyst strongly depends upon the surface area of the photocatalyst as the reactive species use to adsorb onto its surface. It has been reported that the photocatalytic activity of metal oxides is strongly dependent on their morphology properties (Rosales et al., 2019). For the T-B (without catalyst) the results show that TC could hardly be degraded after 120 min under LED light irradiation excluding the possibility of self-photolysis in this system. Kinetics of photocatalytic degradation of TC by TiO_2 nanostructures were investigated using the linear transform of Ln C_0/C = f(t) in Fig. 4.9 (b). The results showed that the photocatalysis kinetics follow pseudo-first order and it is the conversion of the photocatalytic degradation of TiO_2 nanostructures.

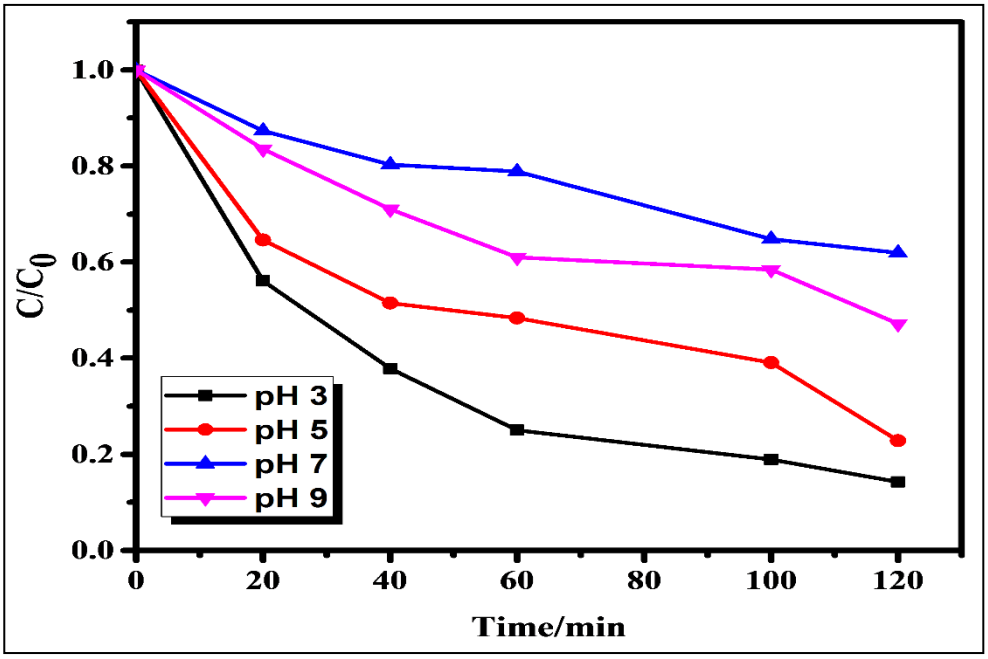

Figure 4. 10: Effect of pH on the degradation of TC by T-NF.

The effect of pH on the photocatalytic degradation of TC by T-NF under LED light was also studied in Fig. 4.10. The experiments were performed by varying the pH value from 3 to 9 using 0.1 M HCl and 0.1 M NaOH respectively. The pH is considered as a critical parameter in the photocatalytic degradation process. The photocatalytic activities of T-NF at pH 3, 5, 7 and 9 were (95%), (84%), (49%) and (64%) in 120 min respectively. According to the results, pH 3 showed a higher activity because the point of zero charge (pzc) for TiO_2 is at pH 6.5. Therefore, the TiO_2 surface is positively charged in acidic solution and negatively charged in basic solution. The acidic solution favours adsorption of tetracycline onto the photocatalyst surface.

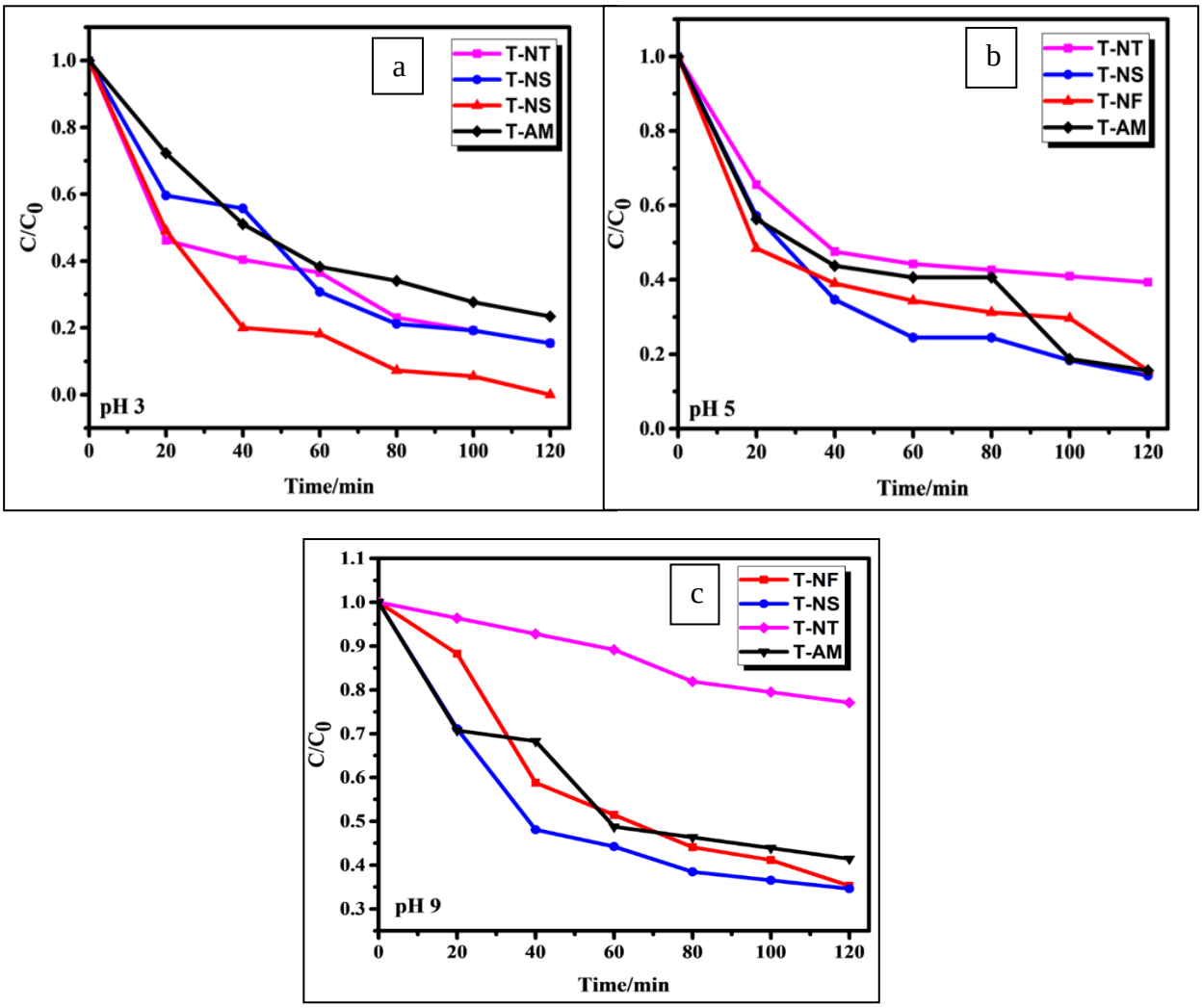

Figure 4. 11: % Degradation of TC for TiO_2 nanostructures samples at (a) pH 3; (b) pH 5 and (c) pH 9.

Three experiments were performed at different pH values (3, 5 and 9) in using HCl and NH_4OH to adjust the pH of the TC solutions respectively. In Fig. 4.11 (a), it is observed that the acidic pH 3 improves the removal conversion of TC principally in the T-NF sample it reached 100% conversion and T-NS reached 86% conversion in Fig. 4.11 (b) at acidic pH 5. The same is not observed for alkaline pH 9, where only the T-NS sample reached 65% conversion in Fig. 4.11 (c). Hence the pH is considered as a critical parameter in the photocatalytic degradation process (Camposeco *et al.* 2016). Although there are basic structural differences between T-NF and T-NS; differences such as shape, elemental compositions, surface and optical properties seem to be the main cause that the T-NS refers to cation vacancies with poor electron densities whilst T-NF present anion vacancies with rich

electron densities; these facts can be the reason of the different behaviours at pH 3, 5 and 9 in the photocatalytic degradation environment. Another explanation of the behaviour at pH 3, 5 and 9 in the solution for the T-NS and T-NF is that the zero-point charge of TiO_2 has been located between 5.8 and 6.8. The T-NF sample is positively charged on the surface below the pH at the zero-point charge and the molecules of TC are found negatively charged; this is the reason for the high conversion at pH 3.

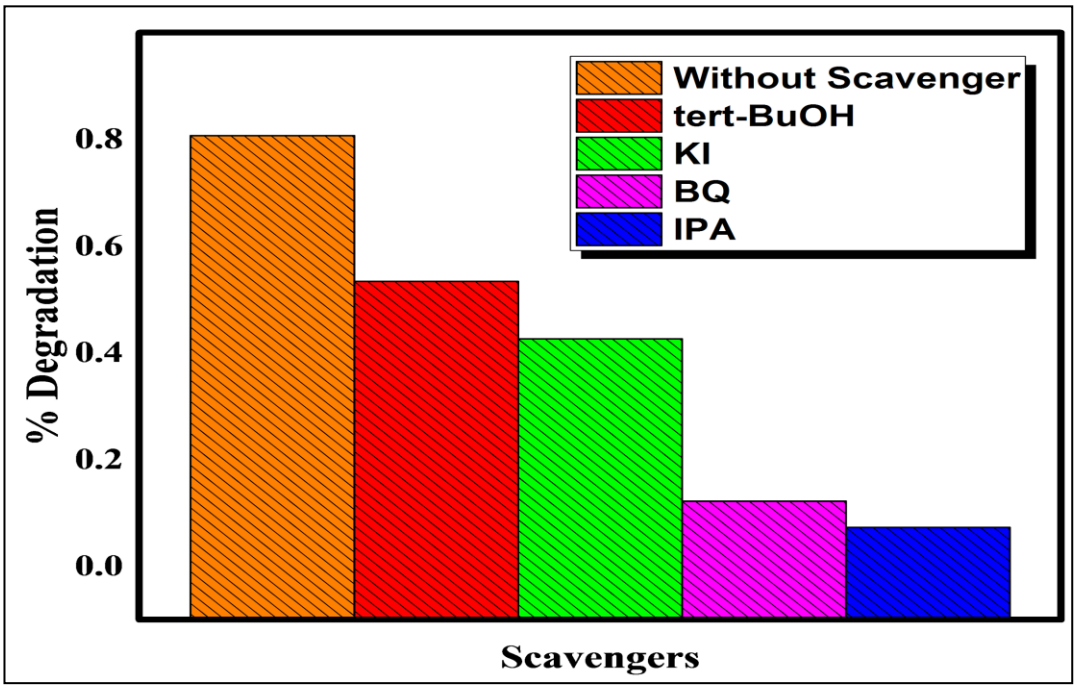

Figure 4. 12: Effect of various scavengers on photocatalytic degradation of TC using Synthesized T-NF (pH: 3, Photocatalyst dosage: 0.05 g/L, TC concentration: 5 mg/L, irradiation time: 120 min).

To investigate the role played by oxidant species and charge carriers on the mechanism of tetracycline degradation; the contribution of reactive species in degradation of TC by Synthesized T-NF catalyst was investigated by the addition of four different scavengers iso-propanol (13 M) (85.2%), tert-Butanol (10.42 M) (91.2%), potassium iodide (0.3 M) (80%) and benzoquinone (0.3 M) (85.3%) as electron, hydroxyl radical and hole scavengers. The effect of various scavengers on degradation efficiency of TC is presented in Fig. 4.12. The quenching effects of tert-BuOH, IPA, KI and BQ allow verifying the holes of the total

hydroxyl radicals both in the solution and the surface of the catalyst ($OH^{\bullet}$), the hydroxyl radicals in solution (OH_{free}), and $O_2^{\bullet}$ / $HO_2^{\bullet}$ radicals respectively. The degradation rate of TC sharply decreased upon addition of tert-BuOH and the removal of TC is achieved after 120 min of the reaction with 91.2 %. This result confirms the major use of hydroxyl radicals in TC degradation. However, iso-propanol was used as ($OH^{\bullet}$) scavenger to determine the role of adsorbed hydroxyl radicals and free radicals. The results showed minimal impact on the TC degradation, which means that only limited free radicals were present in the reaction system. When BQ was added to act as the $O_2^{-\bullet}$ radical the (85.3%) removal of TC degradation was observed. These results clearly demonstrated that adsorbed hydroxyl radicals, free radicals and $O_2^{-\bullet}$ radicals were formed in the T-NF catalytic reaction. Therefore, only the adsorbed hydroxyl radicals were the major reactive species responsible for the catalytic degradation of TC.

4.1.3 Reusability results of T-NF

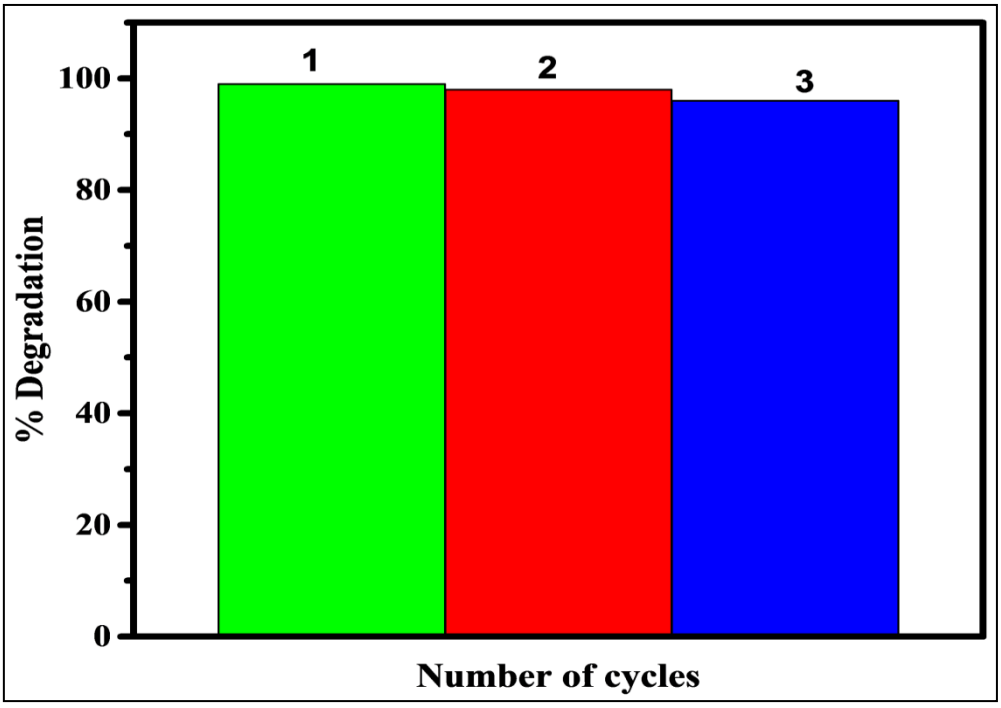

Figure 4. 13: Recyclability characteristics of T-NF in TC degradation.

The stability of the T-NF photocatalyst was evaluated by successive recycling. The experiment was carried out three times in similar conditions. After each run, the catalyst was separated from the reaction suspension and recovered, and then used for the next run; in which the operating conditions of 5 mg/L of TC, 0.05 g of T-NF catalyst and reaction time of 3 hours were applied for the photocatalytic performance and evaluated under LED light irradiation. The degradation achieved in our experiment is shown in Fig. 4.13. It can be deduced from the results that the Synthesized T-NF photocatalyst can maintain its efficiency, activity for several reuses and it is efficient for reducing water pollutant. From experimental results it is seen that degradation rate efficiency of T-NF is better than reused ones. Although reused catalysts also show good catalytic performance for degradation of TC, they can be used three times without having remarkable change in their degradation efficiency (Khan *et al.* 2017).

4.1.4 Electrochemical results of TiO_2 nanostructures

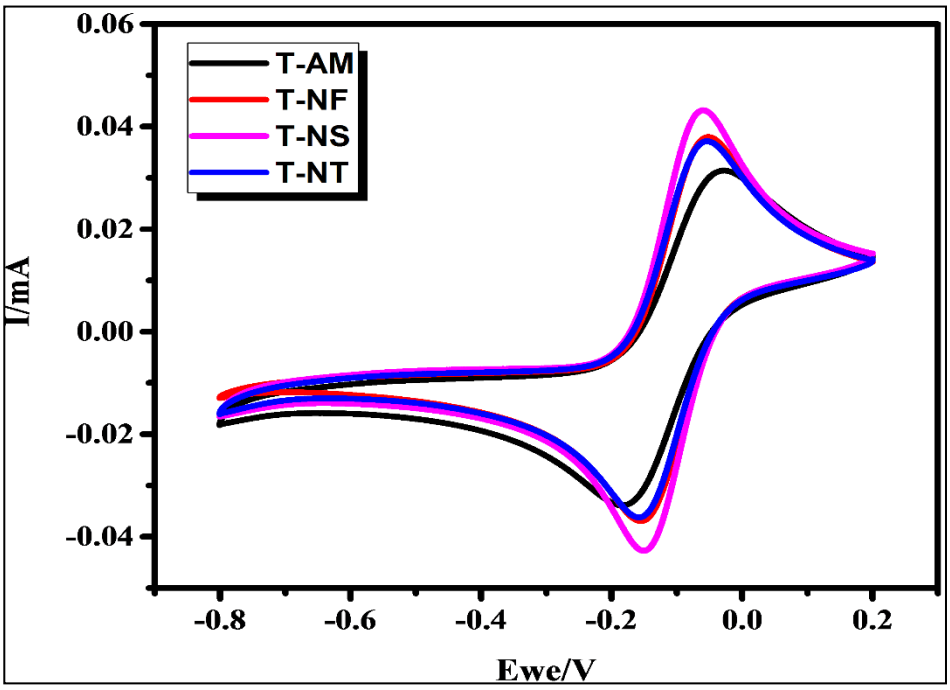

Figure 4. 14: Cyclic voltamograms of TiO_2 nanostructures.

Cyclic voltammetry (CV) was performed to characterize materials in contact with de-aerated electrolyte. TiO_2 nanostructures curves are presented in Figure 4.14. The working electrode was polarized from the rest potential in the anodic direction up to 0.04 mA and back up to -1.0 V. In general, the CV shape for all the TiO_2 nanostructures is typical for anatase structure of TiO_2 nanoparticles materials that is characterized with a very low capacitive current in the anodic potential range but in the cathodic range much rich electrochemical activity is observed (Sobczyński *et al.* 2004). In the negative range, one reduction peak is recorded. According to Bertoluzzi *et al.* (2013) the peak located at -0.18 V could be assigned to the filling of narrow deep trap states. As it could be clearly noticed, CV curves registered for TiO_2 nanostructures differ from each other considering the position of cathodic peak and value of current density.

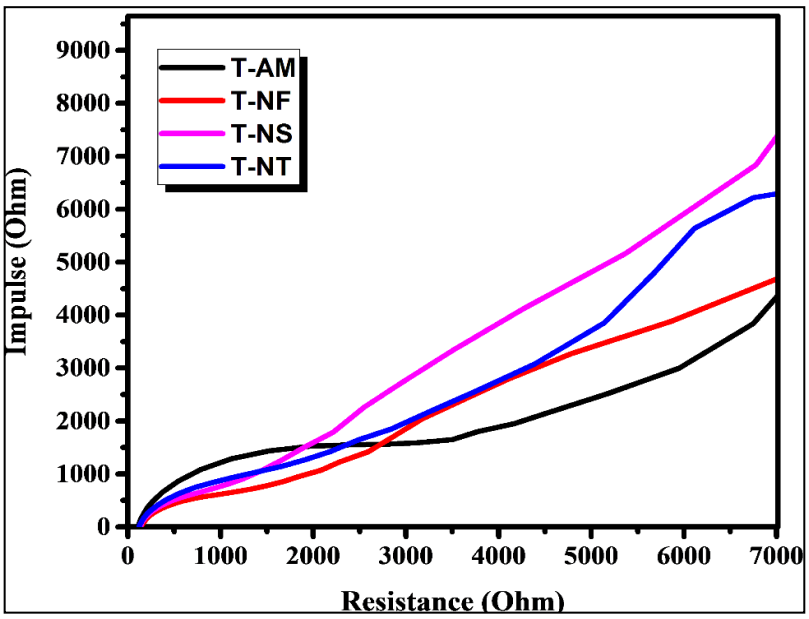

Figure 4. 15: Nyquist plot for the TiO_2 nanostructures.

Fig. 4.15 shows the EIS Nyquist plot of the materials in 0.1 M $K_3[Fe(CN)_6]$ aqueous solution. The Nyquist plot gives information on the charge transfer properties of a semiconductor, such that the radius of the arc on the EIS spectra explains the charge resistance. The reverse is the case when the radius is larger. It can be observed in Fig. 4.15 that the charge transfer resistance of the materials decreased in the order of T-AM >T-NT > T-NS > T-NF. This implies that in the T-NF material there will be a relatively more photogenerated electron-hole separation due to its comparatively fast interfacial charge transfer. Therefore, it is expected that T-NF will be more efficient in the photocatalytic degradation of TC.

4.2 Characterization of CDs/TiO_2 composite nanofiber (CD/TNF)

This section of results discusses the performance and most photocatalytic TiO_2 nanostructure in tetracycline solution. It was found from the previous section of results that T-NF is the most photocatalytic. Therefore, in this section T-NF is doped with carbon dots and we have a successfully Synthesized CD/TNF composite nanofiber material, and the results are discussed in this section.

4.2.1 Characterization results of CD/TNF

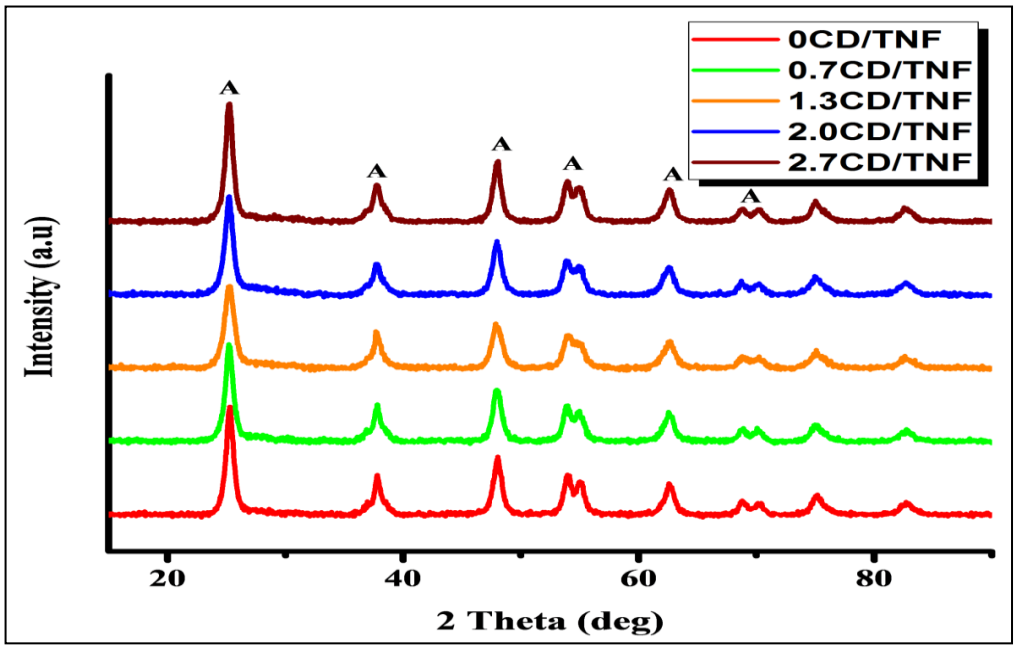

Figure 4. 16: XRD diffraction patterns of CDs/TiO_2 composite nanofiber.

The crystalline structures of CDs/TiO_2 composite nanofiber were investigated by the X-ray diffraction as shown in Fig. 4.16. The composite exhibit strong and sharp diffraction peaks at $2\boldsymbol{\theta}$ values of 25.3˚, 37.8˚, 47.97˚ and 54.15˚ corresponding to the planes of [101], [004], [2 0 0] and [211], respectively. When we increased the CDs content of sample no further characteristic diffraction peaks detected from CDs could be found in CDs/TiO_2 composite nanofiber on the XRD pattern which may be due to their high dispersion and poor crystallinity of doped CDs. By applying the Scherrer equation in $2\boldsymbol{\theta}$ = 25.3˚ and the [101] reflection of the anatase phase was found that the crystallite size for CDs/TiO_2 composite nanofiber was found to be 9.1 nm for the 0CD/TNF sample, 11.2 nm for the 0.7CD/TNF sample, 10.1 nm for 1.3CD/TNF and 2.0CD/TNF samples and 12.6 nm for the 2.7CD/TNF.

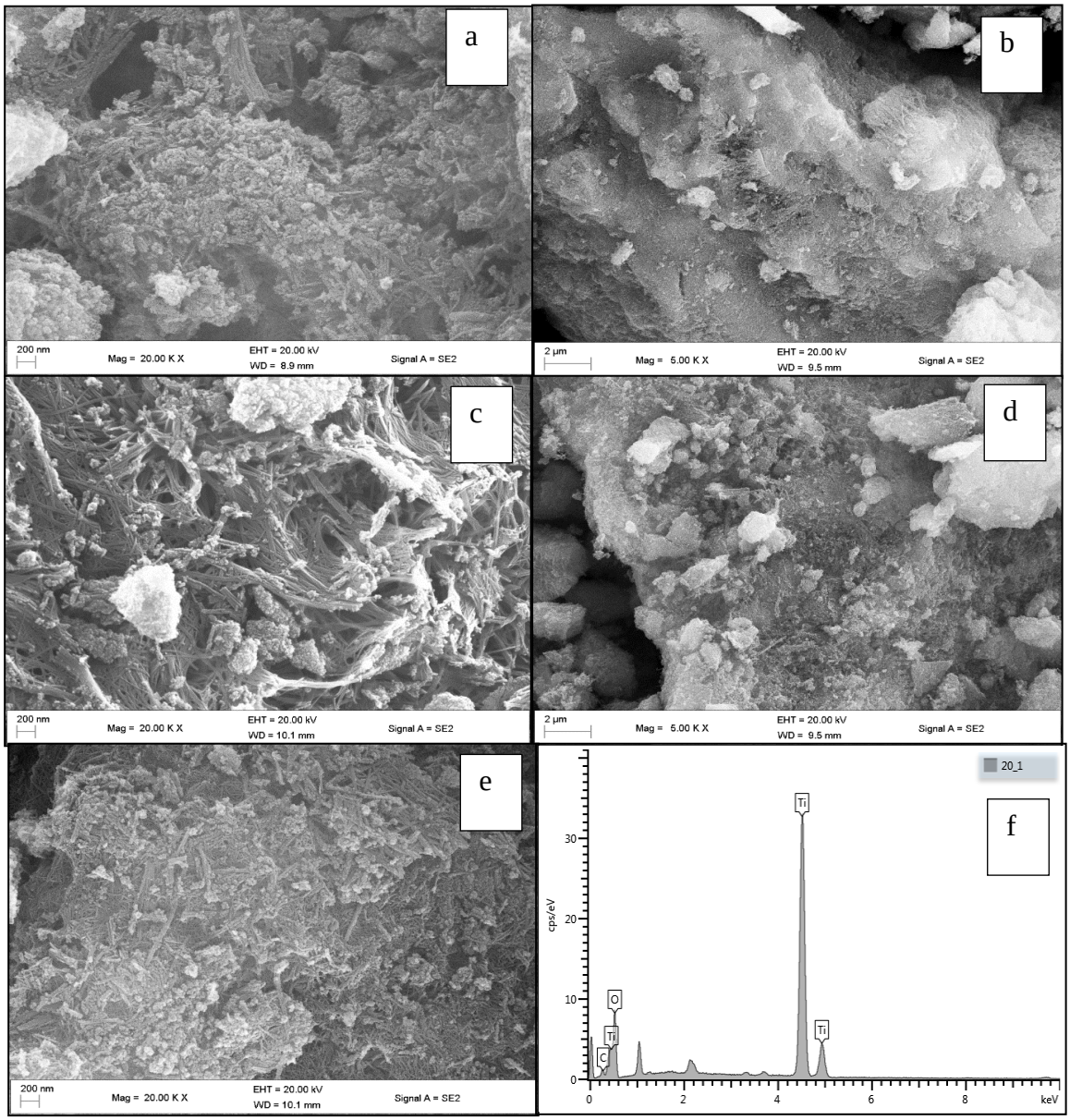

Figure 4. 17: The SEM images of CDs/TiO_2 composite nanofiber a) 0CD/TNF b) 0.7CD/TNF c) 1.3CD/TNF d) 2.0CD/TNF e) 2.7CD/TNF and f) EDX spectra for the 1.3CD/TNF.

To investigate the morphologies and structures of CDs/TiO_2, SEM images were provided in Fig. 4.17 (a-e). The SEM micrographs of 0CD/TNF in Fig. 4.17(a) have fibers-like particles with high aggregation. Fig. 4.17 (b) & (d) showed fiber-like particles of CDs much clearer which are agglomerate. In Fig. 4.17 (c) the CDs were able to be incorporated on the surface of TiO_2-nanofibers. Due to the loading of CDs in Fig. 4.17 (e), their distribution could be

seen on the fibers as packed clusters and the particles are agglomerate. Meanwhile, Fig. 4.17 (f) shows EDS spectrum of CDs/TiO_2 would be the least due to the presence of CDs would be the least due to the presence of CDs.

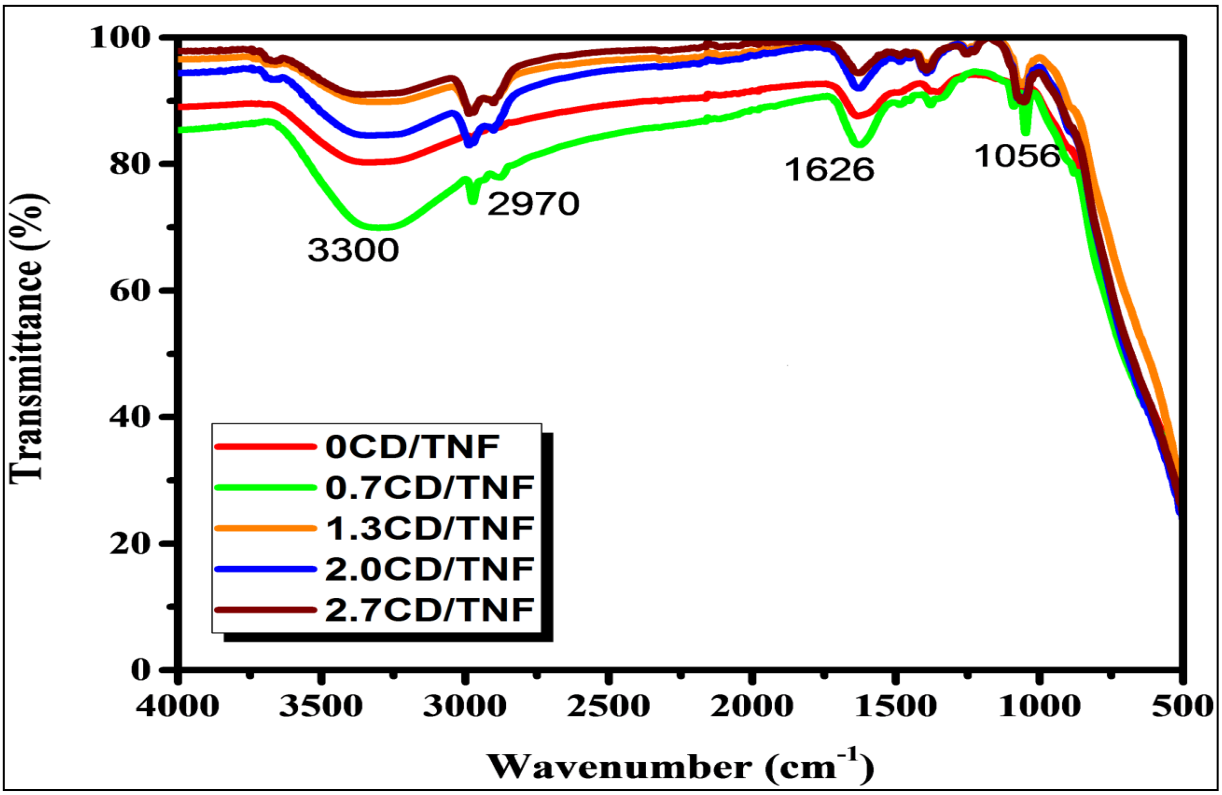

Figure 4. 18: FTIR spectra of CDs/TiO_2 composite nanofiber.

Fourier transform infrared (FTIR) spectra were used to further confirm the functional groups present in the CDs/TiO_2 composite nanofiber (CD/TNF) materials. As shown in Fig. 4.18, it can be clearly seen that the FTIR spectra of CD/TNF composite materials exhibits a strong and broad hydroxyl O-H stretching vibrations and O-H bending due to the functional groups or physically adsorbed water molecules were attributed at 3300 cm^{-1} and 1626 cm^{-1} respectively. Moreover, the small shoulder at 2970 cm^{-1} is assigned to the C-H as-symmetric and symmetric stretching. On the other side, the absorption band below 1000 cm^{-1} which indicates the presence of TiO_2 is attributed to the combination of the Ti-O-Ti and Ti-O-C vibrations and suggests that the coupling of TiO_2 and CDs is achieved by the formation of the Ti-O-C bond. These results indicate that the as-prepared composite consist of CDs and TiO_2.

Therefore, the as-prepared CD/TNF composite nanofiber have excellent stability in water due to the functional groups present in CD/TNF composite nanofiber.

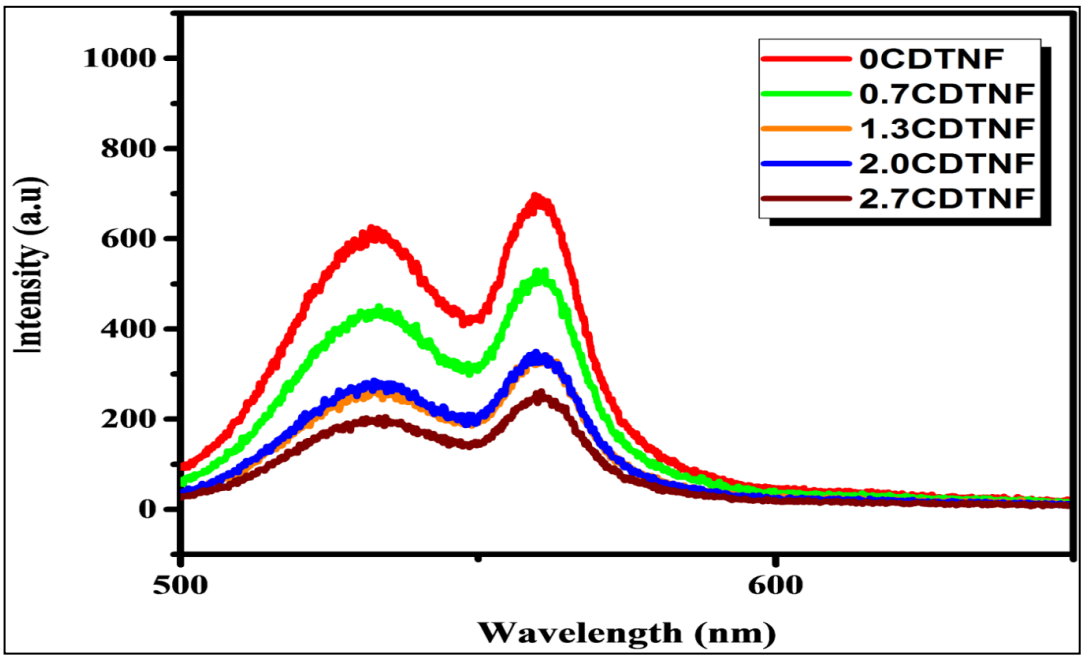

Figure 4. 19: PL spectrum of CDs/TiO_2 composite nanofiber under the excitation wavelength of 360 nm.

The PL emission spectra of CDs/TiO_2 composite nanofiber (CD/TNF) materials were taken to understand the recombination rate of electron-hole or separation efficiency of charge carriers trapping, migration and transfer, as shown in Fig. 4.19. Generally, a stronger PL intensity represents a higher recombination rate of electron-hole pairs under visible light irradiation. As shown in Fig. 4.19, all the composite nanofiber materials show a broad PL emission spectrum in the 500-600 nm region, which can be assigned to the radiative recombination of self-trapped exciting. It is noted that 2.7CD/TNF and 1.3CD/TNF have the greatest ability to absorb light in the observation wavelength range (500-600 nm) as compared to the other CD/TNF composite materials. Therefore, it can be observed that 2.7CD/TNF and 1.3CD/TNF exhibit lower emission intensity than that of 0CD/TNF. The lower PL intensity indicates low recombination rate, which is preferable in case of utilizing the materials as catalyst in photoreactions. Since 2.7CD/TNF and 1.3CD/TNF exhibit lower emission intensity than that of 0CD/TNF, it can be concluded that the introduction of carbon

dots (CDs) can efficiently accelerate the separation of electron-hole pairs. Hence, 2.7CD/TNF and 1.3CD/TNF are more 0CD/TNF.

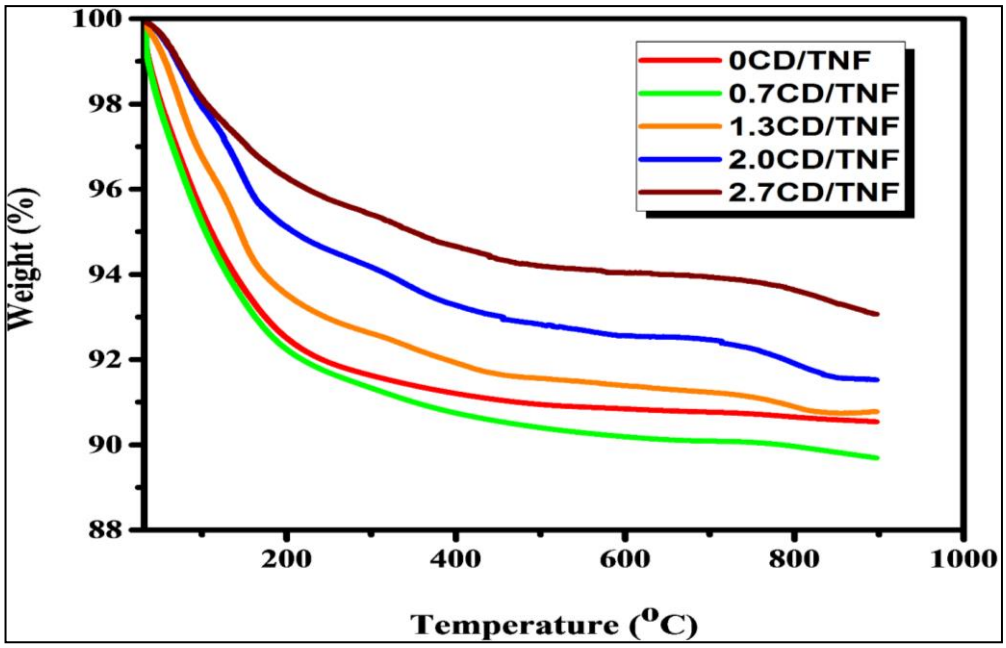

Figure 4. 20: The TGA curves of CD/ TiO_2 composite nanofiber.

The Thermogravimetric analysis (TGA) curves of all CD/TNF composites were shown in Fig. 4.20 to determine the number of CDs loaded on CD/TNF composites. The CD/TNF composites were thermally stable as compared to TNF which is good for the practical applications; the weight losses are larger than that of TNF. All the curves showed two stages of weight losses below 300 ˚C, the 8% 0.7CD/TNF, 7.8% 0CD/TNF, 6.2% 1.3CD/TNF, 4.2% 2.0CD/TNF and 3% 2.7CD/TNF weight losses are contributed to the water removal of adsorbed water. 500 ˚C to 900 ˚C corresponds to a larger endothermic peak which resulted from the removal of CD in the composites since the catalysts start to evaporate at 500 ˚C. Meanwhile there are no exothermic peaks at around 450 ˚C appearing on the curve. The weight losses were mainly due to the surface attached, -OH groups and residual organic compound. Therefore, the weight loss observed in all the CD/TNF composites can be assigned to the combustion of CDs. In the process of combining CDs aqueous solution with TiO_2-nanofiber (TNF) in the reaction solution, as the concentration of CDs increases, CDs increases the probability of the combination of the two by interaction between the surface

groups and TNF. The actual compound proportion of CDs and TNF will affect the factors above.

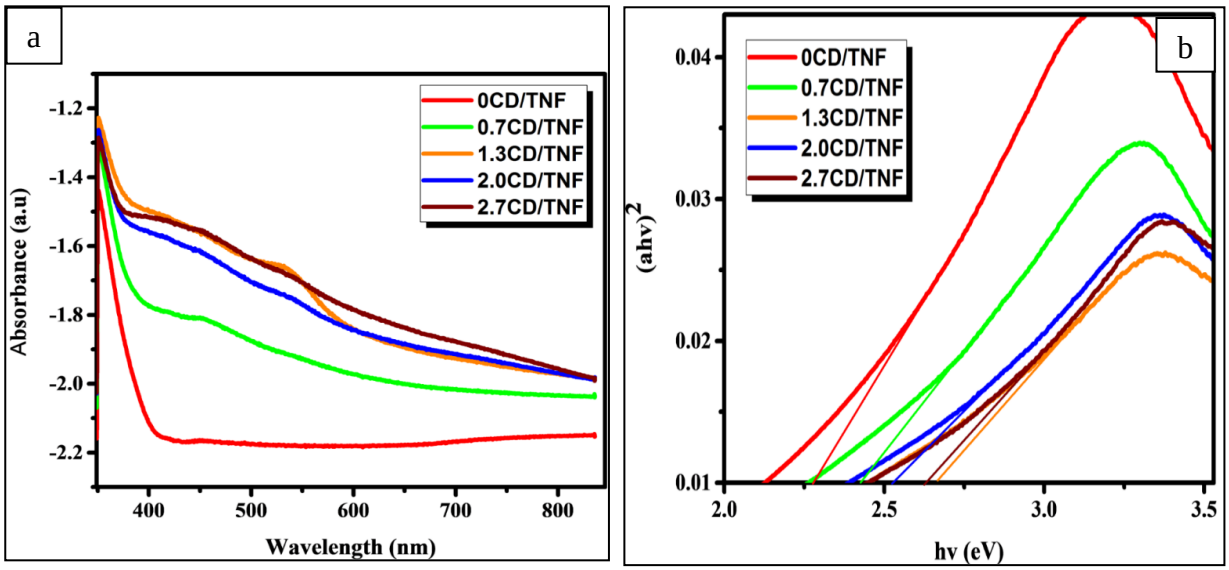

Figure 4. 21: UV-Vis diffuse reflectance (a) and Tauc plots (b) to the CDs/ TiO_2 composite nanofiber.

To investigate the optical absorption properties of CDs/TiO_2 composite nanofiber (CD/TNF) photocatalysts in order to disclose the uses of CQDs for further excellent visible photocatalytic of CD/TNF composites, the UV-Vis diffuse reflectance spectra were performed as seen in Fig. 4.21 (a). Merging of CDs on the surface of the TNF photocatalyst caused considerable optical response in the visible range. As presented in Fig. 4.21 (a) for all CD/TNF samples, a substantial absorption edge is around 410 nm. Above all, after the addition of CDs, the CD/TNF composite materials give a clear advanced absorption in the visible region, which is effective to improve photocatalytic efficiency. Whilst, according to the tauc plot equation (2), the band gap energies of 0CD/TNF, 0.7CD/TNF, 2.0CD/TNF, 1.3CD/TNF and 2.7CD/TNF composite materials are approximated to be 2.28 eV, 2.43 eV, 2.67 eV, 2.54 eV and 2.63 eV respectively in Fig. 4.21 (b). It is important to mention that the reduction of the band gap of CDs/TiO_2 is achieved by manipulating the synthesis conditions during the sol-gel and hydrothermal methods.

4.2.2 Photocatalytic activity results of CD/TNF

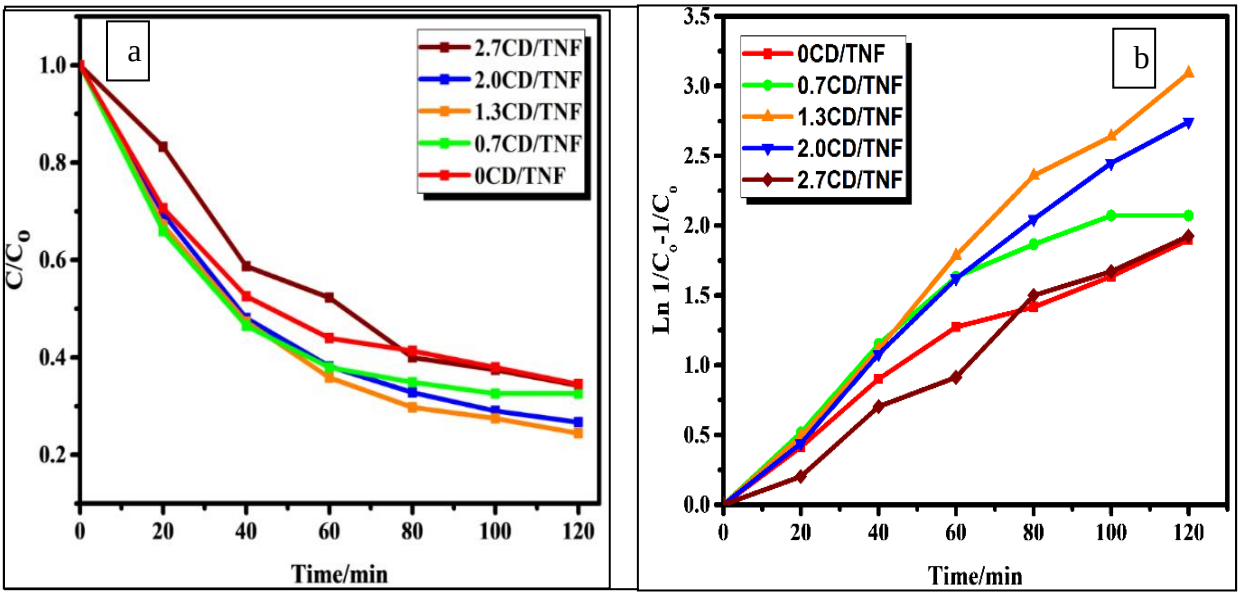

Figure 4. 22: a) The photocatalytic degradation of tetracycline under visible light irradiation CDs/TiO_2 composite nanofiber b) Degradation 2nd order kinetics by CDs/TiO_2 composite nanofiber.

The photocatalytic activities of the CDs/TiO_2 composite nanofiber (CD/TNF) materials were evaluated from photodegradation of TC solution under UV-Vis light irradiation as shown in Fig. 4.22. Initially, before switching on the LED, the light suspensions were stirred under dark conditions for 1 hour to attain adsorption-desorption equilibrium (Martins *et al.* 2017). Insignificant adsorption of TC on the materials was observed after equilibrium. After 2 hours of the photocatalytic experiment, amongst the material Synthesized, 1.3CD/TNF exhibited the best photocatalytic performance (76%) while 0CD/TNF had the least performance (65%). Therefore, the existence of carbon in the material (0.7 CD/TNF and 1.3CD/TNF) helped in improving the photocatalytic performance of TiO_2 by acting as an electron sink. However, there was a slight drop in the photocatalytic performance as the amount of CD on the TNF increased (2.0 CD/TNF and 2.7 CD/TNF). This may have resulted from an excessive amount of CD on the TNF such that CD becomes the site for electron-hole recombination. Oseghe

and Ofomaja (2018) also reported a reduced electron-hole recombination and improved photocatalytic degradation of methylene-blue when carbon dots were added on TiO_2. In addition, TC degradation by the photocatalysts followed a pseudo-second-order kinetic model as shown in Fig. 4.22 (b). 1.3CD/TNF photocatalyst yielded a rate constant (0.0025 $Lmg^{-1}min^{-1}$) for degradation which was higher than 0CD/TNF, 0.7CD/TNF, 2.0CD/TNF and 2.7CD/TNF photocatalyst respectively. This further suggests that 1.3CD/TNF exhibited high photocatalytic performance.

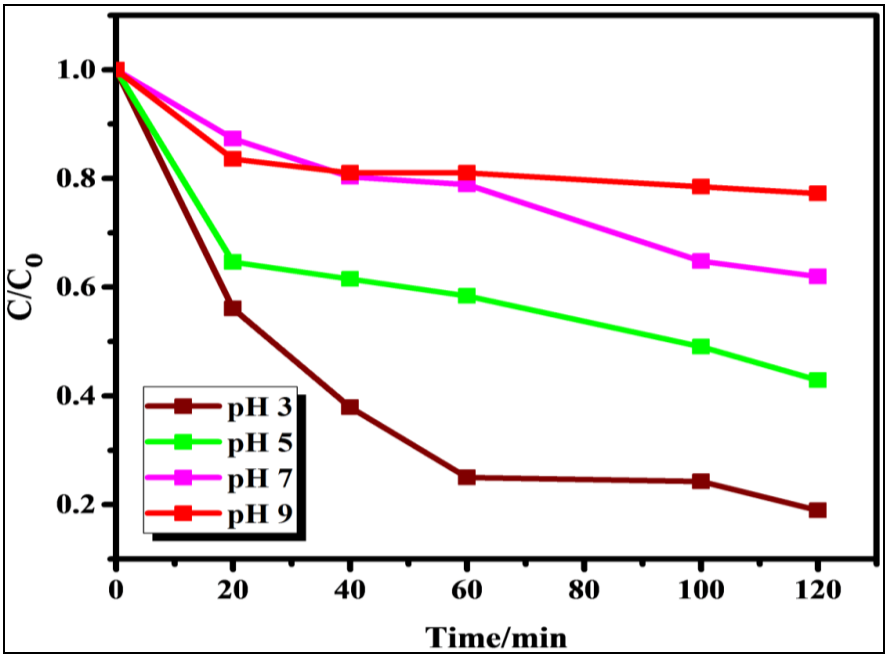

Figure 4. 23: The effect of pH on the degradation of TC by 1.3CD/TNF composite nanofiber.

The effect of pH on the visible LED light photocatalytic degradation of TC was studied as shown in Fig. 4.23. The pH value could affect the photocatalytic activity of the 1.3CD/TNF composite nanofiber as is considered to be one of the most important factors. The 1.3CD/TNF composite exhibited the best photocatalytic activity at pH value of 3. This means the catalyst is able to degrade TC under acidic conditions to produce more hydroxyl radicals on the surface of the catalyst. On the other hand, the potential of hydroxyl radicals for oxidation of organic pollutants at the low pH values is more than basic conditions.

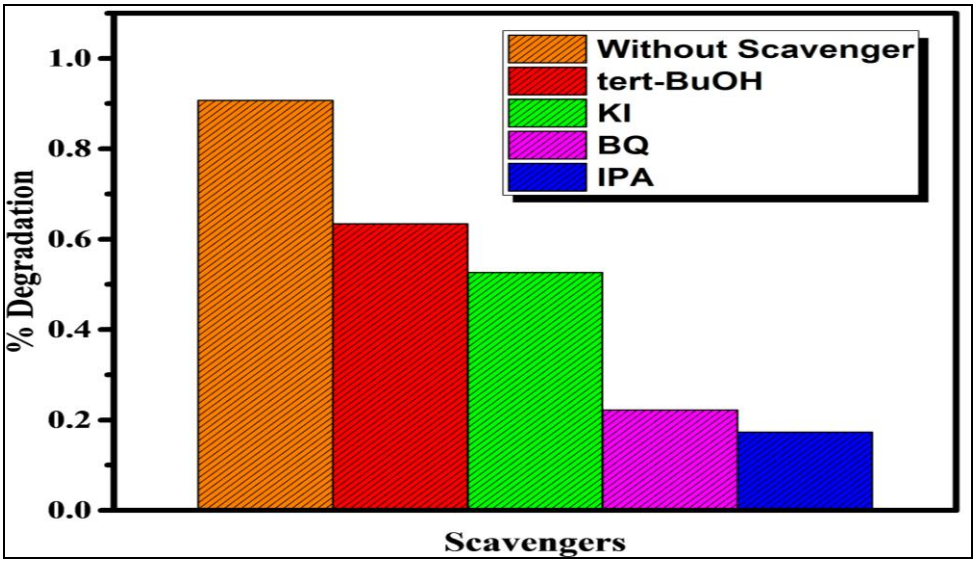

Figure 4. 24: Trapping experiment of active species during the photocatalytic degradation of TC over CDs/TiO_2 composite nanofiber.

It is important to determine the main active species in the photocatalytic reaction process. Four sacrificial agents including isopropanol (IPA), tert-Butanol (tert-BuOH), potassium iodide (KI) and benzoquinone (BQ) were applied as $OH^{\bullet}$, H^{+} and $O_2^{\bullet-}$ scavengers respectively (Fig. 4.24). It can be seen that with 0.3 M of KI as a H^{+} scavenger added into the solution, the degradation rate of TC over 76% 1.3CD/TNF sample is not obviously affected indicating that the H^{+} is not the main reactive species. However, when IPA as $OH^{\bullet}$ scavenger and BQ as $O_2^{\bullet-}$ scavenger are applied, the photodegradation process slowed down and it indicates the main reactive species. We can conclude that all reactive species shows effect on the photocatalytic performance. However, hydroxyl and superoxide radical had higher activity on their performance than H^{+} radicals. The result of trapping experiment reveals that the $OH^{\bullet}$ and $O_2^{\bullet-}$ radicals take more important effects in photocatalysis process. The electrons and holes of T-NF can be separated efficiently under visible light irradiation, where the electrons are transferred to the conduction band (CB), leaving the holes on the valence band. Generally, these photo-generated electrons and holes would quickly recombine and only a spot of charges could take part in the photocatalytic reaction. Significantly, after combining CDs with the highly active facets of T-NF to form 1.3CD/TNF composite, large numbers of the CDs consequently the electrons on the CDs readily combine with oxygen in the solution to

form $O_2^{\bullet-}$, which is a strong oxidizing agent to degrade TC, resulting in efficient electron-hole pairs separation and thus an enhanced photocatalytic activity.

4.2.3 Reusability results of CD/TNF

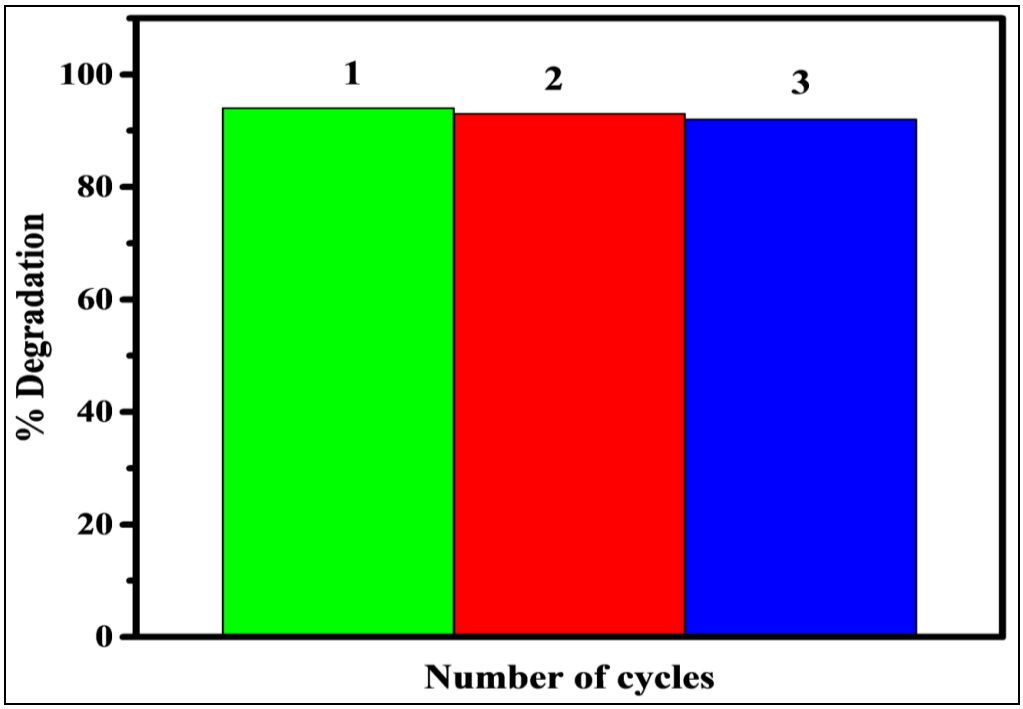

Figure 4. 25: The catalytic reusability of up to three cycles over CDs/TiO_2 composite nanofiber.

For investigating 1.3CD/TNF composite material, the photocatalytic degradation of TC under UV-Vis light irradiation was performed during 3 cycles. As seen in Fig. 4.25, the photodegradation efficiency of 1.3CD/TNF composite on TC suggests reuse of photocatalyst in the photocatalytic process and showed no significant changes up to three cycles. This suggests that the photocatalytic activity has good reusability, considerable stability and being of significance for industrial use of the photocatalyst. Therefore, this study indicates that the structure of the 1.3CD/TNF composite was not affected or chemically transformed to other organic compounds during the photocatalytic process. Hence the 1.3CD/TNF composite has

good reproducibility photocatalytic activity towards photocatalytic degradation of TC under UV-Vis light irradiation, which is of great significance for practical use.

4.2.4 Electrochemical results of CD/TNF

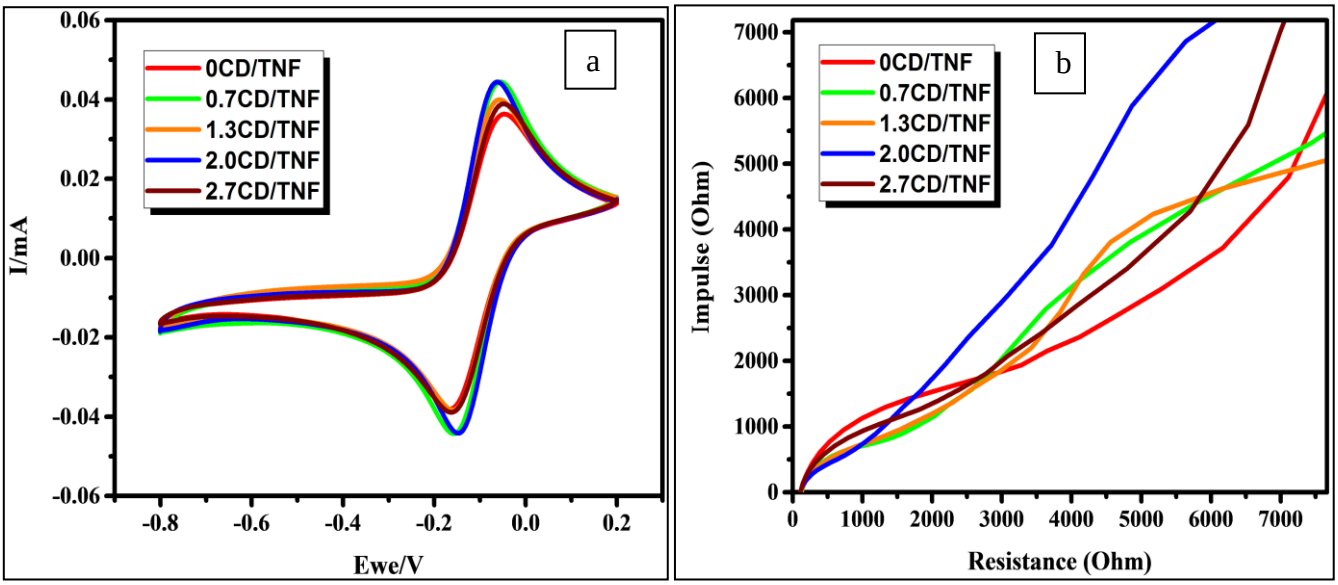

Figure 4. 26: a) Cyclic voltamograms of CDs/TiO_2 composite nanofiber b) Nyquist plot for the CDs/TiO_2 composite nanofiber.

Cyclic voltammetry (CV) was performed to characterize CD/TNF composite nanofiber materials in contact with a deaerated electrolyte. CD/TNF composite nanofiber curves are shown in Fig. 4.26 (a) The working electrode was polarized from the rest potential in the anodic direction up to 0.04 mA and back up to -0.1 V. In the first cycle, the first cathodic peak at -0.1 V is generally ascribed to an irreversible reduction peak. The reduction peak could be assigned to the filling of narrow deep trap states. Fig 4.26 (b) shows the EIS Nyquist plot of the CD/TNF composite material in 0.1 M $K_3[Fe(CN)_6]$ aqueous solution. The Nyquist plot gives information on the charge transfer properties of a semiconductor, such that the radius is larger. It can be observed in Fig. 4.26 (b) that the charge transfer resistance of the CD/TNF composite nanofiber materials decreased in the order of 2.0 CD/TNF > 2.7 CD/TNF > 0 CD/TNF > 0.7 CD/TNF > 1.3 CD/TNF. This implies that in the 1.3 CD/TNF composite nanofiber there will be a relatively more photogenerated electron-hole separation due to its

comparatively fast interfacial charge transfer. Therefore, it is confirmed that 1.3 CD/TNF is the most photocatalytic degradation of TC.

-50 min (pure tetracycline solution without the catalyst (blank))

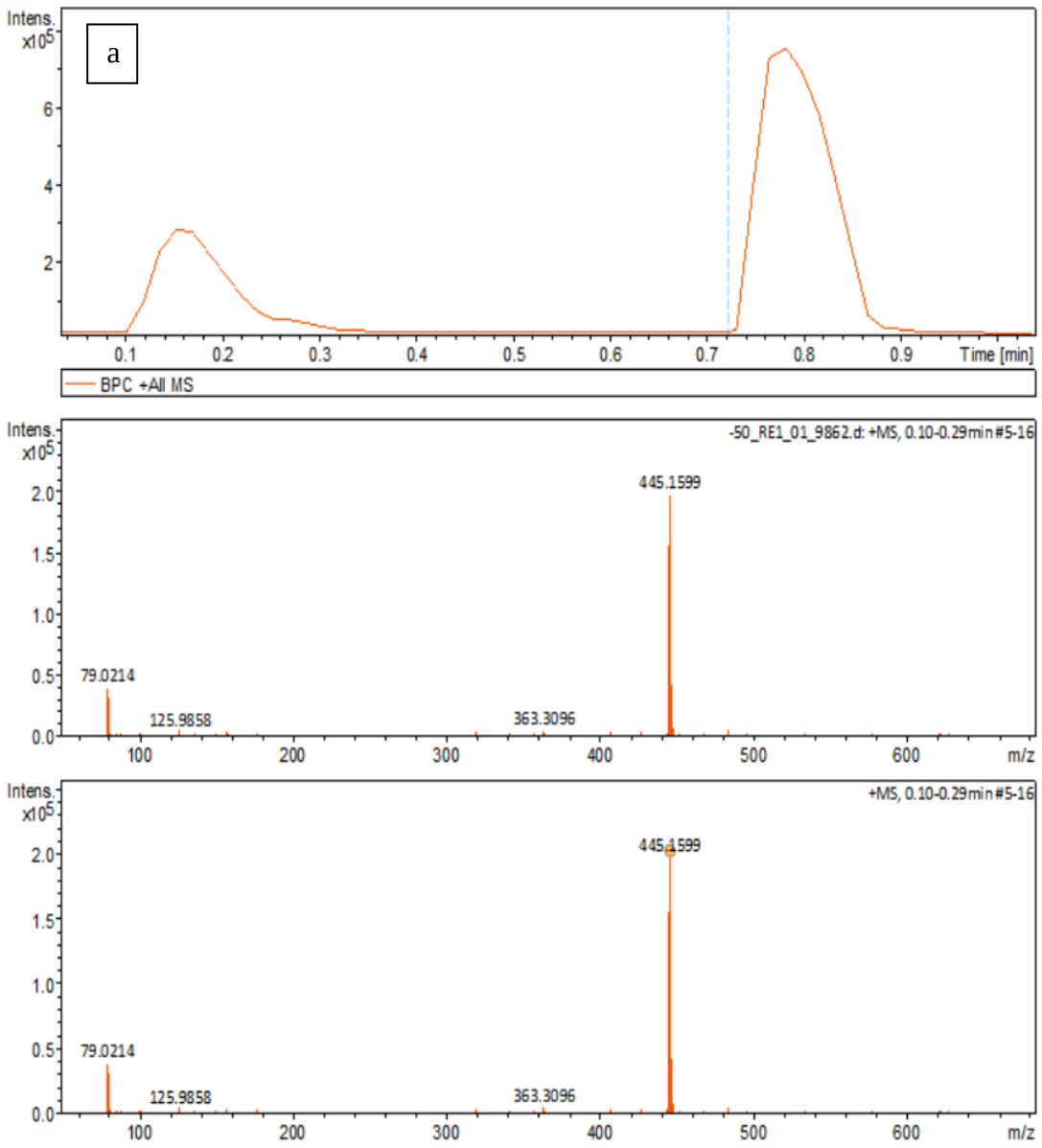

0 min

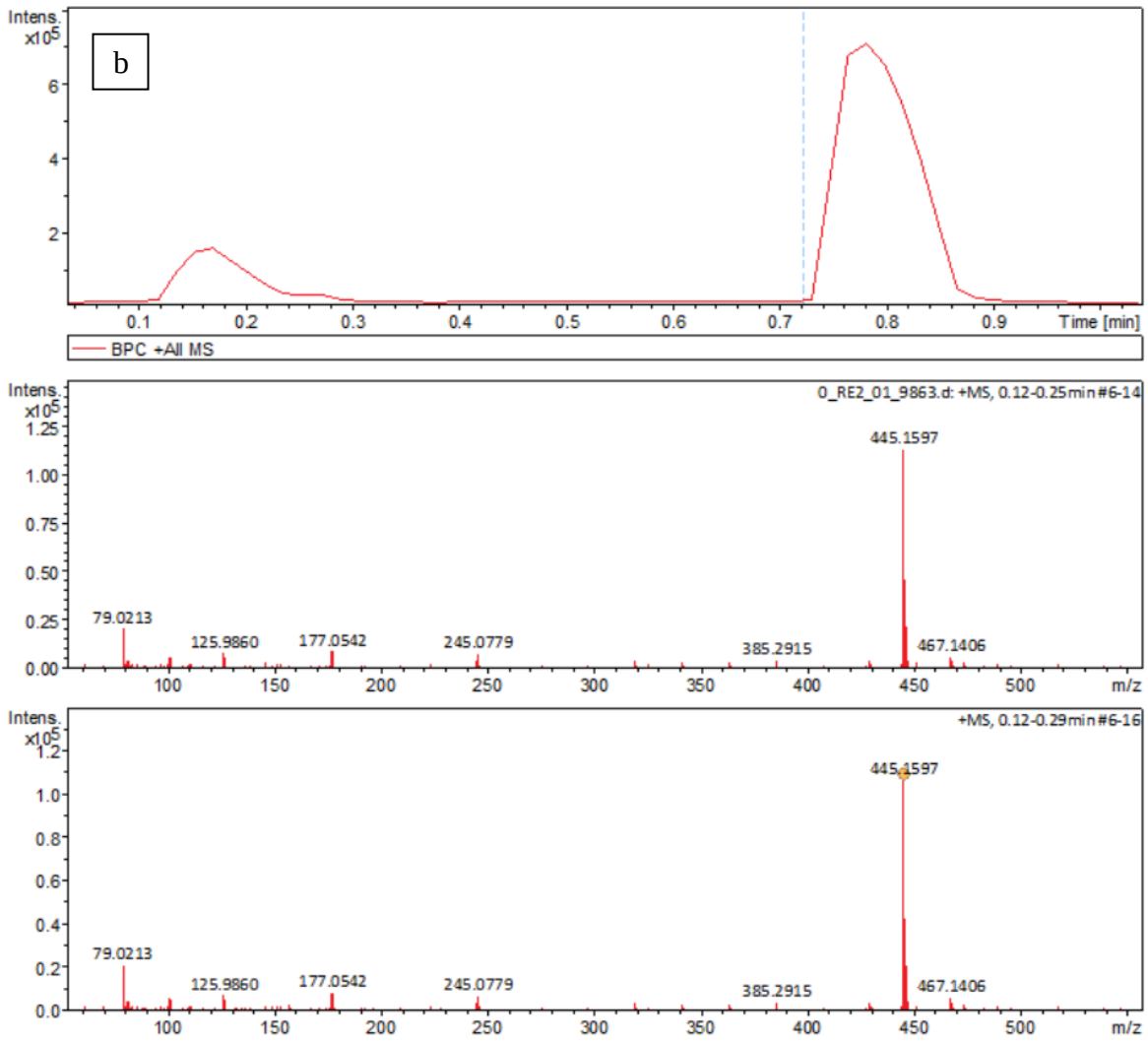
b
Intens.
x10^5
6
4
2
0.1
0.2
0.3
0.4
0.5
0.6
0.7
0.8
0.9
Time [min]
BPC +All MS
0_RE2_01_9863.d: +MS, 0.12-0.25min #6-14
445.1597
79.0213
125.9860
177.0542
245.0779
385.2915
467.1406
m/z
+MS, 0.12-0.29min #6-16
445.1597
79.0213
125.9860
177.0542
245.0779
385.2915
467.1406
m/z

120 min

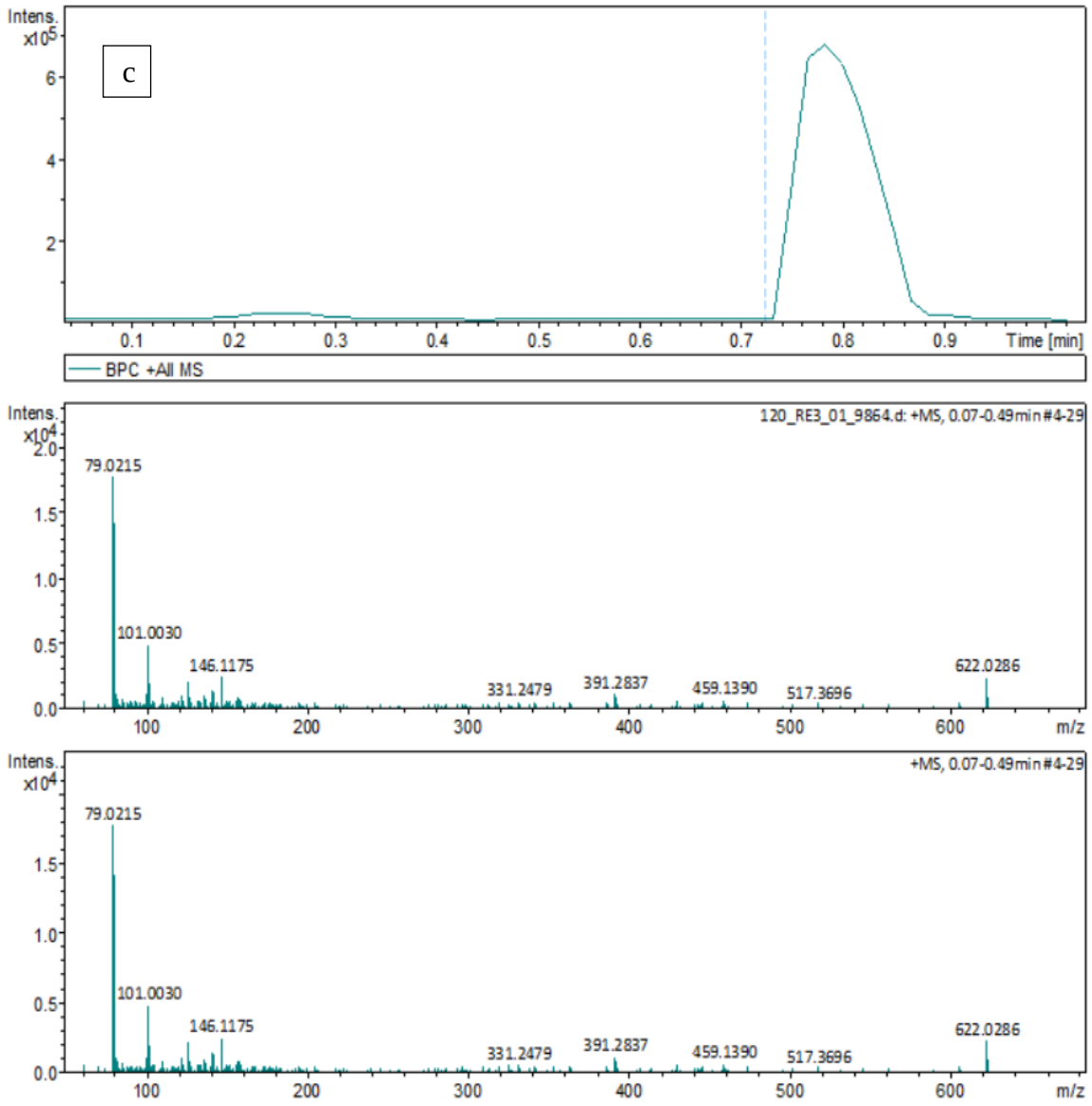
C
Intens.
x10^5
6
4
2
0.1
0.2
0.3
0.4
0.5
0.6
0.7
0.8
0.9
Time [min]
BPC +All MS
Intens.
x10^4
120_RE3_01_9864.d: +MS, 0.07-0.49min #4-29
79.0215
101.0030
146.1175
331.2479
391.2837
459.1390
517.3696
622.0286
100
200
300
400
500
600
m/z
Intens.
x10^4
+MS, 0.07-0.49min #4-29
79.0215
101.0030
146.1175
331.2479
391.2837
459.1390
517.3696
622.0286
100
200
300
400
500
600
m/z

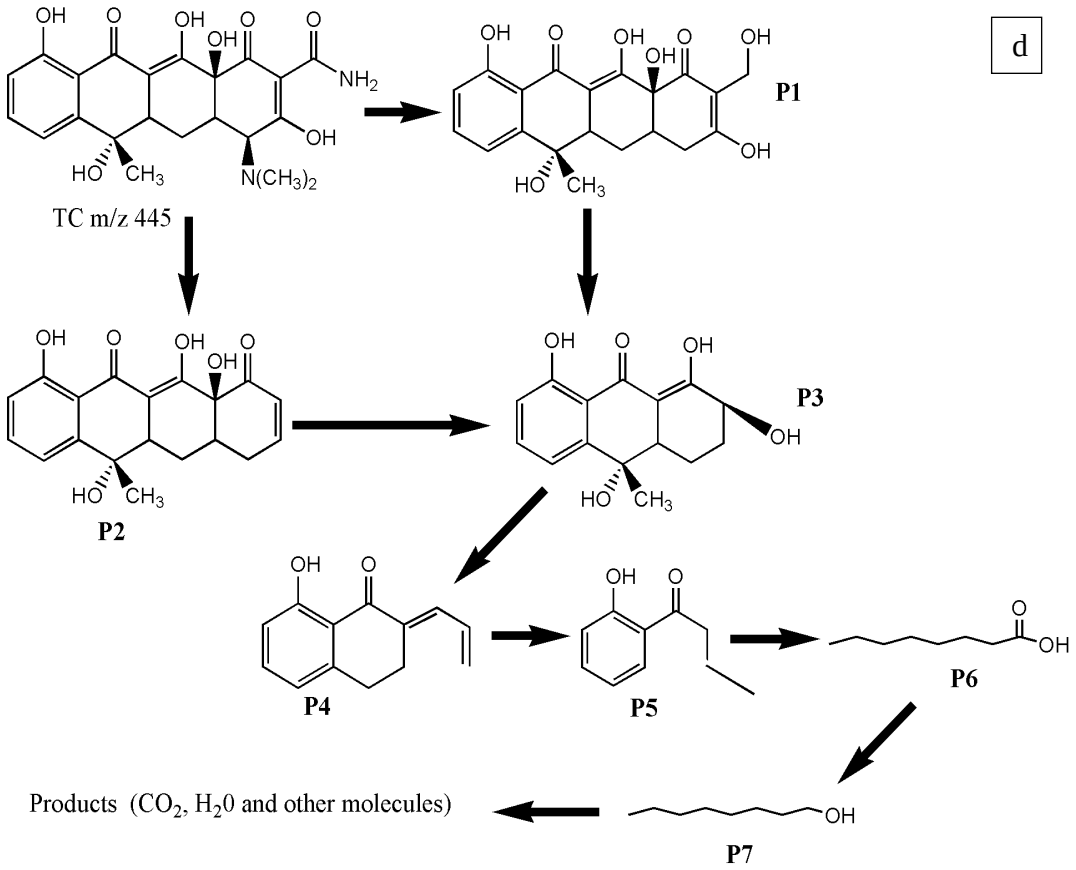

Figure 4. 27: Degradation intermediates of TC in 1.3CD/TNF at **a)** -50 min **b)** 0 min and **c)** 120 min **d)** The possible degradation pathways of TC in 1.3 CD/TNF system.

HPLC-MS/MS was employed to detect the degradation intermediates of TC in CD/TiO_2 composite nanofiber system and the results are shown above in Fig. 4.27 (a) -50 min (sampling of the tetracycline solution without the catalyst), (b) 0 min and (c) 120 min time intervals. The two possible degradation pathways of TC were proposed. Fig. 4.27 (d) for the pathway P1 with m/z = 445 was generated from the dehydration process of TC which was also reported by Li *et al.* (2019). The intermediates with P2 was formed through the N-demethylation reaction of P1 and the ring opening products including P3, P4, P5, P6 and P7 were assigned as the further oxidation products of P2 by OH· and $SO_4^{\cdot-}$ attack (Li *et al.* 2019). In addition, the degradation intermediates of TC at -50 min, 0 min and 120 min; it can be observed that there were changes during those time intervals as shown in Fig. 4.27 (a-c).

4.3 CDs/TiO_2/Fe_2O_3 composite nanofiber with different 1, 3 and 5% Fe_2O_3 Results and Discussion

This section of results discusses the CD/TNF composite nanofiber doped with different percentages of Fe_2O_3. CD/TNF/Fe_2O_3 composite was successfully Synthesized.

4.3.1 Characterization results of CDs/TiO_2/Fe_2O_3 composite nanofiber with different 1, 3 and 5% Fe_2O_3

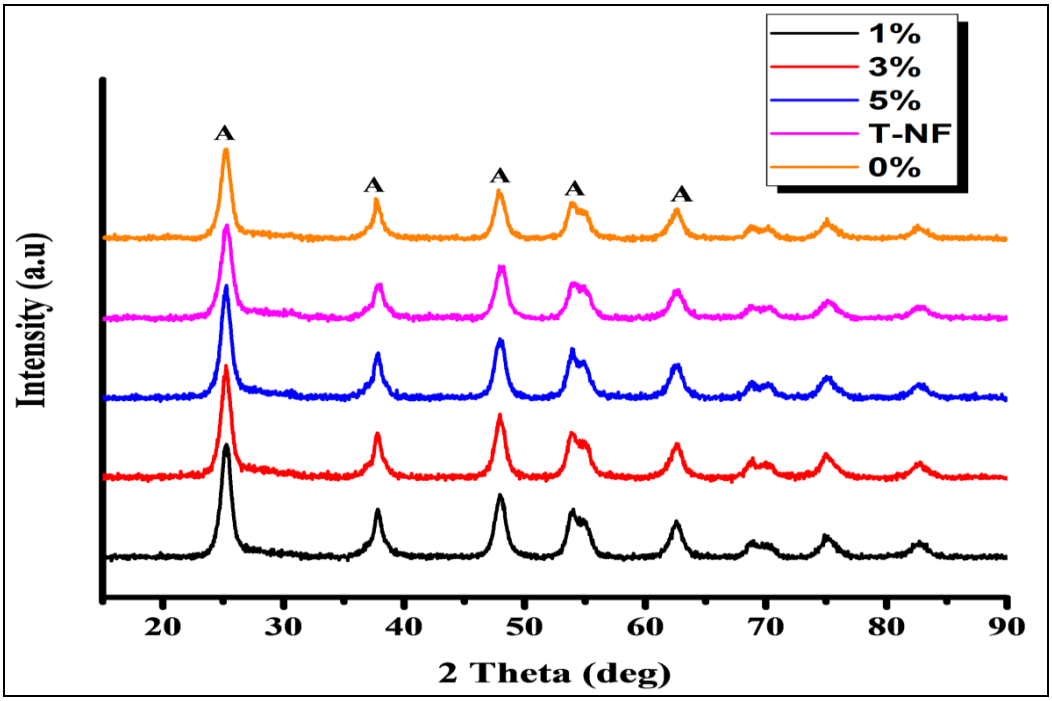

Figure 4. 28: XRD patterns of CDs/TiO_2/Fe_2O_3 composite nanofiber with different 1, 3 and 5% Fe_2O_3.

Fig. 4.28 shows the XRD patterns of CDs/TiO_2/Fe_2O_3 composite nanofiber with different 1, 3 and 5% Fe_2O_3. The XRD pattern of CDs/TiO_2/Fe_2O_3 shows peaks at $2\boldsymbol{\theta}$ = 25.2˚, 37.7˚, 54.02˚ and 62.8˚ corresponding respectively to the crystal planes [012], [110], [204] and [300] (JCPDS: 033-0664). Therefore, the results obtained proves the effective coupling between TiO_2 and Fe_2O_3. By applying the Scherrer equation, the crystallite size of [012] plane indicates 7.2 nm for 1% Fe_2O_3 and 9.8 nm for both 3 and 5% Fe_2O_3. Meanwhile, at low loading, 1% Fe_2O_3 cationic lattice substitution is obtained whereas at high loading an interstitial addition is perceived probably due to size effects. That possible substitution to occur in the 1% Fe_2O_3/CDs/TiO_2 sample is expected to create oxygen ion vacancy positions. On the contrary, 3 and 5% Fe_2O_3 patterns exhibit an increase in intensity implying crystallites size enhancement by giving an average size of 9.8 nm.

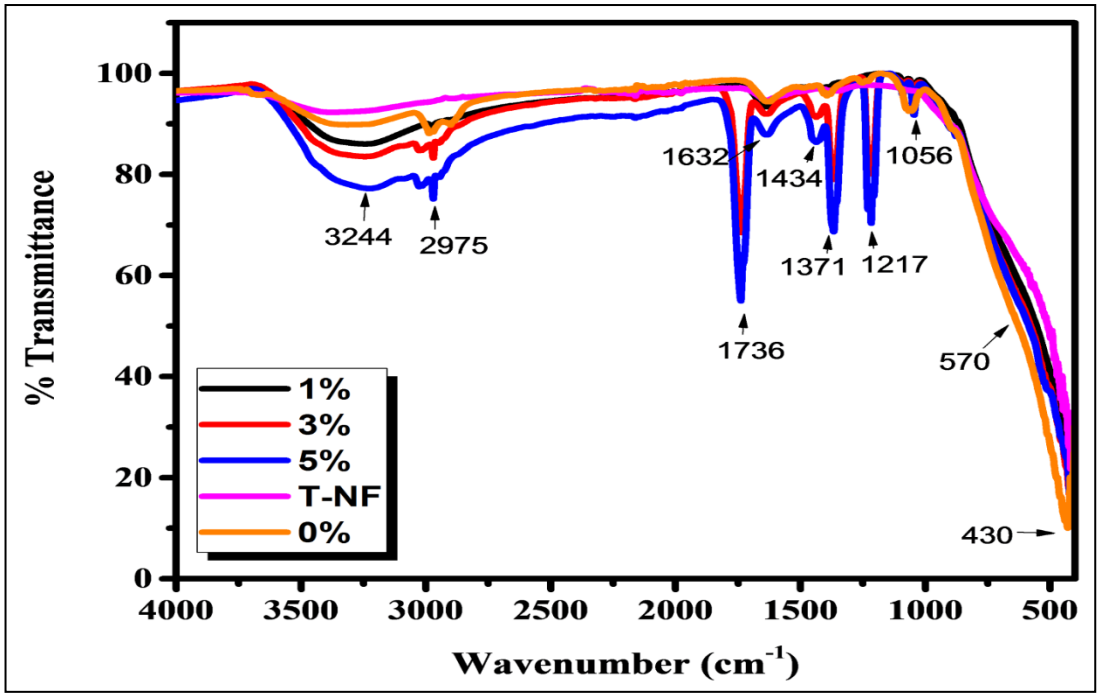

Figure 4. 29: FTIR spectra of CDs/TiO_2 composite nanofiber decorated with respectively indicated weight percentage of Fe_2O_3.

The FTIR spectra of CDs/TNF/Fe_2O_3 samples are shown in Fig. 4.29. The samples show FTIR bands at 3244 cm^{-1} corresponding to the stretching of O-H groups, at 1632 cm^{-1} are

attributed to bending vibration of adsorbed water molecules. The intense broad band below 1000 cm^{-1} is associated with the stretching mode of Ti-O-Ti. The peaks at 2975, 1434 and 1371 cm^{-1} are assigned to sp^3 and sp^2 C-H, unsaturated C-H and C-OH bands indicating that CDs have been loaded to the composites successfully. The band at 430 cm^{-1} is the characteristic of Fe_2O_3. A slight shift of the peak of Fe-O at 570 cm^{-1} can be observed, suggesting the crystal structure of Fe_2O_3 were distorted and Fe-O-C bonds were formed in $CDs/TiO_2/Fe_2O_3$ composite nanofiber.

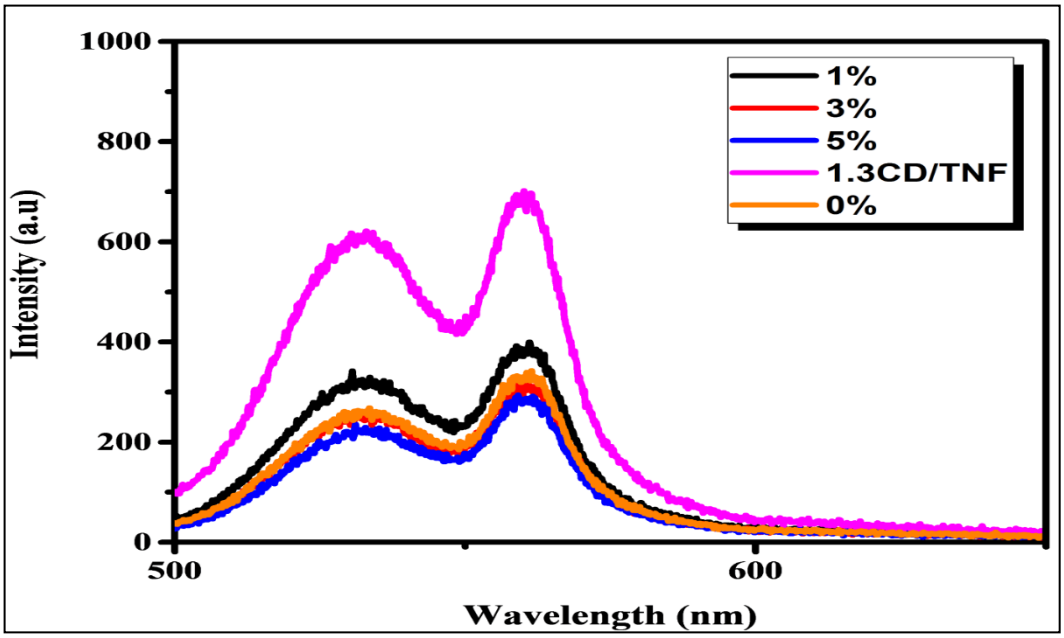

Figure 4. 30: PL spectra of $CDs/Fe_2O_3/TiO_2$ composite nanofiber of different Fe_2O_3 percentage.

From the photoluminescence emission spectra of $CDs/TiO_2/Fe_2O_3$ composite nanofiber materials are shown in Fig. 4.30. It can be observed that the $CDs/TiO_2/Fe_2O_3$ composite nanofiber show a broad PL emission spectrum located at 500 nm-600 nm, which could be attributed to the charge carriers' transition (Wu and Zhang 2019). The PL were used to evaluate the transfer and recombination process of the photoexcited electron-hole pairs, as it is well known. The lower the PL spectra intensity, the higher the efficiency of separation and transfer of electron-hole pairs (Zhang *et al.* 2019). The intensity order of the PL spectra was as follows: 1.3CD/TNF > 1% > 0% > 3% > 5% which simply means that the introduction of Fe^{2+} quenched the PL intensity of the catalyst. Due to the charge transfer process which took

place at the interface between Fe_3O_2 and CDs/TiO_2 composite nanofiber the charge recombination on the surface of TiO_2-nanofiber (TNF) was suppressed, resulting in the decrease of PL intensity.

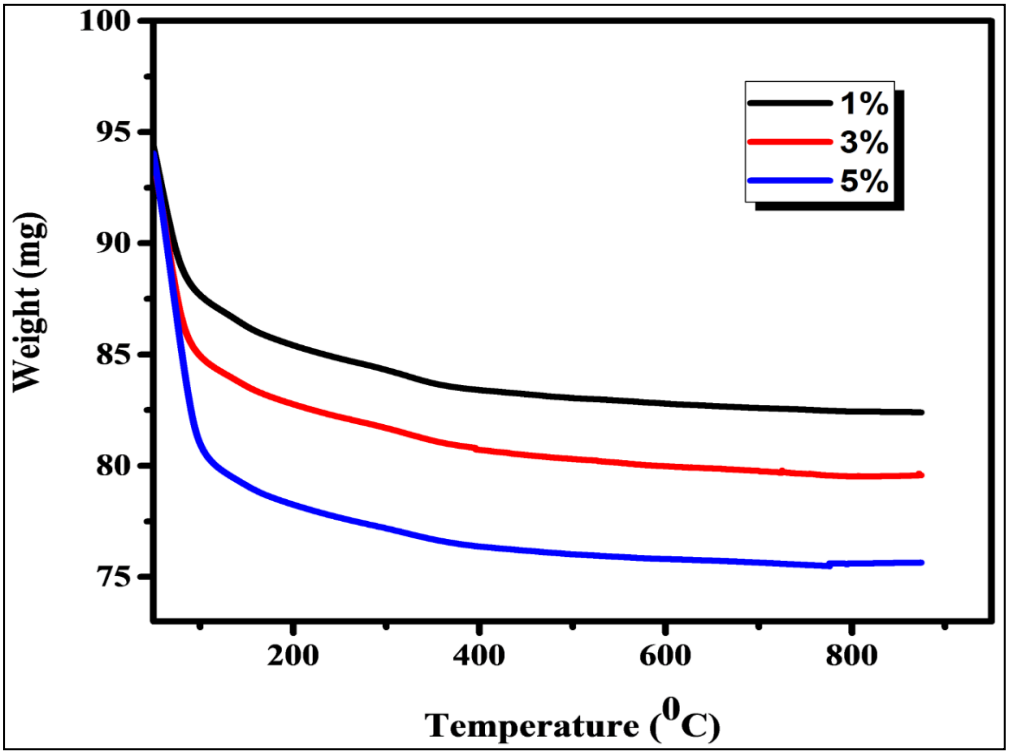

Figure 4. 31: TGA curves of $CDs/Fe_2O_3/TiO_2$ composite nanofiber of different Fe_2O_3 percentage.

Fig. 4.31 shows the thermal gravimetric analysis of $CDs/Fe_2O_3/TiO_2$ composite nanofiber with different percentages of Fe_2O_3 loaded on CDs/TiO_2 composite. The weight loss consists of two main stages. The loss of adsorbed water from room temperature to 100 ˚C is the first stage. The thermal decomposition of the CDs/Fe_2O_3 composite can be attributed at approximately 180 ˚C, thus it takes place at the second stage. The TGA results show the excellent thermal stability of the composite. Therefore, the thermal stability decreases with increasing the Fe_2O_3 percentage.

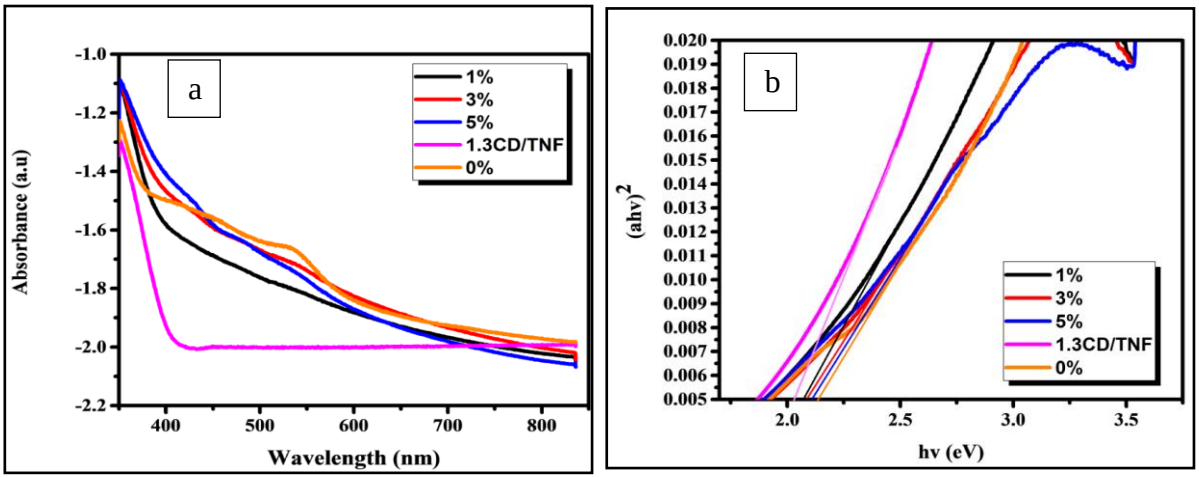

Figure 4. 32: (a) UV-Vis diffuse reflectance spectra (b) and the corresponding Tauc plots of CDs/Fe_2O_3/TiO_2 composite nanofiber.

The UV-Vis optical absorption spectra of different CDs/TiO_2/Fe_2O_3 as well as different Fe loading doped on CDs/TiO_2 composite nanofiber were investigated in the range 300-800 nm in Fig. 4.32 (a). The 1.3CD/TNF composite exhibits the lowest light absorption both in ultraviolet and visible light regions. A red shift in the band gap transition is displayed by the spectra of 1.3CD/TNF. Whereas, 1%-Fe_2O_3/CDs/TiO_2 composite nanofiber shows higher absorption capacity in the wavelength range from 300-450 nm followed by a significant decrease in the visible light range. Both Fe_2O_3 and CDs/TiO_2 composite nanofiber show direct charge transitions brought about via UV absorption and the combined effect of TiO_2 nanofibers and Fe_2O_3 was undoubtedly favorable for the transfer and separation of electrons and holes, effecting to the shift of UV-Vis spectrum. The reduced band gap energy of the CDs/Fe_2O_3/TiO_2 composite nanofiber can be confirmed according to the tauc plot as presented in Fig. 4.32 (b), which is constructed from $(ahv)^2$ versus photon energy (hv) to estimate the band gap between the samples. 1.3CD/TNF composite indicates an indirect transition band gap of 2.04 eV. The values of the band gap energy of samples 1%-Fe_2O_3/CDs/TiO_2, 3%-Fe_2O_3/CDs/TiO_2 and 5%-Fe_2O_3/CDs/TiO_2 are 2.08, 2.10 and 2.13 eV

respectively. It can be indicated that the band gap values of the samples increase by increasing iron oxide content. This is in good agreement with results obtained by (F. Hasany *et al.* 2013).

4.3.2 Photocatalytic activity results of CDs/TiO_2/Fe_2O_3 composite nanofiber with different 1, 3 and 5% Fe_2O_3

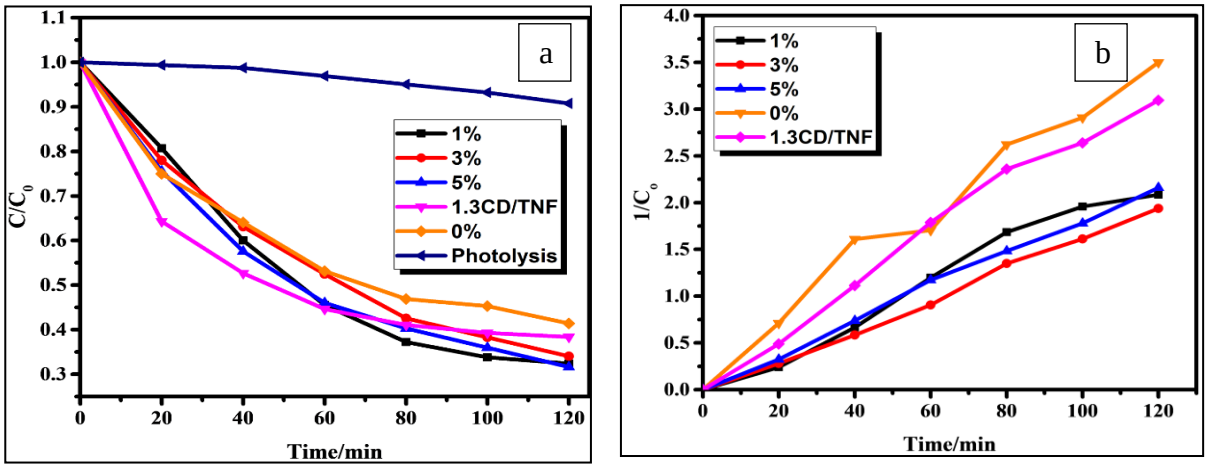

Figure 4. 33: a) The degradation curves of TC by photocatalysts and control samples under visible-light irradiation b) Degradation 2nd order kinetics by CDs/Fe_2O_3/TiO_2 composite nanofiber of different Fe_2O_3 percentages.

The prepared photocatalysts under visible light were assessed by the photocatalytic properties. TC was preferred as a representative pollutant and in Fig. 4.33 (a) the results of photocatalytic degradation experiments are shown. Prior to the TC photodegradation experiments, to eliminate the influence of adsorption on the degradation process dark adsorption was carried out for 1 hour. It can be observed that the photo-induced TC degradation efficiency is up to 69% in 120 min with 1% as the photocatalyst. For comparison 0%, 1%, 3%, 5% and 1.3CD/TNF were used as photocatalysts in the contrast experiments and the activity of all photocatalysts is in the following order: 1% > 5% > 3% > 1.3CD/TNF > 0% > photolysis. Tetracycline degradation by the photocatalyst followed the pseudo-second-order kinetic model as shown in Fig. 4.33 (b).

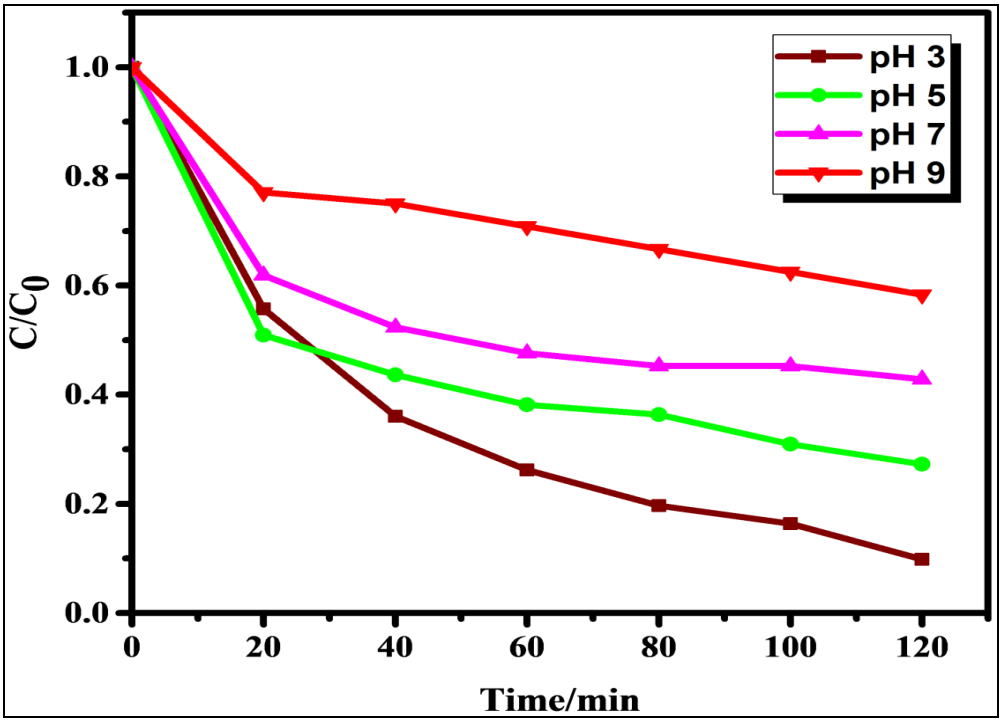

Figure 4. 34: The effect of pH on 1%-Fe_2O_3/CDs/TiO_2 composite nanofiber.

During the photocatalytic degradation process, the pH value is usually considered to be one of the most important factors. As seen in Fig. 4.34, the degradation of TC was carried out at pH values of 3.0, 5.0, 7.0 and 9.0 for the 1%-Fe_2O_3/CDs/TiO_2 composite nanofiber. The degradation rate increased with the decrease in pH values. This is because the magnetite on the catalyst can easily degrade under acidic conditions to produce more hydroxyl radicals on the catalyst surface. Moreover, the generation of reactive iron species on the catalyst surface modifies the physicochemical properties. The presence of surface ferrous species on the catalyst is specially favored under acidic conditions, which plays the most important role in the formation of radical hydroxyl.

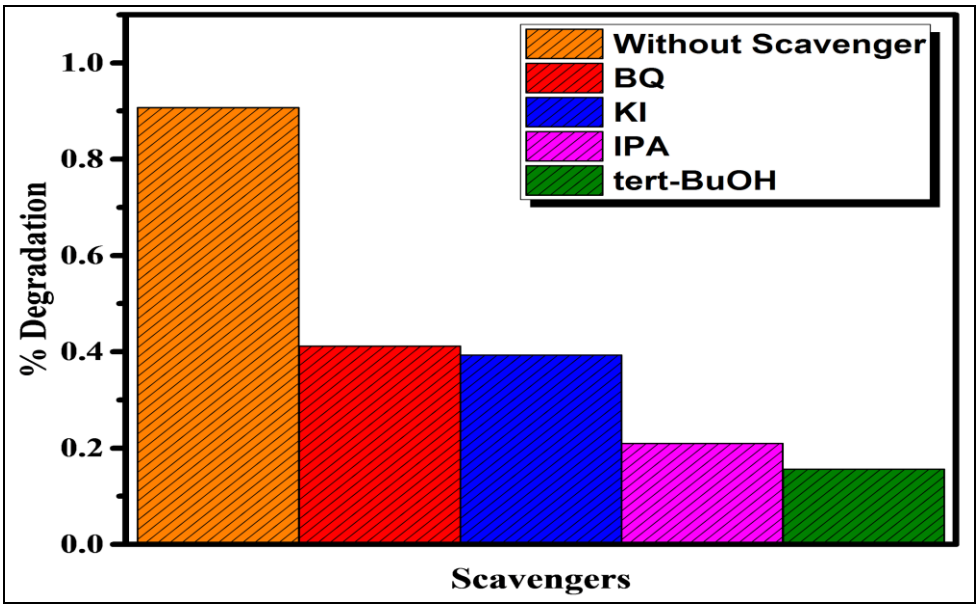

Figure 4. 35: Effect of scavengers on the degradation of tetracycline over 1%-Fe_2O_3/CDs/TiO_2 composite nanofiber.

It is important to indicate the excellent photocatalytic degradation of 1%-Fe_2O_3/CDs/TiO_2 composite nanofiber, it was performed in the absence of H_2O_2 implying the necessity of illustrating the different reactive species that could be displayed during the reaction progressing. In the photocatalytic reaction of CDs/TiO_2/Fe_2O_3 composite nanofiber it can be seen that both $OH^{\bullet}$ and $O_2^{\bullet-}$ play important roles. The effects of addition of tert-Butanol, BQ, KI and IPA were used as scavengers on the catalytic oxidation of the TC over the 1%-Fe_2O_3/CDs/TiO_2 composite nanofiber photocatalyst, it was investigated under similar experimental conditions. In order to understand, a more detailed insight into the effect of active species on photocatalytic processes (oxidation mechanism) is required.

In Fig. 4.35, it has been shown that the reaction rate was relatively retained upon using BQ and KI reflecting the negligible effects of $O_2^{\bullet-}$ and holes species. The experiment with IPA and tert-BuOH scavengers has indicated a significant decrease proposing the influential effect of $OH^{\bullet}$ and electrons. Therefore, the results confirm a major role of hydroxyl radicals in tetracycline degradation.

4.3.3 Reusability results of 1% Fe_2O_3/CDs/TiO_2 composite nanofiber

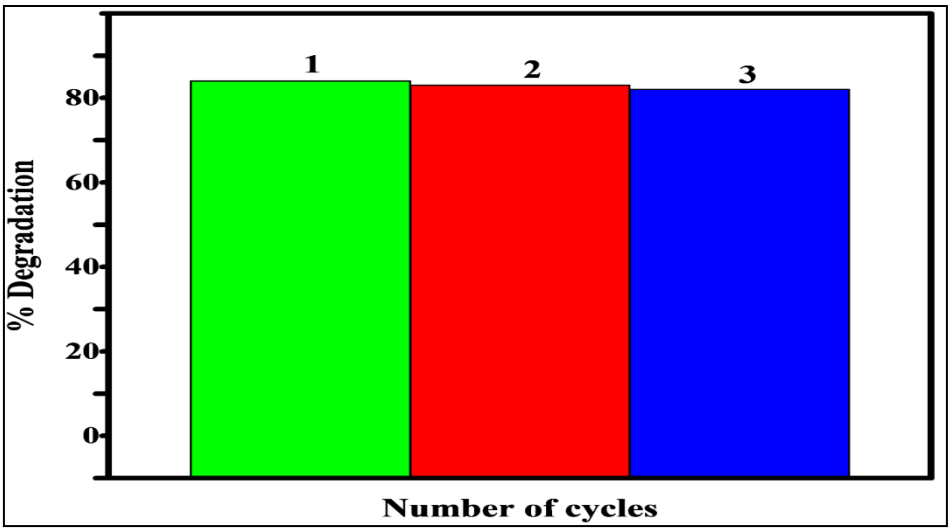

Figure 4. 36: The catalytic reusability of three cycles over 1%-Fe_2O_3/CDs/TiO_2 composite nanofiber.

The reusability of 1%-Fe_2O_3/CDs/TiO_2 composite nanofiber was also studied three times under identical conditions and the results are presented in Fig. 4.36. The catalyst was removed from the reactor and dried in a quartz tube at 60 ˚C overnight under vacuum, at the end of each cycle. However, the TC removal efficiency is still very high which indicated that satisfactory catalytic performance was maintained after three runs after the Fe_2O_3 was slightly dissolved at each cycle. After each run, the catalyst was separated from the reaction suspension and recovered, and then used for the next run. The removal efficiency of 1%-Fe_2O_3/CDs/TiO_2 composite nanofiber to TC decreased slightly compared to the 1st cycle with the increase in the number of cycles, implying that the 1%-Fe_2O_3/CDs/TiO_2 composite nanofiber maintained a good stability and reusability in the process of recycling.

4.3.4 Electrochemical results of CDs/TiO_2/Fe_2O_3 composite nanofiber with different 1, 3 and 5% Fe_2O_3

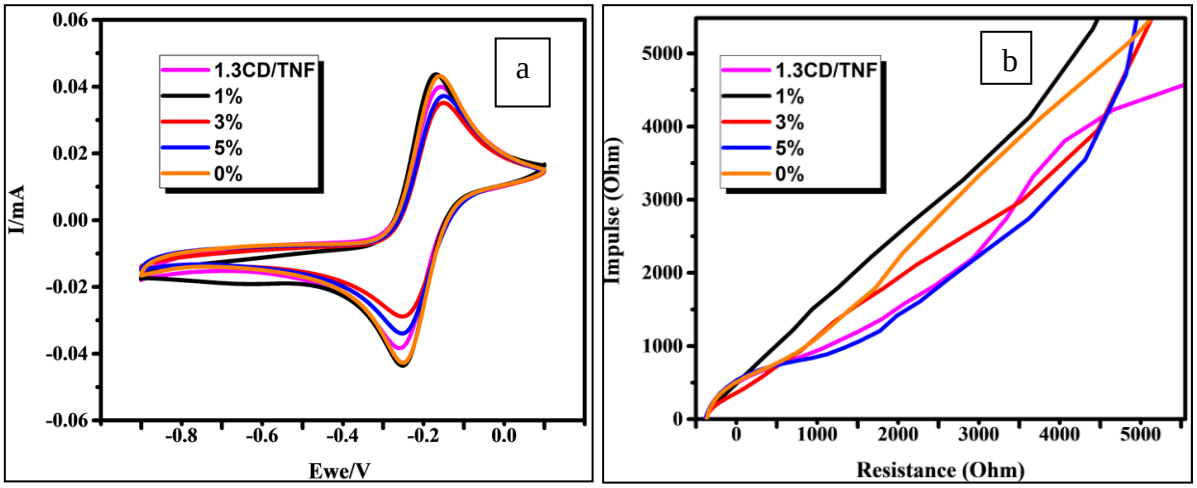

Figure 4. 37: a) Cyclic voltamograms of 1%, 3% and 5%-Fe_2O_3/CDs/TiO_2 composite nanofiber in 0.1M NaOH solution **b)** Nyquist plot for 1%, 3% and 5%-Fe_2O_3/CDs/TiO_2 composite nanofiber.

Cyclic voltammetry (CV) was used to characterize 1%, 3% and 5%-Fe_2O_3/CDs/TiO_2 composite nanofiber materials in contact with a deaerated electrolyte. 1%, 3% and 5%-Fe_2O_3/CDs/TiO_2 composite nanofiber curves are shown in Fig. 4.37 (a) The working electrode was polarized from the rest potential in the anodic direction up to 0.04 mA and back up to -0.25 V. In the first cycle, the first cathodic peak at -0.25 V is generally ascribed to an irreversible reduction peak. Furthermore, reduction of Fe^{3+} ions provide higher electron donor states in the formed 1%, 3% and 5%-Fe_2O_3/CDs/TiO_2 composite nanofiber at negative potentials, resulting in an increase in the capacitance of the space charge layer. Fig 4.37 (b) shows the EIS Nyquist plot of the 1%, 3% and 5%-Fe_2O_3/CDs/TiO_2 composite nanofiber material in 0.1 M $K_3[Fe(CN)_6]$ aqueous solution. The Nyquist plot gives information on the charge transfer properties of a semiconductor, such that the radius is larger. It can be observed in Fig. 4.37 (b) that the charge transfer resistance of the 1%, 3% and 5%-Fe_2O_3/CDs/TiO_2 composite nanofiber materials decreased in the order of 1.3 CD/TNF > 3% > 0% > 5% > 1%. This implies that in the 1%-Fe_2O_3/CDs/TiO_2 composite nanofiber there

will be a relatively more photogenerated electron-hole separation due to its comparatively fast interfacial charge transfer. Therefore, it is confirmed that 1%-Fe_2O_3/CDs/TiO_2 is the most photocatalytic degradation of TC.

References

Bertoluzzi, L., Badia-Bou, L., Fabregat-Santiago, F., Gimenez, S., and Bisquert, J., 2013. Interpretation of cyclic voltammetry measurements of thin semiconductor films for solar fuel applications. *Journal of Physical Chemistry Letters*.

Camposeco, R., Castillo, S., Navarrete, J., and Gomez, R., 2016. Synthesis, characterization and photocatalytic activity of TiO_2 nanostructures: Nanotubes, nanofibers, nanowires and nanoparticles. *Catalysis Today*, 266, 90–101.

Ahmad, R., Ahmad, Z., Khan, A.U., Mastoi, N.R., Aslam, M., and Kim, J., 2016. Photocatalytic systems as an advanced environmental remediation: Recent developments, limitations and new avenues for applications. *Journal of Environmental Chemical Engineering*, 4 (4), 4143–4164.

Akpan, U.G. and Hameed, B.H., 2010. The advancements in sol-gel method of doped-TiO2 photocatalysts. *Applied Catalysis A: General*, 375 (1), 1–11.

Al-Mamun, M.R., Kader, S., Islam, M.S., and Khan, M.Z.H., 2019. Photocatalytic activity improvement and application of UV-TiO2 photocatalysis in textile wastewater treatment: A review. *Journal of Environmental Chemical Engineering*, 7 (5).

Andrade-Guel, M., Díaz-Jiménez, L., Cortés-Hernández, D., Cabello-Alvarado, C., ávila-Orta, C., Bartolo-Pérez, P., and Gamero-Melo, P., 2018. Microwave assisted sol-gel synthesis of titaniumdioxide using hydrochloric and acetic acid ascatalysts. *Boletin de la Sociedad Espanola de Ceramica y Vidrio*, 1–7.

Archana, T., Vijayakumar, K., Arivanandhan, M., and Jayavel, R., 2019. TiO2 nanostructures with controlled morphology for improved electrical properties of photoanodes and quantum dot sensitized solar cell characteristics. *Surfaces and Interfaces*, 17 (May), 100350.

Asha Jhonsi, M. and Thulasi, S., 2016. A novel fluorescent carbon dots derived from tamarind. *Chemical Physics Letters*, 661, 179–184.

Awfa, D., Ateia, M., Fujii, M., Johnson, M.S., and Yoshimura, C., 2018. Photodegradation of pharmaceuticals and personal care products in water treatment using carbonaceous-TiO2 composites: A critical review of recent literature. *Water Research*, 142, 26–45.

Bakre, P. V., Volvoikar, P.S., Vernekar, A.A., and Tilve, S.G., 2016. Influence of acid chain length on the properties of TiO2 prepared by sol-gel method and LC-MS studies of methylene blue photodegradation. *Journal of Colloid and Interface Science*, 474, 58–67.

Bertoluzzi, L., Badia-Bou, L., Fabregat-Santiago, F., Gimenez, S., and Bisquert, J., 2013. Interpretation of cyclic voltammetry measurements of thin semiconductor films for solar fuel applications. *Journal of Physical Chemistry Letters*.

Bokare, A.D. and Choi, W., 2014. Review of iron-free Fenton-like systems for activating H2O2 in advanced oxidation processes. *Journal of Hazardous Materials*.

Camposeco, R., Castillo, S., Navarrete, J., and Gomez, R., 2016. Synthesis, characterization and photocatalytic activity of TiO2 nanostructures: Nanotubes, nanofibers, nanowires and nanoparticles. *Catalysis Today*, 266, 90–101.

Cao, M., Wang, P., Ao, Y., Wang, C., Hou, J., and Qian, J., 2016. Visible light activated photocatalytic degradation of tetracycline by a magnetically separable composite photocatalyst: Graphene oxide/magnetite/cerium-doped titania. *Journal of Colloid and Interface Science*, 467, 129–139.

Chansri, P. and Sung, Y.M., 2016. Reprint of "Investigations of electrochemical luminescence characteristics of ZnO/TiO2 nanotubes electrode and silica-based gel type solvents". *Surface and Coatings Technology*, 307, 1139–1143.

Choi, D., Ham, S., and Jang, D.J., 2018. Visible-light photocatalytic reduction of Cr(VI) via carbon quantum dots-decorated TiO2 nanocomposites. *Journal of Environmental Chemical Engineering*, 6 (1), 1–8.

Cuerda-Correa, E.M., Domínguez, J.R., Muñoz-Peña, M.J., and González, T., 2016. Degradation of Parabens in Different Aqueous Matrices by Several O3-Derived Advanced Oxidation Processes. *Industrial and Engineering Chemistry Research*.

Dedual, G., Macdonald, M.J., Alshareef, A., Wu, Z., Tsang, D.C.W., and Yip, A.C.K., 2014. Requirements for effective photocatalytic oxidative desulfurization of a thiophene-

containing solution using TiO2. *Journal of Environmental Chemical Engineering*.

Dhaka, S., Kumar, R., Lee, S. hun, Kurade, M.B., and Jeon, B.H., 2018. Degradation of ethyl paraben in aqueous medium using advanced oxidation processes: Efficiency evaluation of UV-C supported oxidants. *Journal of Cleaner Production*.

F. Hasany, S., Ahmed, I., J, R., and Rehman, A., 2013. Systematic Review of the Preparation Techniques of Iron Oxide Magnetic Nanoparticles. *Nanoscience and Nanotechnology*.

Fazal, T., Razzaq, A., Javed, F., Hafeez, A., Rashid, N., Amjad, U.S., Ur Rehman, M.S., Faisal, A., and Rehman, F., 2020. Integrating adsorption and photocatalysis: A cost effective strategy for textile wastewater treatment using hybrid biochar-TiO2 composite. *Journal of Hazardous Materials*, 390 (May 2019), 121623.

Gaur, N., Narasimhulu, K., and PydiSetty, Y., 2018. Recent advances in the bio-remediation of persistent organic pollutants and its effect on environment. *Journal of Cleaner Production*, 198, 1602–1631.

Hama Aziz, K.H., Miessner, H., Mueller, S., Kalass, D., Moeller, D., Khorshid, I., and Rashid, M.A.M., 2017. Degradation of pharmaceutical diclofenac and ibuprofen in aqueous solution, a direct comparison of ozonation, photocatalysis, and non-thermal plasma. *Chemical Engineering Journal*.

Han, F., Kambala, V.S.R., Srinivasan, M., Rajarathnam, D., and Naidu, R., 2009. Tailored titanium dioxide photocatalysts for the degradation of organic dyes in wastewater treatment: A review. *Applied Catalysis A: General*.

Hanaor, D., Michelazzi, M., Chenu, J., Leonelli, C., and Sorrell, C.C., 2011. The effects of firing conditions on the properties of electrophoretically deposited titanium dioxide films on graphite substrates. *Journal of the European Ceramic Society*.

Hantusch, M., Bessergenev, V., Mateus, M.C., Knupfer, M., and Burkel, E., 2018. Electronic properties of photocatalytic improved Degussa P25 titanium dioxide powder. *Catalysis Today*, 307 (October 2017), 111–118.

Haque, F.Z., Nandanwar, R., and Singh, P., 2017. Evaluating photodegradation properties of anatase and rutile TiO2 nanoparticles for organic compounds. *Optik*, 128, 191–200.

Heponiemi, A. and Lassi, U., 2012. Advanced Oxidation Processes in Food Industry Wastewater Treatment – A Review. *In*: *Food Industrial Processes - Methods and Equipment*.

Horikoshi, S. and Serpone, N., 2020. Can the photocatalyst TiO2 be incorporated into a wastewater treatment method? Background and prospects. *Catalysis Today*, 340 (August 2018), 334–346.

Hou, L., Wang, L., Royer, S., and Zhang, H., 2016. Ultrasound-assisted heterogeneous Fenton-like degradation of tetracycline over a magnetite catalyst. *Journal of Hazardous Materials*, 302, 458–467.

Hou, Y., Lu, Q., Wang, H., Li, H., Zhang, Y., and Zhang, S., 2016. One-pot electrochemical synthesis of carbon dots/TiO2 nanocomposites with excellent visible light photocatalytic activity. *Materials Letters*, 173, 13–17.

Huang, Y., Liang, Y., Rao, Y., Zhu, D., Cao, J.J., Shen, Z., Ho, W., and Lee, S.C., 2017. Environment-Friendly Carbon Quantum Dots/ZnFe2O4 Photocatalysts: Characterization, Biocompatibility, and Mechanisms for NO Removal. *Environmental Science and Technology*, 51 (5), 2924–2933.

Jia, J., Li, D., Wan, J., and Yu, X., 2016. Characterization and mechanism analysis of graphite/C-doped TiO2 composite for enhanced photocatalytic performance. *Journal of Industrial and Engineering Chemistry*, 33, 162–169.

Kalantari, K., Kalbasi, M., Sohrabi, M., and Royaee, S.J., 2016. Synthesis and characterization of N-doped TiO2 nanoparticles and their application in photocatalytic oxidation of dibenzothiophene under visible light. *Ceramics International*, 42 (13), 14834–14842.

Kalantari, K., Kalbasi, M., Sohrabi, M., and Royaee, S.J., 2017. crossmark, 43 (August 2016), 973–981.

Karci, A., Arslan-Alaton, I., Olmez-Hanci, T., and Bekbölet, M., 2012. Transformation of 2,4-dichlorophenol by H 2O 2/UV-C, Fenton and photo-Fenton processes: Oxidation products and toxicity evolution. *Journal of Photochemistry and Photobiology A: Chemistry*.

Khairy, M. and Zakaria, W., 2014. Effect of metal-doping of TiO2 nanoparticles on their photocatalytic activities toward removal of organic dyes. *Egyptian Journal of Petroleum*, 23 (4), 419–426.

Khalid, N.R., Majid, A., Tahir, M.B., Niaz, N.A., and Khalid, S., 2017. Carbonaceous-TiO2 nanomaterials for photocatalytic degradation of pollutants: A review. *Ceramics International*, 43 (17), 14552–14571.

Khan, S.B., Hou, M., Shuang, S., and Zhang, Z., 2017. Morphological influence of TiO 2 nanostructures (nanozigzag, nanohelics and nanorod) on photocatalytic degradation of organic dyes. *Applied Surface Science*, 400, 184–193.

Khodadadi, M., Ehrampoush, M.H., Ghaneian, M.T., Allahresani, A., and Mahvi, A.H., 2018. Synthesis and characterizations of FeNi3@SiO2@TiO2 nanocomposite and its application in photo- catalytic degradation of tetracycline in simulated wastewater. *Journal of Molecular Liquids*, 255, 224–232.

Kim, H., Jin, C., Park, S., Lee, W.I., Chin, I.J., and Lee, C., 2013. Structure and optical properties of Bi2S3 and Bi2O3 nanostructures synthesized via thermal evaporation and thermal oxidation routes. *Chemical Engineering Journal*.

Kommineni, S., Zoeckler, J., Stocking, A., Liang, S., Flores, A., Kavanaugh, M., Rodriguez, R., Browne, T., Roberts, R., Brown, A., and Stocking, A., 2000. *Advanced Oxidation Processes: Literature Review, Removal of Methyl Tertiary Butyl Ether (MTBE) from Drinking Water: Air Stripping, Advanced Oxidation Process, Granular Activated Carbon, Synthetic Resin Sorbents*. National Water Research Institute.

Krishnan, S., Chandran, K., and Sinnathambi, C.M., 2016. Wastewater treatment technologies used for the removal of different surfactants: A comparative review. *International Journal of Applied Chemistry*.

Kumar, S., Sharma, S., Sood, S., Umar, A., and Kansal, S.K., 2016. Bismuth sulfide (Bi2S3) nanotubes decorated TiO2 nanoparticles heterojunction assembly for enhanced solar light driven photocatalytic activity. *Ceramics International*, 42 (15), 17551–17557.

Li, Z., Guo, C., Lyu, J., Hu, Z., and Ge, M., 2019. Tetracycline degradation by persulfate activated with magnetic Cu/CuFe2O4 composite: Efficiency, stability, mechanism and

degradation pathway. *Journal of Hazardous Materials*, 373 (March), 85–96.

Lin, C.C., Ho, J.M., and Wu, M.S., 2015. Continuous preparation of Fe3O4 nanoparticles using a rotating packed bed: Dependence of size and magnetic property on temperature. *Powder Technology*.

Liu, C., Li, Y., Wei, L., Wu, C., Chen, Y., Mei, L., and Jiao, J., 2014. CdS quantum dot-sensitized solar cells based on nano-branched TiO2 arrays. *Nanoscale Research Letters*.

Lu, J., Wang, Z., Zhang, Y., and Zhou, X., 2013. Hydrothermal synthesis of Bi2S3 nanorods from a single-source precursor and their promotional effect on the photocatalysis of TiO2. *Journal of Nanomaterials*.

Mahshid, S., Askari, M., Sasani Ghamsari, M., Afshar, N., and Lahuti, S., 2009. Mixed-phase TiO2 nanoparticles preparation using sol-gel method. *Journal of Alloys and Compounds*.

Martins, A.C., Cazetta, A.L., Pezoti, O., Souza, J.R.B., Zhang, T., Pilau, E.J., Asefa, T., and Almeida, V.C., 2017. Sol-gel synthesis of new TiO2/activated carbon photocatalyst and its application for degradation of tetracycline. *Ceramics International*, 43 (5), 4411–4418.

Martins, N.C.T., Ângelo, J., Girão, A.V., Trindade, T., Andrade, L., and Mendes, A., 2016. N-doped carbon quantum dots/TiO2 composite with improved photocatalytic activity. *Applied Catalysis B: Environmental*, 193, 67–74.

Matongo, S., Birungi, G., Moodley, B., and Ndungu, P., 2015. Pharmaceutical residues in water and sediment of Msunduzi River, KwaZulu-Natal, South Africa. *Chemosphere*, 134, 133–140.

Matsuzawa, S., Tanaka, J., Sato, S., and Ibusuki, T., 2002. Photocatalytic oxidation of dibenzothiophenes in acetonitrile using TiO2: Effect of hydrogen peroxide and ultrasound irradiation. *Journal of Photochemistry and Photobiology A: Chemistry*.

Mohamed, M.M., Bayoumy, W.A., Goher, M.E., Abdo, M.H., and Mansour El-Ashkar, T.Y., 2017. Optimization of α-Fe 2 O 3 @Fe 3 O 4 incorporated N-TiO 2 as super effective photocatalysts under visible light irradiation. *Applied Surface Science*, 412, 668–682.

Muruganandham, M., Suri, R.P.S., Jafari, S., Sillanpää, M., Lee, G.J., Wu, J.J., and

Swaminathan, M., 2014. Recent developments in homogeneous advanced oxidation processes for water and wastewater treatment. *International Journal of Photoenergy*.

Oseghe, E.O. and Ofomaja, A.E., 2018a. Study on light emission diode/carbon modified TiO2 system for tetracycline hydrochloride degradation. *Journal of Photochemistry and Photobiology A: Chemistry*, 360 (April), 242–248.

Oseghe, E.O. and Ofomaja, A.E., 2018b. Facile microwave synthesis of pine cone derived C-doped TiO2 for the photodegradation of tetracycline hydrochloride under visible-LED light. *Journal of Environmental Management*, 223 (July), 860–867.

Panneerselvam, P., Morad, N., and Tan, K.A., 2011. Magnetic nanoparticle (F3O4) impregnated onto tea waste for the removal of nickel(II) from aqueous solution. *Journal of Hazardous Materials*, 186 (1), 160–168.

Park, Y., Kim, W., Park, H., Tachikawa, T., Majima, T., and Choi, W., 2009. Carbon-doped TiO2 photocatalyst synthesized without using an external carbon precursor and the visible light activity. *Applied Catalysis B: Environmental*.

Ren, Y.N., Xu, W., Si, Z.X., Zhou, L.X., and Zheng, Y.Q., 2018. Photocatalytic degradation of tetracycline antibiotics under visible light using uranyl isophthalate coordination polymers. *Polyhedron*, 152, 195–201.

Rimoldi, L., Meroni, D., Cappelletti, G., and Ardizzone, S., 2017. Green and low cost tetracycline degradation processes by nanometric and immobilized TiO2 systems. *Catalysis Today*, 281, 38–44.

Sadeghi-Niaraki, S., Ghasemi, B., adeh, A.H., Ghasemi, E., and Ghahari, M., 2019. Preparation of (Fe,Cr)2O3@TiO2 cool pigments for energy saving applications. *Journal of Alloys and Compounds*, 779, 367–379.

Sadeghi-Niaraki, S., Ghasemi, B., Habibolahzadeh, A., Ghasemi, E., and Ghahari, M., 2019. Nanostructured Fe2O3@TiO2 pigments with improved NIR reflectance and photocatalytic ability. *Materials Chemistry and Physics*, 235 (May), 121769.

Safari, G.H., Hoseini, M., Seyedsalehi, M., Kamani, H., Jaafari, J., and Mahvi, A.H., 2014. Photocatalytic degradation of tetracycline using nanosized titanium dioxide in aqueous solution. *International Journal of Environmental Science and Technology*, 12 (2), 603–

616.

Saitoh, T., Shibata, K., and Hiraide, M., 2014. Rapid removal and photodegradation of tetracycline in water by surfactant-assisted coagulation-sedimentation method. *Journal of Environmental Chemical Engineering*, 2 (3), 1852–1858.

Shao, S., Hu, Y., Cheng, C., Cheng, J., and Chen, Y., 2018. Simultaneous degradation of tetracycline and denitrification by a novel bacterium, Klebsiella sp. SQY5. *Chemosphere*, 209, 35–43.

Sharma, S., Dutta, V., Singh, P., Raizada, P., Rahmani-Sani, A., Hosseini-Bandegharaei, A., and Thakur, V.K., 2019. Carbon quantum dot supported semiconductor photocatalysts for efficient degradation of organic pollutants in water: A review. *Journal of Cleaner Production*, 228, 755–769.

Sharma, S., Umar, A., Sood, S., Mehta, S.K., and Kansal, S.K., 2018. Photoluminescent C-dots: An overview on the recent development in the synthesis, physiochemical properties and potential applications. *Journal of Alloys and Compounds*, 748, 818–853.

Shen, G.R., Cheng, Y.T., and Tsai, L.N., 2005. Synthesis and characterization of Ni-P-CNT's nanocomposite film for MEMS applications. *IEEE Transactions on Nanotechnology*.

Shen, T., Wang, Q., Guo, Z., Kuang, J., and Cao, W., 2018. Hydrothermal synthesis of carbon quantum dots using different precursors and their combination with TiO2 for enhanced photocatalytic activity. *Ceramics International*, 44 (10), 11828–11834.

Sobczyński, A., Duczmal, L., and Zmudziński, W., 2004. Phenol destruction by photocatalysis on TiO2: An attempt to solve the reaction mechanism. *Journal of Molecular Catalysis A: Chemical*.

Song, Z., Ma, Y.L., and Li, C.E., 2019. The residual tetracycline in pharmaceutical wastewater was effectively removed by using MnO2/graphene nanocomposite. *Science of the Total Environment*, 651, 580–590.

Sun, D., Cao, Y., Xu, Y., Zhang, G., and Sun, Y., 2016. Tunable synthesis of core-shell α-Fe2O3/TiO2 composite nanoparticles and their visible-light photocatalytic activity. *Chemical Research in Chinese Universities*.

Tomić, N., Grujić-Brojčin, M., Finčur, N., Abramović, B., Simović, B., Krstić, J., Matović, B., and Šćepanović, M., 2015. Photocatalytic degradation of alprazolam in water suspension of brookite type TiO2 nanopowders prepared using hydrothermal route. *Materials Chemistry and Physics*.

Totito, T.C., 2013. Photocatalytic activity of supported TiO 2 nanocrystals, (November), 1–153.

Tran, M.H. and Jeong, H.K., 2018. Modification of titanium dioxide by solution plasma. *Journal of Physics and Chemistry of Solids*, 121 (April), 292–297.

Tseng, Y.H., Kuo, C.S., Huang, C.H., Li, Y.Y., Chou, P.W., Cheng, C.L., and Wong, M.S., 2006. Visible-light-responsive nano-TiO2 with mixed crystal lattice and its photocatalytic activity. *Nanotechnology*.

Wang, D., Xiao, L., Luo, Q., Li, X., An, J., and Duan, Y., 2011. Highly efficient visible light TiO2 photocatalyst prepared by sol-gel method at temperatures lower than 300°C. *Journal of Hazardous Materials*, 192 (1), 150–159.

Wang, J.Y., Yu, J.X., Liu, Z.H., He, Z.K., and Cai, R.X., 2005. A simple new way to prepare anatase TiO2 hydrosol with high photocatalytic activity. *Semiconductor Science and Technology*.

Wang, Q., Zheng, H., Long, Y., Zhang, L., Gao, M., and Bai, W., 2011. Microwave-hydrothermal synthesis of fluorescent carbon dots from graphite oxide. *Carbon*.

Wu, M.C., Huang, W.K., Lin, T.H., and Lu, Y.J., 2019. Photocatalytic hydrogen production and photodegradation of organic dyes of hydrogenated TiO 2 nanofibers decorated metal nanoparticles. *Applied Surface Science*, 469 (August 2018), 34–43.

Wu, Q. and Zhang, Z., 2019. The fabrication of magnetic recyclable nitrogen modified titanium dioxide/strontium ferrite/diatomite heterojunction nanocomposite for enhanced visible-light-driven photodegradation of tetracycline. *International Journal of Hydrogen Energy*, 44 (16), 8261–8272.

Xu, D., Xiao, Y., Pan, H., and Mei, Y., 2019. Toxic effects of tetracycline and its degradation products on freshwater green algae. *Ecotoxicology and Environmental Safety*, 174 (December 2018), 43–47.

Yang, L., Sun, W., Luo, S., and Luo, Y., 2014. White fungus-like mesoporous Bi2S3 ball/TiO2 heterojunction with high photocatalytic efficiency in purifying 2,4-dichlorophenoxyacetic acid/Cr(VI) contaminated water. *Applied Catalysis B: Environmental*.

Yu, Y., Yu, J.C., Yu, J.G., Kwok, Y.C., Che, Y.K., Zhao, J.C., Ding, L., Ge, W.K., and Wong, P.K., 2005. Enhancement of photocatalytic activity of mesoporous TiO2 by using carbon nanotubes. *Applied Catalysis A: General*, 289 (2), 186–196.

Zhang, B., Maimaiti, H., Zhang, D.D., Xu, B., and Wei, M., 2017. Preparation of coal-based C-Dots/TiO2 and its visible-light photocatalytic characteristics for degradation of pulping black liquor. *Journal of Photochemistry and Photobiology A: Chemistry*, 345, 54–62.

Zhang, J., Kuang, M., Wang, J., Liu, R., Xie, S., and Ji, Z., 2019. Fabrication of carbon quantum dots/TiO2/Fe2O3 composites and enhancement of photocatalytic activity under visible light. *Chemical Physics Letters*, 730 (May), 391–398.

Zheng, X., Fu, W., Kang, F., Peng, H., and Wen, J., 2018. Enhanced photo-Fenton degradation of tetracycline using TiO2-coated α-Fe2O3 core–shell heterojunction. *Journal of Industrial and Engineering Chemistry*, 68, 14–23.

Zhu, J., Chen, F., Zhang, J., Chen, H., and Anpo, M., 2006. Fe3+-TiO2 photocatalysts prepared by combining sol-gel method with hydrothermal treatment and their characterization. *Journal of Photochemistry and Photobiology A: Chemistry*, 180 (1–2), 196–204.

Zhu, Z., Cai, H., and Sun, D.W., 2018. Titanium dioxide (TiO2) photocatalysis technology for nonthermal inactivation of microorganisms in foods. *Trends in Food Science and Technology*, 75 (February), 23–35.

Chapter 5 CONCLUSIONS AND RECOMMENDATIONS

5.1 Conclusion

In summary, four types of TiO_2 nanostructures (nanotubes, nanofibers, nanospheres and amorphous) were successfully Synthesized by the sol-gel and hydrothermal method, by adjusting the NaOH concentration and reaction temperature.

Photocatalysis depends on the pH in the photocatalytic degradation of organic pollutants.

The experiments were performed at different pH values respectively, and pH is considered as a critical parameter in photocatalytic degradation.

According to the results obtained, the T-NF sample exhibited excellent photocatalytic activity at pH 3 and degrading tetracycline under visible light irradiation.

Regarding the photocatalytic degradation of tetracycline under visible light irradiation, according to the results obtained it was found that it strongly depends on the type of TiO_2 nanostructures and the pH medium.

The results obtained show that the T-NF are believed to have potential applications in the field of environmental remediation.

After coupling T-NF with CDs, the CDs/TiO_2 composite nanofiber displays weaker PL intensity and higher photocatalytic degradation activity of TC than T-NF under visible light irradiation, which may be due to the enhanced absorptivity of pollutants and higher separation efficiency of electron hole pairs.

CDs can accept and transfer photogenerated electrons through Ti-O-C and Fe-O-C bonds formed between the CDs and TiO_2/Fe_2O_3, effectively separating electrons and holes.

CDs can improve the utilization of photogenerated electrons and the introduction of CDs enhances the role of O_2^- radicals in the photocatalytic process of CDs/TiO_2/Fe_2O_3 composite nanofiber.

The new as-Synthesized CD-TiO_2-Fe_2O_3 composite nanofiber material has been Synthesized by the hydrothermal method and it has been successfully applied as a catalyst for

photodegradation of TC using visible light irradiation. The CD-TiO_2-Fe_2O_3 composite nanofiber displayed excellent visible light photocatalytic activity in the degradation of TC. Therefore, this reveals that CD-TiO_2-Fe_2O_3 composite nanofiber have potential as economically friendly photocatalysts for wastewater treatment due to their reusability.

5.2 Recommendations

- The photodegradation needs to be monitored with total organic carbon (TOC) analyzer to determine the concentration of organic carbon.
- The photocatalytic activity of the TiO_2 composite nanofiber should be investigated on other model organic pollutants such as methylene blue (MB) and Rhodamine B.
- The magnetic properties of the 1%,3%,5%-Fe_2O_3/CDs/TiO_2 composite nanofiber using the vibrating sample magnetometry (VSM) needs to be measured.